Investigating inhibition of porphyrin (heme) synthesis as a novel treatment option for prostate cancer

Georgina Lucy Meecham Davis

Supervisor: Dr Greg Brooke

A thesis submitted in accordance with the requirements of the University of Essex for the degree of MSc by Dissertation in Biochemistry

School of Biological Sciences

University of Essex

Date of Submission: October 2019

Statement of Originality:

I clarify that this thesis is my own work and that all sources used have been acknowledged.

Abstract

Prostate cancer (PC) affects 1 in 8 men in the UK. Hormone therapy is used to initially treat men diagnosed with non-organ confined disease. PC growth is dependent upon the androgen receptor and hence therapies for non-organ confined disease aim to disrupt this signalling axis. However, over time cancer cells adapt and become therapy resistant. For this stage of the disease, there are limited treatment options and there is a need for new therapies that can target these resistant forms of PC.

Metabolism is a process often modified in cancer cells. It has been shown that porphyrin synthesis is increased in multiple cancers and targeting this pathway may be a viable treatment option for PC. Crystal violet assays demonstrated that the porphyrin synthesis inhibitor succinyl acetone (SA) reduced the proliferation of PC3, LNCaP and DU145 cells and heme depletion assays confirmed that SA does decrease cellular heme content. Flow cytometry demonstrated that SA induced a low level of caspase independent cell death, but when combined with ROS damage the percentage number of cells undergoing cell death increased significantly. The data suggest that cell death is not as a result of apoptosis, necroptosis or ferroptosis, suggesting a different type of cell death is occurring.

This study also aimed to express and purify the enzymes responsible for the first step in heme synthesis, performed by ALAS 1 or 2. ALAS 2 T was able to be purified in Rosetta cells in a pET28a vector and ALAS 1 T was expressed in pET21a vector in T7 shuffle cells. Heme synthesis was further validated as a novel therapeutic target for PC and the successful expression of ALAS1 and 2 will facilitate future drug discovery programs.

Acknowledgements

I would first like to thank my supervisor Dr Greg Brooke for his incredible support and encouragement throughout the last year, without which, this work would not be possible. I would also like to acknowledge all that Dr Filippo Prischi has also contributed with his support throughout. A big thank you to all the girls in the GB lab for continued encouragement whenever I needed it. Also, to Julie Arvidson for her kind guidance and to Emma Revill for her time and support.

Abbreviations

AIM	Auto induction media
AKT	Protein Kinase B
ALA	5-Aminolevulinate
ALAD	ALA dehydratase
ALAS	5-Aminolevulinate synthase
AR	Androgen receptor
ATP	The Adenosine triphosphate
BCL-2	B-cell lymphoma 2
BCL-XL	B-cell lymphoma-extra large
CICD	Caspase independent cell death
DAMPs	Damage related pattern molecules
DD	Death domain
ddH_2O	Double distilled water
DED	Death effector domain
DHT	5α- dihydrotestosterone
DNA	Deoxyribonucleic acid
Dntp	Deoxyribonucleotide triphosphate
DR	Death receptor
DRE	Digital rectal examination
EDTA	EDTA Ethylenediaminetetraacetic
FACS	FACS fluorescence-activated cell sorting
FADD	Fas-associated death domain-containing
FBS	Foetal bovine serum
FSH	Follicle-stimulating hormone
HO	Hydroxyl radical
HO-1	1 Heme oxygenase 1
ICE	Interleukin-1β converting enzyme
LB	Luria broth
LH	Luteinising hormone
LHRH	Luteinising-hormone-releasing hormone

MLKL	Mixed linkage domain like
NEMO	NF-kB essential modulator
NF	Nuclear factor
NSCLC	Non-small cell lung cancer
P13K	Phosphoinositide 3-kinase
PBS	Phosphate buffered saline
PBS-T	Phosphate buffered saline-Tween
PC	Prostate cancer
PFA	Paraformaldehyde
PI	Propidium iodide
PSA	Prostate specific antigen
PSG	Penicillin Streptomycin-Glutamine
PTEN	Phosphatase and tensin homolog
PVDF	Polyvinylidene fluoride
RHIM	Homotypic interaction motif
RIPK1/3	Receptor Interacting Protein Kinases 1/3
RNA	Ribonucleic acid
ROS	Reactive oxygen species
RPMI	Rosewell Park Memorial Institute
SA	Succinyl acetone
SDS	Sodium dodecyl sulphate
SOC	Super optimal broth with catabolite repression
TAE	Tris acetic acid
TEMED	Tetramethyl ethylenediamine
TNF	Tumour Necrosis Factor
TN	Tumour Necrosis Factor Receptor
TRAIL TNF	TNF related apoptosis inducing ligand
UGS	Urogenital sinus
UROD	Uroporphyrinogen decarboxylase
WT	Wild type

Contents

List of Figures

1.0 Chapter one; Introduction

1. 1. 0 The prostate gland

The prostate is a gland that is heavily involved in male fertility. It is the approximate size of a walnut and continues to get bigger as a man gets older. The prostate glands' function is to secrete a fluid that makes up 30 % of the total volume of semen with seminal vesicle fluid and spermatozoa (male germ cells) (Huggins et al., 1942). The total seminal plasma is made up of many fluids secreted from male accessory glands (including the prostate), epididymis and testes. These different organs interact simultaneously to create this seminal plasma. Prostatic fluid, containing citrate, kallikreins and Zn^{2+}, is important for the synchronised cascade of actions that allow for a sperm to access an egg to enable fertilization as well as nourishing and protecting spermatozoa after ejaculation (Verze et al., 2016; Hoover and Naz 2012).

1. 1. 1 Development of the prostate gland

The prostate is formed from the urogenital sinus (UGS). During the first 5 weeks of foetal development, the mammalian cloaca is used as an excretory method. By 6 weeks this is then split into digestive and urinary tracts. In response to androgens, produced by cells of Leydig found within male testicles, the UGS differentiates to become sexually dimorphic at 8 weeks. Prostatic development is initiated at 10 weeks from the UGS. Formation of solid cords and ducts, epithelial buds, and a branched glad develop after this. In humans, the prostate grows as one organ containing glandular areas that, after sexual maturity, become histologically distinct (Meeks and Schaeffer 2013).

The prostate and seminal vesicle depend, specifically, on the presence of stimuli, in the form of androgens (Mann 1974) The androgenic stimuli signal through an androgen receptor to induce proliferation and prostate development (Meeks and Schaeffer 2013).

1. 1. 2 Location and structure of the prostate gland

The prostate is located just under the bladder surrounding the urethra (Figure 1). The prostate is composed of ducts formed of two compartments: the inner epithelium and the outer stroma. Normal development and homeostasis are maintained by these compartments influencing each other via signalling pathways.

There are three main zones recognised within the prostate, the central zone, the transition zone and the peripheral zone. The central zone is found around the ejaculatory ducts and under the bladder. The transition zone is found around the urethra, next to the ejaculatory ducts and lastly the peripheral zone makes up the front, back and lateral parts of the prostate. These can be clinically described as two lobes and a central sulcus (Verze et al., 2016).

The stroma ensures the optimal environment for the inner epithelial section and contains many supportive signals to maintain homeostasis in both healthy and regenerative conditions. The epithelial inner section is responsible for the main glandular functions of the prostate as it secretes the fluids needed for the ejaculate (Verze et al., 2016).

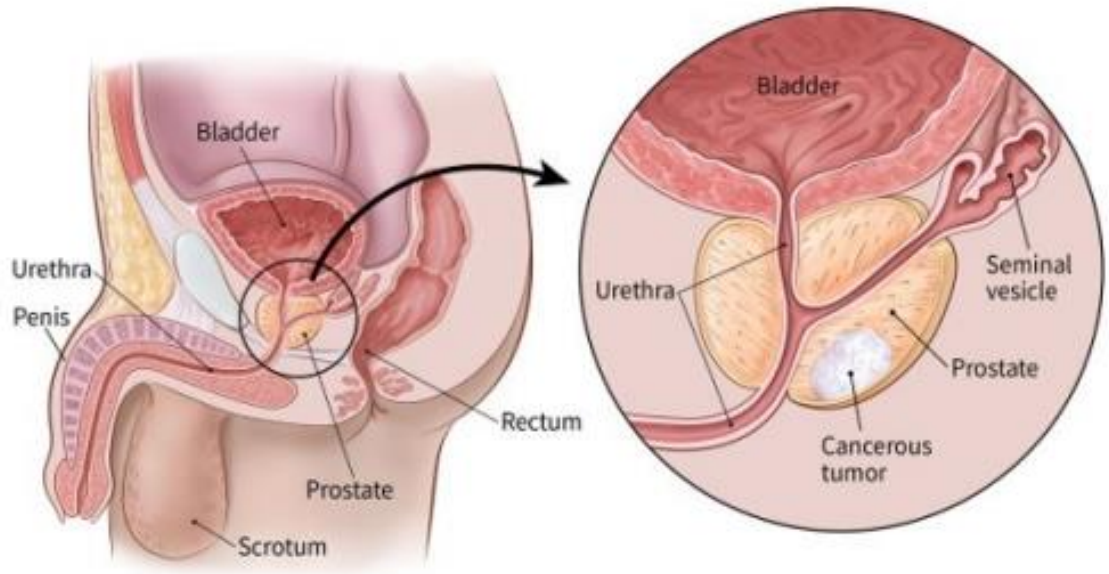

Figure 1 Image to show the positioning of the prostate around the urethra and under the bladder. *The right shows an example of where a cancerous prostate tumour could be situated. (ACS, 2018).*

1. 2. 0 Diseases of the prostate gland

There are many common diseases that target the prostate and can affect the fertility of a man at different ages. Prostatic diseases and an unhealthy prostate can affect male fertility via spermatozoa function (Verze et al., 2016). One of which is prostatitis syndrome, a common disease affecting 11-13 % of adult men, having serious implications on a person's quality of life. Chronic bacterial prostatitis can be associated with a development of infertility (Verze et al., 2016). A pathogen that is having a direct negative affect on spermatozoa are considered to be within one of three categories: a pathogen causing damage directly to spermatozoa, an immune-mediated damage response or the indirect effect of sperm dysfunction due to decreased prostate secretion ability. A bacterial infection within the reproductive tract is thought to result in damaging the secretory abilities of the prostate, having a negative effect on morphology and motility of the semen. An infection of Escherichia coli can have many effects on the semen parameters such as membrane alterations, mitochondrial changes and a reduction of the number of sperm cells within the fluid with the ideal mitochondrial membrane potential. It can also cause changes to spermatozoa immobilization and decrease the viability and motility of sperm (Verze et al., 2016).

Bacterial prostatitis can be caused by *Chlamydia trachomatis. C. trachomatis* can potentially cause inflammation that inhibits the normal function of the prostate gland (Verze et al., 2016). Another disease of the prostate is benign prostatic hyperplasia or otherwise known as prostate enlargement. Although the causes for prostate enlargement are unknown, it still poses a large public health problem. It is a disease with high prevalence within older men and is a result of the prostate gland growing via non-malignant unregulated growth. In extreme cases it can cause a person to experience irreversible bladder damage, kidney failure, sepsis and even death (Parsons 2006).

Obesity, and the glucose homeostasis irregularities that are associated with obesity, are considered risk factors for prostate enlargement as they may be able to influence prostate growth and therefore

the development of benign prostatic hyperplasia. It is also believed that androgens also play an important role in the causation of prostate enlargement (Parsons 2006).

1. 2. 1 Prostate cancer

Approximately 1 in 8 men, across the UK, will get prostate cancer at one point in their lifetime and it is the most common cancer in men in the UK (PCUK 2018) and the second most common cancer in men in the world (Wenpeng and Henneberg 2018). There has been a 44 % increase in prostate cancer incidence since the early 1990s in the UK (CRUK 2018) and it is a large public health concern in most developed countries and is gradually becoming a greater problem in developing countries (Bratt and Lamb 2018).

As prostate cancer develops slowly it is often symptomless during the early stages. Some cases of prostate cancer grow so slowly that there may be no symptoms at all throughout the man's life (Lloyd et al., 2015). Often symptoms only occur if the prostate grows near the urethra and large enough to put pressure on it and change the way a person urinates. This can include symptoms such as difficulty beginning to urinate or to empty the bladder, needing to urinate more – especially at night and a sudden need to urinate.

An increase in life expectancy of men and therefore increase in the rise of prostate cancer incidence has inflated the economic burden of prostate cancer in Europe. The total costs of prostate cancer for Europe has been estimated to exceed 8.43 billion euros. Most of the costs are related to the first year of diagnosis (Mottet et al., 2016).

1. 2. 2 Diagnosis of prostate cancer

Prostate cancer screening is a controversial topic as there is little solid evidence that mass Prostate specific antigen (PSA) screening is cost effective by reducing prostate cancer deaths. Screening can also be associated with over diagnosis and over treatments (Mottet et al., 2016). Findings have shown

a strong argument against a population systematic screening in all countries. A risk adapted strategy based on the individual can be used for early detection and could be offered to a man who is well informed and has 10-15 years life expectancy at least. This may still give rise to over diagnosis and so a careful analysis of the patients risks and the likelihood of them benefiting from an early diagnosis (Mottet et al., 2016).

There are some new biological markers and genetic markers that have been found to increase specificity when used with PSA meaning a lower level of over diagnosis, however there is still too little data on population bases survival benefit (Mottet et al., 2016). Clinical diagnosis usually begins with a suspicious digital rectal examination and/or PSA levels. A prostate biopsy is used to then confirm the diagnosis. The DRE (digital rectal examination) can detect incidence of prostate cancer when the volume is larger than 0.2ml. Some prostate cancers can even be detected by only the DRE (~18%) regardless of PSA levels and an unusual DRE can represent the risk of a high Gleason score (higher the score the more aggressive the cancer and the worse the prognosis) and demonstrate a need for a biopsy (Mottet et al., 2016). PSA has been used as a serum marker. However, it is specific to the organ, not the cancer and so it can show high levels in response to benign prostatic hyperplasia, prostatitis and other non-cancerous ailments (Mottet et al., 2016).

1. 2. 3 Risk factors for prostate cancer

Some of the risk factors of prostate cancer include age, ethnicity – with black men having a higher risk - weight and genetics. Having a first degree relative with diagnosed prostate cancer or breast cancer can mean a higher risk (Lloyd et al., 2015). Studies have found that in the UK black men have a 2-3 times higher risk of developing prostate cancer than white men (Ben-Shlomo et al., 2008; Jack et al., 2010). A meta-analysis and systematic review found that black men diagnosed with prostate cancer had a poorer prognosis in comparison to white men (Evans et al., 2008). However, as these studies

were all based in the USA with reduced access to health care, as it is required to pay for treatment, this could be because of an underprivileged socioeconomic position rather than a higher risk of a more aggressive form of prostate cancer (Lloyd T et al., 2015).

There has been strong evidence that there is a genetic predisposition for prostate cancer based on family history. It has been found that there are 100 common susceptibility loci that can add to a person's risk of prostate cancer. For a person to have true hereditary prostate cancer they are defined as having more than 2 affected relatives or at least two relatives with a form of the disease before the age of 55. These people usually develop the disease 6-7 years before a non-hereditary form of the cancer, however, after this initial diagnosis there is no difference in the progression of the disease (Mottet et al., 2016).

Inflammation of the prostate may have a role in causing the complicated progression of the degeneration of the prostate eventually leading to prostate carcinogenesis. An inflammatory injury causing prostate tissue remodelling could promote changes to the structure that are often linked to malignancies and benign disease (Ficarra et al., 2014). Inflammatory infiltrates are often found to be present in prostate biopsy or prostatectomy tissue (Wagenlehner et al., 20087). Viral and bacterial DNA found within prostate cancer cells show they have the potential to act to increase genotoxic activity by the induction of oxidative stress on the cell. Some prostatectomy specimens show RNA sequences from bacteria in patients with benign prostatic hyperplasia (Verze et al., 2016). One study induced chronic inflammation in a mouse model via injection of *E. coli* causing reactive hyperplasia linked to oxidative stress, showing that there is a definite link between inflammation, oxidative stress causing DNA damage and carcinogenesis (Elkahwaji et al., 2007).

1. 2. 4 Current treatment options for prostate cancer

To reduce over treatment, active surveillance is used to ensure the correct timing for treatment of a selected low risk patient. A patient remains under close regular surveillance and with consideration of the person's life expectancy, a predefined threshold that suggests the disease is becoming life threatening indicates the need for commencement of treatment (Mottet et al., 2016).

A radical prostatectomy is carried out to remove the disease while ensuring continence and potency are preserved. The entire prostate gland is removed between the urethra and the bladder. Resection of both seminal vesicles and enough surrounding tissue to ensure disease eradication. This is usually done alongside a pelvic lymph node dissection (Mottet et al., 2016). Patients of increasing age are of a higher risk of incontinence and so a patient's life expectancy is a necessary part of the counselling process when discussing this surgical treatment option.

Radiation therapy is another treatment option for prostate cancer patients. This involves a localised dose of radiation on the malignant cells to destroy them. The method aims to use the highest dose possible on the cancer cells but whilst causing as little damage as possible to surrounding healthy body tissue. Radiation causes damage to the tumour cells halting their reproduction and therefore shrinking the tumours volume. However, the radiation can also do significant damage to the surrounding healthy cells (Sadeghi et al., 2010).

Hormone therapy is achieved by depriving the tumour of androgen. This is done via suppressing the secretion of testicular androgens or by suppressing the action of circulating androgen. These methods can also be combined and cause a "complete androgen blockade". Surgical castration is one way to deprive the cancer cells of androgen. This is achieved by bilateral orchiectomy or subcapsular pulpectomy; a simple (almost complication free) procedure that can be done under local anaesthetic and achieves castration quickly – under 12 hours. However, it is irreversible and makes intermittent treatment not possible. Luteinising-hormone-releasing hormone (LHRH) antagonists are synthetic analogues of LHRH and can be administered via injection on a regular basis, the frequency of which

depends on the patient. Exposure to the LHRH antagonists inhibits LHRH receptors and suppresses LH (luteinising hormone) and FSH (follicle-stimulating hormone) production and so testosterone production is also down regulated usually achieving a castration level after 2-4 weeks (Mottet et al., 2016).

1. 2. 5 Androgen receptor and prostate cancer

Hormone therapy is one of the main therapies used to initially treat men diagnosed with the disease. Prostate cancer growth is dependent upon the androgen receptor and hence these therapies aim to block androgen production or action. The androgen receptor is a transcriptional activator within prostate cells which initiates gene expression needed for many functions of the cell some of which are involved in metabolism and proliferation. The normal function of this receptor is needed for the normal healthy development of the prostate (Han., 2018).

Accumulation of citrate and Zn^{2+}, Krebs cycle inhibition and the release of prostatic fluid are all regulated by androgens, or male sex steroids, via the androgen receptor, which acts as the effector. The androgen receptor is a part of a subfamily of 48 nuclear receptors in humans. They have a double function of being intracellularly located and ligand activated transcription factors. Testosterone is converted within the prostate to androgen, 5α- dihydrotestosterone (DHT) which has a higher binding affinity for the androgen receptor. There are many genes within the prostate epithelium, lots being important for prostate homeostasis, that are under the regulation of DHT (Verze et al., 2016).

DHT dependent expression is essential for ensuring a healthy homeostasis of the epithelial section of the prostate and for decreasing progression of malignancy's (in prostate cancer cases). As a male human gets older their circulating testosterone levels and prostatic DHT levels decrease. This impairs the function of the prostate gland and reduces its ability to keep healthy levels of Zn^{2+}, citrate and kallikreins in the prostatic fluid. Therefore, male fertility is progressively debilitated as a person grows

older. This age-depended impairment also causes a metabolic change that favours an epithelial cell in a cancer-prone status, causing full ATP production by respiration and terminal oxidation by the mitochondria, this facilitates prostate cancer initiation and progression (Verze et al., 2016).

Hormone dependant prostate cancer requires androgen receptor signalling and tumour growth is driven by the androgen receptor. Its activity can be inhibited by androgen-deprivation therapies in patients with metastatic prostate cancer and they are treated with medical or surgical castration (Han 2018). The androgen receptor has an altered cistrome for the initial stages of prostate cancer. In prostate cancer cells the androgen receptor gains control of and begins to target new oncogenes. These include the ETS family and SOX9 the expression of which alters the androgen receptor binding, routine in cancer cells. Many epigenetic regulators can reprogram the chromatin binding of the androgen receptor by altered expression of the epigenetic factors themselves. A study carried out on radical proctectomy tumours proposes that during tumorigenesis the androgen receptor has been reprogramed alongside FOXA1 and HOXB13 (Pomerantz et al., 2015). Castration resistant prostate cancer has also been found with androgen receptor reprograming. One mechanism for this could be the higher levels of expression of some androgen receptor splice variants (Han 2018).

1. 2. 6 Prostate cancer Therapy Resistance

Over time cancer cells adapt and become able to grow and spread without high levels of androgens, therefore promoting therapy resistance. The cancer then becomes castration-resistant or androgen-independent. For this stage of the disease, there are limited treatment options and therefore there is a need for new therapies that can target these resistant forms of prostate cancer.

A recurrence of the cancer is often because of residual androgens contributing to continued androgen receptor activity and so many castration resistant patients benefit from further androgen suppression therapy. Unfortunately, many of these patients still relapse before 1-2 years and with increased

expression levels of androgen receptor and high levels of genes regulated by the androgen receptor show that androgen receptor levels are re-established. There is therefore a need for improvement on the current therapies that act on targeting androgen receptor activity (Han 2018).

Castration resistance is thought to be due to two mechanisms: androgen receptor independent and androgen receptor dependant. In castration resistant prostate cancer there is a higher level of androgen noted compared to cells that are sensitive to androgen and androgen receptor expression is seen suggesting an adapted system. Two new compounds that target castration resistance are abiraterone acetate and enzalutamide. Abiraterone acetate is a CYP17 inhibitor (CYP17 catalyse synthesis of androgens from precursors, 17α-hydroxy and 17,20-lyase) (Vasaitis et al., 2012). Blocking the CYP17 cellular testosterone levels are decreased by inhibiting its synthesis at the adrenal stage as well as within the cells themselves. Enzalutamide is a new anti-androgen that has an increased affinity for the androgen receptor, it blocks androgen receptor transfer and therefore inhibits agonist activity (Mottet et al., 2016).

1. 3. 0 Metabolism in cancer cells

Cancer cells have many alterations from healthy cells to enable them to survive and proliferate uncontrollably. Metabolism is one of the prosseses often modified in cancer cells. The metabolism within tumour cells occurs at a much faster rate this is because a large supply of cellular energy is needed to maintain the unlimited cell growth during tumour development. The tumours also have a metabolic flexibility that allows them to produce ATP for energy whilst using resources for biosynthesis, needed for cell growth and proliferation (Martinez-Outschoorn 2017). Normal cells are able to produce enough energy mainly via oxidative phosphorylation during the electron transport chain. Cancer cells, however, often produce ATP via an accelerated rate of aerobic glycolysis and lactic acid fermentation. This is known as the Warburg effect. It has a lower efficiency of ATP production but increases metabolite production potentially useful for increased cell proliferation (Vander Heiden

2010). An enhanced glycolytic flux in cancer cells is not dependant on decreased respiration or oxygen consumption (Kaambre 2012; Whitaker-Menezes 2011).

Heme is an essential component for the generation of cellular energy by electron transport and oxidative phosphorylation as it is an important prosthetic group in many proteins that transport and store oxygen e.g. cytochromes and haemoglobin. It also is a direct regulator of the processes within systems that use oxygen or sense oxygen. So, heme can affect growth and survival of cells via its action on proteins needed for energy generation (Hooda et al., 2013). Two studies show that mitochondrial respiration is amplified in human breast cancer cells (Kaambre 2012; Whitaker-Menezes 2011). Whilst other recent studies have shown that metabolism alterations are a hallmark of cancer and that these alterations are more complex than was originally thought (Birsoy et al., 2012).

These results show that mitochondrial respiration is important to cancer cell metabolism. Heme is a key factor in mitochondrial function and is necessary in every process involved in oxygen metabolism, working as a prosthetic group in haemoglobin and myoglobin as well as other globin's that are used to transport and store oxygen and in oxygenase's using oxygen for biosynthetic reactions and degradation reactions. Heme is also used in enzymes to detoxify oxygen (Hooda et al., 2013). This difference in the metabolism of healthy cells and cancer cells allows a possibility for drugs to be developed that can selectivity target the abnormal metabolism taking place in cancer cells. Therefore, making it a promising new therapeutic strategy.

1. 3. 1 Metabolism within prostate cells

Synthesis of citrate and oxidation during the Krebs cycle are key metabolic pathways in aerobic cells. The complete oxidation of fats and glucose are carried out by citrate synthesis followed by its oxidation which allow cells to generate a cellular energy supply of ATP. The Krebs cycle and its intermediates create pathways for biosynthesis and degradation reactions of amino acid metabolism. Citrate synthesis ensures an acetyl-coA source for lipogenesis and is therefore a key part of the normal

metabolism system ensuring normal function, growth and reproduction abilities of human cells (Costello and Franklin 2000).

The prostate has a unique relationship with its metabolism that is not seen in any other human tissues. Prostatic epithelial cells are the only healthy human cells that produce energy by glycolysis (a hallmark of proliferating cancer cells) rather than the Krebs cycle (Verze et al., 2016). In addition, one of the main functions of the prostate involves secretion of a high level of citrate and zinc, a function that is linked specifically to the epithelium in the peripheral zone. These cells are therefore specialised for this function of zinc and citrate accumulation. The central zone does not have this function. The cells in the central zone, however, behave like most other human cells by oxidizing citrate and not accumulating zinc. This is a unique characteristic of the cells in the peripheral zone as no other body cells carry out this metabolic function. The accumulation of citrate for secretion means that, instead of citrate being an oxidizable intermediate for metabolism, it becomes the end product. This is achieved by limiting m-aconitase activity and this ensures citrate oxidation is in turn limited. Because this occurs at the start of the Krebs cycle the continuing of the cycle is abandoned in these cells (Costello and Franklin 2000).

1. 3. 2 The importance of Heme pigments and uses within proteins

A heme protein is characterised by the presence of an iron-porphyrin compound presented as a prosthetic group of the protein. This compound is known as “heme” and would be conjugated with a protein, the properties of the heme proteins are created by the existence of the heme prosthetic group within the protein (Wyman 1948). Tetrapyrrole heme is potentially one of the most important pigments within biology. It is needed for molecular, energy and electron transport, oxygen and carbon dioxide sensing and many enzymatic reactions (Astner et al., 2005). Almost all animal cells can synthesise heme, with mature erythrocytes and potentially some other cells that are highly differentiated being the exception (Ponka 1997).

Haemoglobin, peroxidases, myoglobin, catalases, cytochromes as well as many other mitochondrial respiratory complexes utilise heme as a prosthetic group (Kalainayakan et al., 2018). Heme is able to promote most oxidation processes within a biological system and therefore carries out functions that are vital for cell and whole organism homeostasis. Heme is used as a prosthetic group in proteins that are involved in oxygen transport, respiration within the mitochondria (electron transport), steroid biosynthesis, signal transduction processes and drug metabolism. Heme is synthesised just for incorporation into haemoglobin within erythroid cells. The main haemoprotein that is needed for oxygen storage in muscle tissues is myoglobin and all respiring tissues need heme for incorporating into cytochromes (Ryter and Tyrrell 2000).

Heme is able to regulate cellular processes such as cell cycle, death as well as transcription and translation and it has an action on respiratory proteins that are needed for energy production within the cell. Heme influences cell growth and survival (Ye and Zhang 2004). Therefore, unusual heme levels can indicate many diseases some of which include anaemia, porphyria, neurodegenerative disorders, type two diabetes, heart disease and this could further be applied to cancer cells such as lung, pancreatic and colorectal cancers (Kalainayakan et al., 2018).

1. 3. 3 Heme synthesis pathway

The precursor for all biologically synthesized heme is 5-Aminolevulinate (or ALA). This is produced (in animals) from glutamate in a single step. This first step of the heme biosynthetic pathway is carried out in the mitochondria and catalysed by 5-Aminolevulinate synthase (ALAS), a homodimeric pyridoxal 5'-phosphate-dependent enzyme. The full pathway of heme synthesis including all of the enzymes involved and where the reactions take place within the cell is shown below in figure 2. The mitochondria exports amino levulinate to the cytoplasm for further steps of the heme biosynthesis pathway including tetrapyrrole assembly and side chain decarboxylation (Ryter and Tyrrell 2000).

Through a series of four enzyme catalysed reactions aminolevulinate acid is converted to coproporphyrinogen III (as shown figure 2).

The coproporphyrinogen III created is then transported back into the mitochondria where the last few stages of heme synthesis that involve side chain oxidation and dehydrogenation are carried out converting the coproporphyrinogen III in to proroporphyrin IX. Iron will then be incorporated into the pathway by enzyme mitochondrial ferrochelatase. This will generate protoheme by adding ferrous iron Fe (II) into protoporphyrin IX. The heme iron then reversibly oxidises to ferriprotoporphyrin – the ferric form (Ryter and Tyrrell 2000). The heme synthesis pathway is regulated by inhibition. The end product inhibits ALAS mitochondrial translocation and synthesis (Ryter and Tyrrell 2000).

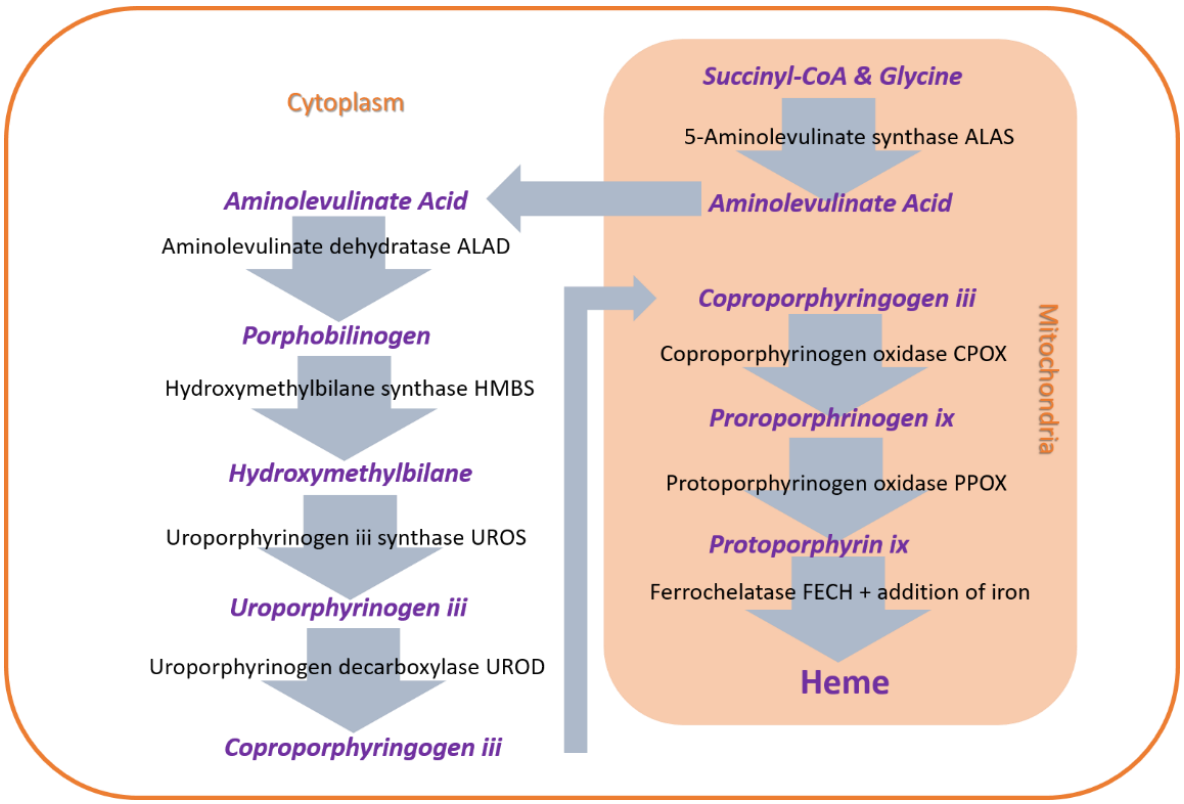

***Figure 2 Diagram showing the heme synthesis pathway occurring within a cell**. The orange outline representing the cell and the orange box the mitochondria. The blue arrows represent the order of the reactions within the pathway. Black lettering are the enzymes involved and purple lettering are each intermediate compound formed by the enzymes.*

1. 3. 4 The enzymes ALAS1 and ALAS2 from the heme synthesis pathway

ALAS was first discovered by Shemin and Neuberger (Shemin 1958; Gibson 1958) and exists and two isoenzymes: ALAS1 and ALAS2, ALAS1 is expressed in all cell types and ALAS2 is produced only in developing erythrocytes (Riddle 1989). The ALAS enzymes are related to other members of a subfamily that has been named the "CoA-dependant acetyltransferase or a-oxoamine synthase subfamily" including serine palmitoyl transferase and 8-amino-7-oxononanoate synthase catalyse. These four enzymes use small amino acids, CoA esters and aminoketones to catalyse reactions. Together they make up a family with tremendous biological importance due to their functions within heme synthesis, biotin synthesis and sphingolipid synthesis (Hunter and Ferreira 2009).

ALAS works as a homodimer, converting succinyl-CoA and glycine into ALA, CoA CO_2 (Hunter 2009). This works via an ordered kinetic mechanism whereby glycine binds first then followed by succinyl-CoA and amino levulinate being released last, after CoA and Carbon dioxide (Zhang and Ferreira 2002). This process follows a three steps kinetic reaction as there is a formation of an intermediate Michaelis complex. This synthesis of ALA is regulated by the levels of heme present in the cell and is the rate limiting step, due to the slow release of ALA (Ferreira 1993). The ALA then moves into the cytoplasm where ALA dehydratase (ALAD) condenses and cyclizes two molecules of ALA (Del 1993). The very last step of the pathway takes place in the mitochondria and involves incorporating iron into Protoporphyrin requiring the enzyme ferrochelatase (Peng 2008).

Rhodobacter capsulatus ALAS has a 49 % sequence identity with the catalytic core of human ALAS. The *Rhodobacter capsulatus* ALAS has been solved as a crystal structure holoenzyme with glycine and succinyl-CoA bound. This structure has helped to discover properties of the enzyme such as the positions of the substrates and cofactors. The cofactor was found to be 20 Å down from the active site at the centre of the enzyme. Active site residues were also able to be found (Hunter and Ferreira 2009).

The structure of human ALAS2 was solved by Bailey et al. (2018) and has been deposited on the PDB (code: 6HRH) is currently unpublished. The structure shows two binding pockets for the ligand pyridoxal-5'-phosphate (C8 H10 N O6 P / vitamin B6) in both chains. This is shown above (Figure 3). The structure for ALAS1 however is still unsolved and so we investigated methods for expression for purification of both isoenzymes. ALAS1 has been found by the Brooke group (unpub) to be upregulated in prostate cancer cells and so is of interest for prostate cancer treatment. The structure of ALAS2 however, does give us some insight as to structural properties of ALAS1 as they are isoenzymes.

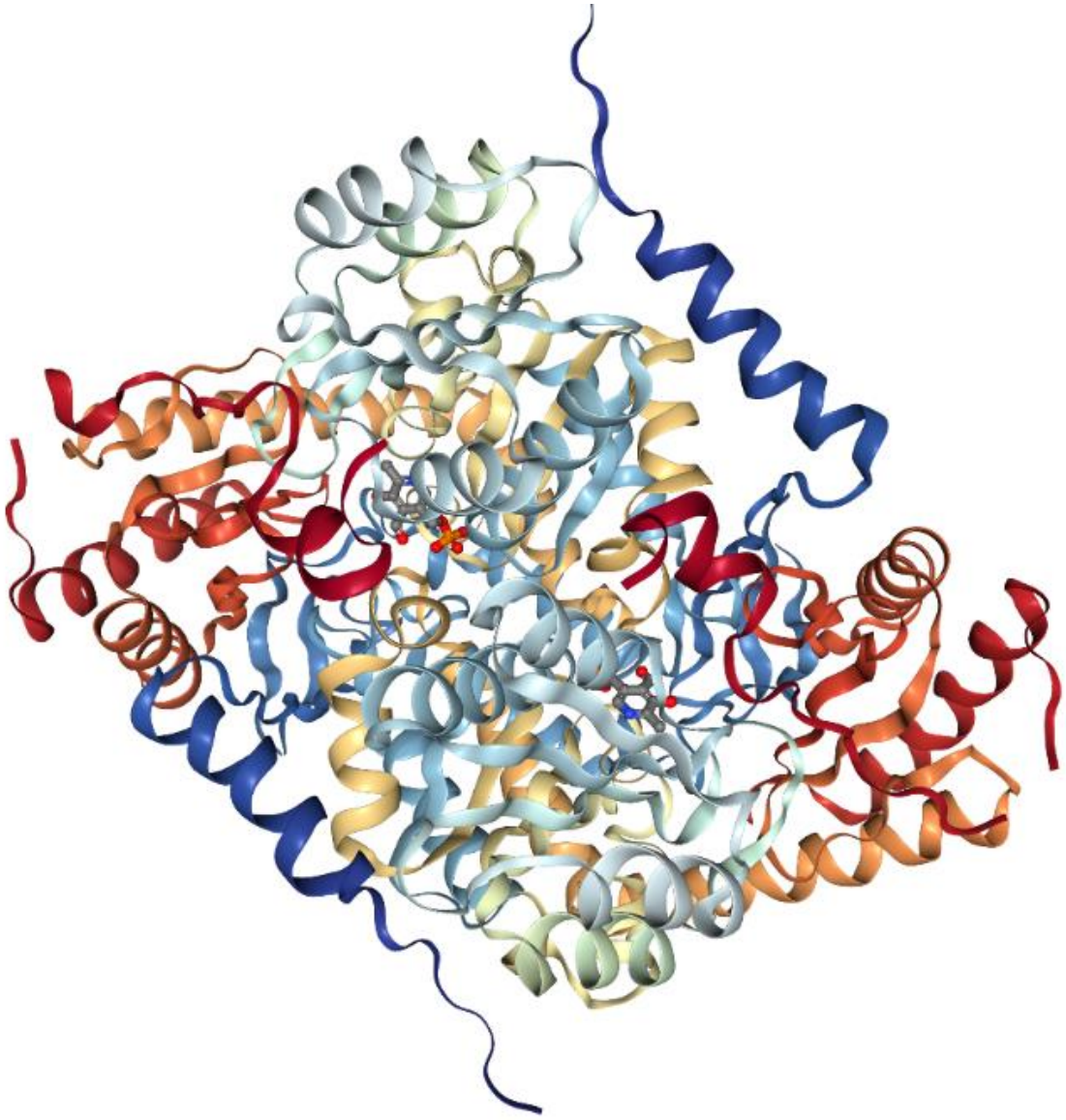

Figure 3 Structure of human erythroid-specific 5'-aminolevulinate synthase, ALAS 2, in a truncated form of 469 residues. *Images created with 6HRH Bailey et al. (2018), NGL viewer: web-based molecular graphics for large complexes. Bioinformatics, and RCSB PDB.*

1. 3. 5 Heme synthesis in cancer cells

Research into heme synthesis aspect of altered metabolism in cancer cells is a promising area as it has been shown that porphyrin (heme) synthesis in breast cancer tumours is increased (Navone 1990). The function of heme and mitochondria in lung cancer development was investigated by Hooda (2013) to find out if metabolic vulnerabilities could be an effective target to inhibit lung cancer progression. It was found that in non-small-cell lung cancer cells oxygen consumption rates and heme biosynthesis are intensified compared to the rates in normal cells. Proteins promoting heme synthesis, function and uptake were found to be in increased levels in these tumour types. It was also found that reducing heme uptake and biosynthesis (by lowering mitochondrial respiration) oxygen consumption was reduced. Cancer cell migration, colony formation and proliferation were also reduced (Hooda 2013). Showing that inhibiting respiratory and heme function can interrupt lung cancer progression. Lung cancer cells have shown, in vitro, to accumulate heme and they require it for invasion and proliferation (Kalainayakan et al., 2018).

While another study (Ye 2004) investigated the function of heme and mitochondria in lung cancer development to find out if metabolic vulnerabilities could be an effective target to inhibit lung cancer progression. Investigations into HeLa cells has shown that inhibition of heme synthesis induces cell cycle arrest and expression of senescence and apoptosis cellular markers. It was found that heme deficiency induced p53 and p21 expression while decreasing the activation of RAF in the MAP kinase signalling pathway and so heme has been shown to be able to control expression levels of key cell cycle regulators (Ye 2004). There are also several cancers that have shown a higher risk associated with intake of heme (Kalainayakan et al., 2018). Previous work from the Brooke group (unpub) suggests that targeting heme synthesis may be a viable treatment option for prostate cancer. This study therefore aims to further evaluate the efficacy of targeting this pathway as a therapeutic approach for this disease.

1. 3. 6 Heme synthesis inhibitor Succinyl acetone

Heme synthesis inhibitor Succinyl acetone (4,6-Dioxoheptanoic acid) inhibits ALAD (ALA dehydrogenase) activity, the second enzyme involved in the heme synthesis pathway. A study where intracellular heme synthesis was measured in PC12 cells treated with Succinyl acetone (1 mM), heme synthesis was reduced more than ten times (Zhu 2002). In non-small-cell lung cancer cells - and normal cells - Succinyl acetone potently inhibited heme synthesis, and has shown this potency across many cell lines, HeLA cells and mouse neuronal cells for example (Hooda 2013). Succinyl acetone (or SA) will be used to inhibit the heme synthesis pathway in initial experiments to show inhibition of heme synthesis is a viable treatment option for cancer.

1. 4. 0 Prostate cancer and Necroptosis

A therapeutic strategy targeting prostate cancer could cause death by a few potential mechanisms, namely apoptosis, necrosis or necroptosis (outlined in sections 1. 4. 1 and 1. 4. 2). The method of prostate cancer cell death could have major therapeutic implications. Characterisation of programmed necrosis mechanisms, like necroptosis, could provide targets to minimise inflammation reducing tissue damage in diseases such as atherosclerosis, pancreatitis or inflammatory bowel disease (Linkermann and Green 2014). This could be done by therapeutically interrupting or promoting necroptosis. Or, in the case of this study, the stimulation of necroptosis within cancer cells could be useful for those resistant to apoptosis. Necroptosis has a benefit over apoptosis in that apoptosis contains its immunogenic proteins within the dead cell whereas necroptosis can initiate an immune response by other healthy cells (Linkermann and Green 2014). Upon recruiting these healthy cells there will be an immune response towards the cancer cells already targeted (Galluzzi and Kroemer 2008) enhancing tumour death. TNF related apoptosis inducing ligand (TRAIL) is an important inducer of apoptosis within cancer cells and can mediate tumour immune surveillance i.e. the healthy

immune system monitors and kills cancer cells before tumour can cause harm (Jouan-Lanhouet et al., 2012).

1. 4. 1 Mechanisms of cell death

Necrosis has been defined as a form of cell death from the mid-19th century and was known to be a consequence of disease. Apoptosis was defined a century later and is now understood as the primary form of programmed cell death driven by a pathway of molecular mechanisms in advanced/developed animals (Linkermann and Green 2014). It was first assumed that necrosis was different from apoptosis in that it appears to be an unregulated form of cell death observed in reaction to stress, that it does not display an ordered death that was programmed by molecular events, unlike what is seen in apoptosis. However, it was eventually found that in certain settings there is a cell mediated, programmed type of necrosis (Hitomi et al., 2008).

There are many forms of evidence that show necrosis can be a form of programmed cell death in its mechanism and in its incidence (Hitomi et al., 2008). Studies have found that regulated necrosis has been involved in embryonic development and tissue homeostasis. It can be induced by ligands binding to membrane receptors and it is regulated by many genetic or epigenetic factors (Golstein and Kroemer 2007; Galluzzi and Kroemer 2008).

A form of programmed necrosis has been termed “necroptosis” (Galluzzi and Kroemer 2008). Apoptosis has distinct morphological characteristics such as nuclear fragmentation, membrane blebbing, chromatin condensation and formation of apoptotic bodies. Necroptosis has the morphological features of unprogrammed cell death like cellular swelling and rupture. The rupture causes a release of the cell contents which triggers an immune response (Pasparakis and Vandenabeele 2015). DAMPs or damage related pattern molecules, such as mitochondrial DNA and HMGB1 or nuclear high mobility group box-1 protein, are recognised in the blood by immune cells (Pasparakis and Vandenabeele 2015) making necroptosis an inflammatory form of cell death.

1. 4. 2 Necroptosis pathway

During apoptotic cell death, caspase proteases are activated causing the morphological features of apoptosis sequentially causing cell death. Whereas Receptor Interacting Protein Kinases 1 and 3 (RIPK1 and 3) initiate necroptosis. Necroptosis requires the activity of these RIPKs and the ligation of Tumour Necrosis Factor Receptor (TNFR) by Tumour Necrosis Factor (TNF) (Galluzzi and Kroemer 2008). TNF is the initial trigger to necroptosis, along with the involvement of pan-caspase inhibitors. TNFR1, antigen receptors and toll-like receptors can trigger necroptosis by the inhibition of caspase-8, together with the cell expression of RIPK3 and its substrate; mixed linkage domain like (MLKL). This works to inhibit apoptosis at the same time as activating necroptosis (Linkermann and Green 2014).

TNF receptor 1 activation of necroptosis is the most studied program of necroptosis (Figure 4) Ligation of TNFR1 by TNF induced the formation of a receptor-proximal complex including RIPK1 (described as complex 1 in the Figure). Ubiquitination and phosphorylation events within this complex of RIPK1 and NEMO (NF-kB essential modulator) lead to activation of the NF (nuclear factor) -kB transcriptional program or MAP kinase activation (Orozco et al., 2014). RIPK1 is deubiquitinated and becomes able to translocate to the cytosol where it can form the necrosome. The necrosome supports and scaffolds RIPK3 activation via deubiquitylation. Once RIPK3 has been deubiquitinated by ubiquitinases it no longer has pro-survival functions and is able to promote cell death by phosphorylating MLKL (Yoon et al., 2017).

Some structural studies have shown that RIPK3 activation via RIPK1 within the necrosome involves formation of oligomers. These oligomers are formed by interactions between domains that are present on both the RIPK proteins 1 and 3. This domain has been termed RHIM (or RIP homotypic interaction motif) (Orozco et al., 2014). RIPK1 can inhibit and promote the oligomerization of RIPK3 and necroptosis. RIPK1 contributes to the TNF regulated activation of RIPK3, however, RIPK1 would normally repress spontaneous RIPK3 oligomerization in the cytosol. Cells that have no RIPK1 have increased RIPK3 dependant death via spontaneous oligomerization of accumulated RIPK3. However

inhibited or inactivated RIPK1 within cells still protect the cell from RIPK3 cell necroptosis. This data suggests that RIPK1 activates RIPK3 in response to TNF signalling but that without that signal it acts as a regulator of RIPK3 (Orozco et al., 2014).

The formation and regulation of RIPK1 and RIPK3 necrosome complex is still under investigation. There is ongoing research into whether RIPK3 oligomerisation or RHIM amyloid formation or both together are sufficient or necessary for RIPK3 to be activated. Some studies have shown that chemically forced oligomerization of RIPK3 is enough to induce necroptosis without the RHIM domain, RIPK1 activity or stimulation by TNF (Orozco et al., 2014). The idea that necroptosis is dependent on RIPK1 and RIPK3 activation by TNF1 was supported by one study (Newton et al., 2014) looking into how the activity of RIPK3 can determine whether a cell dies via necroptosis or apoptosis. It was found that the introduction of wildtype RIPK3 can cause necroptosis again in RIPK3 deficient cells but not inactivated RIPK3 mutant, showing that the kinase activity of the RIPK3 is crucial for necroptosis initiation (Newton et al., 2014).

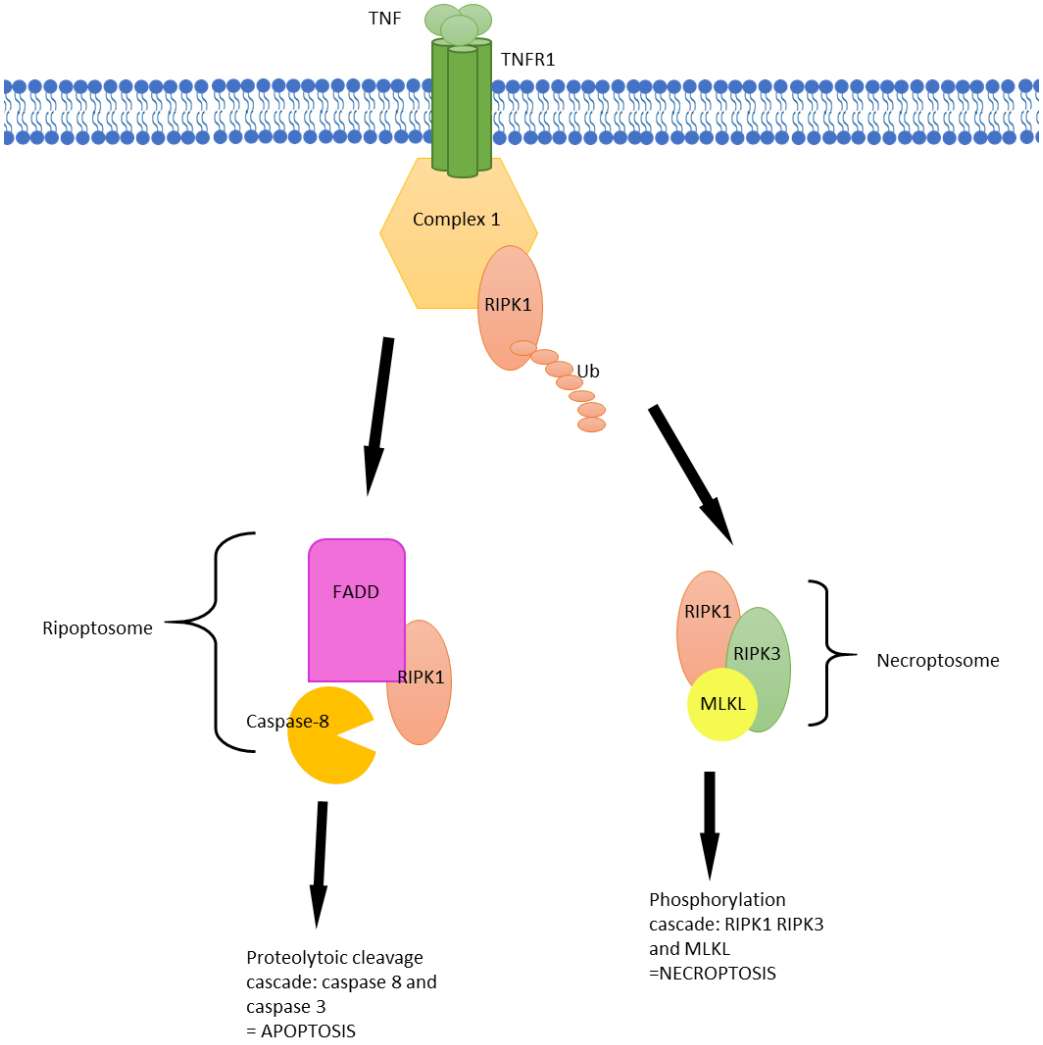

Figure 4 Diagram depicting the initiation of the signalling pathways of apoptosis (left) and necroptosis (right).

1. 5. 0. Hypothesis and aims

Hypothesis

Targeting heme synthesis is a novel therapeutic approach to inhibit prostate cancer growth.

Aims

1, to investigate the effect of porphyrin synthesis inhibition upon prostate cancer proliferation

2, to identify co-therapies to enhance the specificity and efficacy of porphyrin synthesis inhibition

3, to investigate the method in which prostate cancer cells die when porphyrin synthesis is inhibited

4, to clone, express and purify ALAS1 and ALAS2 using a bacterial expression system

2. 0 Methods

2. 1.0 Tissue culture methods

2. 1.1 General tissue culture

PC3, LNCaP and DU145 cells were obtained from ATCC. Cell lines were maintained in RPMI 1640 enriched with 10 % FBS (foetal bovine serum) and PSG (Penicillin Streptomycin-Glutamine). Standard sterile tissue culture techniques were used for cell culture and the cells were stored at 37 °C, humidified and with 5 % CO_2.

2. 1. 2 Passaging of mammalian cells

Cells were split each time they reached a confluency of approximately 70-80 %. Excess media was aspirated, and the cells were washed with 5 ml PBS for a few minutes (PBS containing 8 g NaCl, 0.2 g KCl, 1.44 g Na_2HPO_4 in to 1 L of ddH_2O, pH of 7.4 with HCl). PBS was removed, 0.25 ml of trypsin was added, and the cells were incubated at 37 °C for a few minutes until they had detached. The reaction was stopped by the addition of 10 ml media. The cells were resuspended into a single cell suspension by pipetting up and down. 1 ml of the resuspended cells were transferred into a T25 flask containing 5 ml pre-warmed media.

2. 1. 3 Cell counting and seeding

Cells were resuspended in 10 ml of media and diluted 1:10 prior to counting. 10 µl of this dilution was placed in a haemocytometer and 10 squares of the grid were counted. The total number of cells per ml was subsequently calculated. The cells were diluted to allow for plating of the correct number of the required number of cells for the experimental design. For 96 well plates 2,000 cells were plated per well, 12 well plates 20,000 cells per well and 6 well plates 200,000 per well.

2. 2 Crystal Violet Proliferation assays

2. 2. 1 Treatment with Succinyl acetone

2,000 cells were seeded per well and incubated overnight prior to treatment. Cells were treated with a dose range of 0-2 M SA (0-2 M) ± X 10 µM heme ± 0-1 M MK2206/A-1155463. Cells were left for 6 days prior to fixation with 100 µL of 4 % PFA (paraformaldehyde). Plates were incubated at room temperature for an hour. The PFA was removed and the plates were washed with ddH_2O three times and air dried. 50 µl of 0.04 % crystal violet (dissolved in PBS) was added to each well and incubated at room temperature for an hour. After this the plates were washed 3 times with ddH_2O and air dried. 100 µl of 10 % acetic acid was added to each well and left shaking at room temperature for an hour before the absorbance (490 nm) was read on an Omega plate reader.

2. 2. 2 Cotreatments

2,000 cells were added per well in a 96 well plate and the surrounding wells were filled with 100 µl of PBS to ensure humidity. The plate was incubated overnight at 37 °C prior to treatment with 0 - 1 mM MK2206 and A-1155463. Half of the cells were also co-treated with 200 µM of SA.

2. 2. 3 Measuring cellular heme content

200,000 cells were seeded per well (6 well plates) and incubated overnight prior to treatment. Cells were treated with a dose range of 0-2 M SA (0-2 M). Cells were left for 6 days prior to harvesting.

Cells were harvested from the plates and the heme content was normalised to total protein count. The protocol by Sinclair et al. (2001) was followed for heme content analysis. Pellets were resuspended in 2 M oxalic acid and kept at 100 °C. 200 µl of each sample was transferred to a white-

walled 96 well plate. An excitation of 400 nm and 662 nm emission was used to measure the fluorescence of porphyrin using a CLARIOstar (BMG LABTECH, UK) plate reader.

2. 2. 4 Quantification of *TNF-α* expression at the RNA level

200,000 cells were seeded per well and incubated overnight prior to treatment with 0-2 M SA. Cells were left for 6 days prior to harvesting. Cells were washed with PBS and collected with a cell scraper. The cells were transferred to 1.5 ml Eppendorf tubes before being centrifuged at 4 °C, 5000 rpm for 5 minutes and the PBS aspirated. During RNA extraction, filter tips and sterile techniques were used to avoid contamination. The cells were lysed in 500 µl of Trizol reagent and incubated for 5 minutes at room temperature. 80 µl of chloroform was added, the cells were mixed by hand and then incubated overnight (24 hours) at -80 °C. The cells were defrosted gradually at room temperature before being centrifuged at 12,000 g 4 °C for 15 minutes. The top aqueous layer was transferred to a new tube containing 1 µl of GlycoBlue and 200 µl of isopropanol was added. The tubes were inverted to mix and incubated again for 5 minutes at room temperature. The tubes were centrifuged at 12,000 g, 4 °C for 10 minutes and the supernatant removed. 400 µl of 75 % ethanol was then used with vortexing to wash the cells before the cells were centrifuged again at 7500 g 4 °C 10 minutes and the supernatant removed. The ethanol wash and centrifugation were repeated before the final ethanol wash was removed and the cells were air dried at room temperature. The dry pellets were resuspended in 30 µl of RNAse-free ddH_2O and incubated at 55 – 60 °C for 10-15 minutes. A NanoDrop® ND-1000 UV/VIS Spectrophotometer (Nanodrop, Thermo Scientific) was used to measure the concentration of RNA in each of the samples.

250 ng RNA was reversed transcribed to make cDNA using the Luna kit (NEB), according to manufacturer's instructions. The reverse transcription was carried out using a T100 Thermal Cycler (Bio-Rad). qPCR was performed using primers specific for *TNF-α* and *L19* (Table 1) was used for normalisation on a Roche LighCycler machine. qPCR data was analysed using the $2^{-\Delta\Delta Ct}$ method.

Table 1: qPCR primers used for gene expression analysis.

Primer	Sequence
TNF-α_F	5’-CTCTTCTGCCTGCTGCACTTTG -3’
TNF-α_R	5’-ATGGGCTACAGGCTTGTCACTC-3’
L19_F	5’-GCAGCCGGCGCAAA-3’
L19_R	5’-GCGGAAGGGTACAGCCAAT-3’

2. 2. 5 TNF-α ELISA

200,000 cells were seeded per well and incubated overnight prior to treatment with ± 200 µM SA. Cells were left for 6 days prior to harvesting. The ELISA was carried out on the supernatant which was collected and concentrated by centrifugation in centrifugal filter units (Millipore). The supernatant was then filtered via a syringe filter or left unfiltered for the ELISA.

The Human Quantikine ELISA Kit (R&D Systems) was used, following the manufacturer's instructions, to measure TNF-α expression. All reagents were brought to room temperature before use. 50 µl of assay diluent was added to each well of the test plate before the addition of 200 µl of standards, sample or control. The wells were then covered with an adhesive strip and incubated at room temperature for 2 hours. Each well was aspirated to remove the liquid and washed with 400 µl of wash buffer 4 times. After removal of the final wash 200 µl of TNF-α conjugate was added to each well, covered with a new adhesive strip and incubated either at 1-hour room. The aspiration and washes were repeated, 200 µl of substrate solution added to each well and the plate incubated for 20 minutes at room temperature protected from the light. 50 µl of stop solution was added to each well and within 30 minutes the optical density of the samples was determined using a microplate reader at 450 nm.

2. 3 Flow cytometry

2. 3. 1 PI Inclusion Assay

DU145, DU145 FADD knock-out (kind gift from Andrea Mohr, University of Essex) were seeded in 12 well plates. Cells were treated ± SA (200 mM), Necrostatin (40 mM), Ferrostatin (10 nM), Z-VAD (20 µM) 24 hours after cells had been seeded. H_2O_2 (200 µM) was added after 5 days and the cells incubated for 24 hours. The media was collected, and the cells were washed with PBS, which was also

collected. The cells were detached through the addition of 100 µl of trypsin before incubation at 37 °C for 3 minutes. The cells were subsequently collected and transferred to the tube containing the media and PBS. 10 µl of propidium iodide (PI) was added and the % PI positive cells were quantified using flow cytometry (Accuri C6).

2. 3. 2 DNA hypodiploidy assay

Cells were seeded, treated and harvested as for the PI inclusion assay and were pelleted by centrifugation at 5000 rpm for 2 minutes. The liquid was aspirated, and the pellet resuspended in 200 µl of Nicoletti buffer. Nicoletti buffer contained 10 g sodium citrate, 10 ml of Triton X-100 diluted in 1 L of ddH_2O. 10 µl of PI was added per ml of nicoletti buffer prior to use. The % of cells undergoing apoptosis were quantified using flow cytometry (Accuri C6).

2. 4 Protein Expression methods

2. 4. 1 LB Agar Plates, LB Media and SOC Media

Luria broth (LB from Sigma) was made by dissolving 10 g of LB broth powder in 500 ml of ddH_2O before being autoclaved. LB agar was made with 35 g of LB agar dissolved into 1 L of ddH_2O. The stock was autoclaved and warmed in a microwave before the necessary antibiotics were added. The mixture was poured into plates and left to set before use. Super optimal broth with catabolite repression medium (SOC) contains 0.5 % yeast extract, 2 % tryptone, 10 mM NaCl, 10 mM $MgSO_4$, 2.5 mM KCl, 20 mM glucose diluted with ddH_2O up to 1 L.

2. 4. 2 Antibiotics

0.1 g of ampicillin was dissolved in 1 ml of ddH_2O to give a stock concentration of 100 mg ml^{-1}. A further 1:1000 dilution in media gave a working concentration of 100 µg ml^{-1} for each growth. Kanamycin was used at a final concentration of 50 µg ml^{-1}. A stock concentration of 50 mg ml^{-1} was made up of 0.5 g kanamycin dissolved in 1 ml ddH_2O.

2. 4. 3 Protein expression in bacteria

A starter culture was made from a single bacterial colony, of BL-21, Rosetta, pGro7 cells containing both the pet28a ALAS 2 T and ALAS 1 T plasmids (appendix figures 2 and 3), BL-21 cells containing the pet28a ALAS1-$T_{C108S,}$ pet28a-ALAS1-197, pet21aALAS1-T, pet21a-ALAS1-197 plasmids (appendix figures 5, 6 and 7) and T7 shuffle cells containing pet28a-ALAS1-197, pet21aALAS1-T, pet21a-ALAS1-197 plasmids. The single colony was picked from a transformation (section 2. 6. 3) and placed in 10 ml LB (containing the appropriate antibiotic) The culture was left to shake at 37 °C overnight. 1 ml of the starter culture was removed and stored for SDS-PAGE analysis as described in 2.5.1- 2.5.2. Auto induction media (AIM) was prepared by dissolving 34.85 g AIM in 1 L ddH_2O. 5 ml of glycerol was added prior to sterilisation by autoclaving. The appropriate antibiotic was added immediately before use (Kanamycin for pet28a vectors and ampicillin for pet21a vector). The remaining starter culture was added to 1 L of the AIM media and shaken in a Brunswick scientific innova.43 incubator for 1.5 hours at 37 °C, after which the temperature was lowered to 20 °C overnight. 0.5 mg/ml of arabinose was added to the pGro7 cultures containing the pet28a ALAS1 T plasmid to induce chaperone expression.

1 ml of the overnight culture was removed and stored for SDS-PAGE analysis as described in 2.5.1-2.5.2. The rest of the culture was centrifuged at 4000 rpm for 15 minutes at 4 °C. The supernatant was removed, and the remaining pellet resuspended in 50 ml lysis buffer (Table 2). The lysate was

subsequently passed through an Emulsiflex for a minimum of 3 times – maximum of 5 times if the mixture was still too viscus. The resulting lysed cells were centrifuged at 17,000 rpm for 45 minutes at 4 °C and the supernatant transferred to a fresh tube. A sample of the supernatant was taken for SDS-PAGE analysis.

2. 4. 4 Protein purification

To equilibrate the HisTrap excel column, 10 ml of lysis buffer (Table 2) was passed through it. The sample was then ran through the column followed by a wash with 50 ml wash buffer. The purified protein was eluted in 20 ml wash buffer with 300 mM imidazole added. The eluted sample was visualised using SDS-PAGE. The wash buffer used followed the same recipe as the lysis buffer outlined in Table 2 but without the addition of the DNAse.

Table 2: Protein expression lysis buffer recipe:

Component	Final concentration
tris pH7.5/8	50 mM
NaCl	500 mM
Beta mecaptoethanol	5 mM
glycerol	5 %
EDTA	0.5 mM
Triton	0.05 mM
DNAse	5 µl, 2 ng ml^{-1}

2. 5. Protein separation analysis

2. 5. 1 Preparation of samples for SDS-PAGE analysis

Cell pellets were resuspended in 30 µl of PBS and 6 µl of 6X loading dye. This was then stored at -20 °C if the samples were not to be used immediately for analysis. Once ready for use the samples were boiled for 30 minutes at 85 °C and then kept on ice until gel loading.

2. 5. 2 SDS polyacrylamide gel electrophoresis

The BioRad MiniProtean SDS PAGE system was used for gel electrophoresis. 10 % acrylamide gels were made using (per gel) 1.65 ml of acrylamide, 1.88 ml of 1 M Tris- HCl pH 8.9 and 1.9 ml ddH_2O, 50 µl of 10 % SDS, 50 µl of 10 % APS. 5 µl TEMED (Tetramethyl ethylenediamine) was added immediately before pouring. The stacking gel was made up of 0.425 ml acrylamide, 0.62 ml 1 M Tris-HCl pH 6.8, 1.1 ml of ddH_2O, 50 µl of 10 % SDS and 50 µl 10 % APS. 2.55 µl of TEMED was added immediately before pouring.

The gel was prepared by pouring 4.5 ml of 10 % acrylamide gel between two glass plates and topped with butanol to ensure that the top of the gel set flat. Once set the butanol was poured off and the top of the gel cleaned with ddH_2O before the stacking buffer and comb was added.

30 µl of the protein sample mixtures were loaded alongside 5 µl of PageRulerTM Plus Prestained Protein Ladder (Bio-Rad). The whole gel was placed within 1 X running buffer and ran at 125 V for 2 hours. A 10x running buffer solution was made up of 144 g glycine, 30.3 g of Tris, 100 ml of 10 % SDS diluted in 1 L of ddH_2O. The 1x running buffer was made up from 100 ml of the 10x running buffer diluted in ddH_2O to make 1 L.

2. 5. 3 Coomassie stain

The stain was made by dissolving 0.25 g of Coomassie brilliant blue R-250 in 45 ml methanol, 45 ml ddH_2O and 10 ml of glacial acetic acid. The solution was filtered and stored at room temperature. Destain was made up from 50 ml H_2O, 40 ml methanol and 10 ml glacial acetic acid.

The gel was covered in Coomassie blue stain, ensuring that it was completely covered, and then heated in a microwave for 10 seconds. The blot was incubated at room temperature for 1 hour. The stain was removed and replaced with destain and left rocking at room temperature overnight before it was photographed.

2. 5. 4 Immunoblotting

Transfer buffer was made from 22.52 g of glycine, 400 ml of methanol and 4.88 g of Tris and diluted in ddH_2O to make 2 L. Polyvinylidene fluoride (PVDF) membrane (Millipore) was activated with methanol and washed with transfer buffer. This was then sandwiched with the SDS-PAGE within two pieces of immunoblotting paper that was soaked in transfer buffer. The proteins were transferred to the PVDF membrane at 15 mA, 100 V for two hours using a semi-dry electro blotting machine (Bio-Rad).

The membranes were blocked with 5 % Milk PBS-0.1 % Tween for 30 minutes. The milk block was removed from the membrane and the primary antibody 6 X HIS – antibody 1:10,000 (abcam) was added and left to incubate over night at 4 °C or for one hour at room temperature (with continuous shaking). The antibody was removed, and the membrane washed with PBS-0.1 % Tween 4 times before a second 5 % milk PBS-T block was carried out for 15 minutes. Secondary antibody (goat anti-mouse HRP, 1:2000) was added to the block and the membrane was left to incubate for 1 hour at room temperature. The secondary antibody was removed, and the membrane washed 4 times before

a final wash of PBS. The bands on the gel were visualised using LuminataTM Forte Western HRP Substrate (Millipore) on a Fusion FX (VILBER LOURMAT).

2. 6. Cloning and transformations

2. 6. 1 Sanger sequencing

Nucleotide sequencing was carried out by EUROFINS and visualised using SnapGene.

2. 6. 2 Site Directed Quick Change Mutagenesis

Primers (described in Table 3) were diluted to 75 ng μl^{-1} and template DNA to ~ 15-20 ng μl^{-1}. The site directed mutagenesis reaction is provided in Table 4 and was performed using the cycling conditions described in Table 5. After the amplification, 1 µl of *Dpn*1 was added to the mixture. The reaction was mixed and centrifuges (13,000 rpm for 1 minute) and incubated at 37 ^{o}C for 1 h.

Table 3: Primers for quick change mutagenesis reaction	
Primer name	**Sequence**
cys108_F	5’-CCAGGAAAGGGTTTTGCTTGCAGTGCCCTG-3’
cys108_R	5’-CAGGGCACTGCAAGCAAAAGCCCTTTCCTGG-3’

Table 4: Components of site directed mutagenesis reaction mix	
Component	**Volume µl**
ddH_2O	21.1
10XPFU Ultra (aligent)	3
DMSO	1.8
dNTP 10 Mm	0.6
DNA template	1
PFU Tubo Hotstart DNA polymerase	0.5
Primer F	1
Primer R	1
Total volume	**30**

Table 5: Cycling conditions of site directed mutagenesis reaction. 15 cycles were carried out		
Step	**Time minutes**	**Temperature °C**
Initial denaturation	2:00	95
Denaturation	0:50	95
Anneal	1:00	55
Extention	13:00	68
hold	∞	12

2. 6. 3 Transforming into competent cells and propagation.

50 µl of competent cells (Rosetta, BL-21, T7 shuffle and pGro7) were defrosted on ice and 20 ng of the DNA template was added to the cells and mixed before being incubated on ice for 30 min. Cells were heat shocked at 42 °C for 45 sec and the cells placed in ice for 2 minutes. 450 µl of SOC growth media (2. 4. 1) was added and the cells incubated at 37 °C for 1 hour with shaking. The cells were centrifuged for 2 minutes at 4000 rpm, 450 µl of the supernatant was discarded and the pellet resuspended in the remaining liquid. The culture was spread onto LB agar plates (2. 4. 1) containing the appropriate antibiotic and incubated at 37 °C for 18 hours. Colonies were picked and grown in 5 ml LB media overnight (18 hours) at 37 ºC.

2. 6. 4 Preparation of competent cells

1 colony picked from a plate was grown in 10 ml LB media overnight at 37 ºC. 8 ml of the 10 ml culture was then added to 400 ml LB media with no antibiotics added. This was left to grow at 37 ºC until OD590 reached 0.4-0.5. 50 ml aliquots were then taken and added to pre-chilled bottles which were further incubated on ice for 5-10 minutes.

The cells were centrifuged at 4000 g at 4 ºC for 15 minutes. After removal of the supernatant the pellet was resuspended in 10 ml ice cold $CaCl_2$ solution (Table 6) and centrifuged again at 4000 g 4 ºC 15 minutes. The pellet was resuspended in ice cold $CaCl_2$ solution before being left on ice for 30 minutes. The samples were centrifuged as before and the pellet resuspended in 2 ml ice cold $CaCl_2$. The resulting solution was aliquoted and frozen at -80 ºC.

Table 6: $CaCl_2$ solution recipe for competent cell preparation. components were gently mixed before filter sterilisation.

Component	Concentration used
$CaCl_2$	60 mM
Glycerol	15 %
PIPES	10 mM
KOH	Ph 7.0

2. 6. 5 Mini Prep

3 ml of liquid culture was used to obtain plasmid DNA. The DNA was extracted using the Monarch miniprep kit (Sigma Aldrich), following the manufacturer's instructions. The bacteria were pelleted by brief centrifugation at 13,000 rpm. The pellet was resuspended in resuspension buffer and lysis buffer added and incubated for 1 minute before neutralization buffer was added and a further 2-minute incubation. The cellular debris were pelleted, and the supernatant applied to the column before being washed and the final DNA eluted with 30 µl ddH_2O.

2. 6. 6 Restriction enzyme digests

1 µg of DNA was digested with 2 µl of the required restriction enzymes (Table 7). Reactions were incubated at 37 °C for 30 min.

Table 7: Restriction enzymes used for each digest reaction	
Reaction	**Enzyme used**
ALAS1 p28 a 197 fragment digest	*NheI* and *HindIII*
ALAS1 p21 a 197 fragment digest	*NheI* and *HindIII*
ALAS1 p21 a T fragment digest	*NheI* and *HindIII*
ALAS1 and ALAS2 plasmid digest	*BglII*
Fragment analytic digest	*NheI* and *HindIII*

2. 6. 7 Agarose gel electrophoresis

1 % agarose gels were prepared by dissolving 0.75 g of agarose in 75 ml TAE (or tris acetic acid EDTA buffer, 40 mM Tris acetate base, 1.114 ml of glacial acetic acid and 1 mM EDTA diluted into a total of 1 L ddH_2O) in a microwave at small intervals at a medium power until boiling and all the agarose had dissolved. Once the mixture cooled enough to touch 3 µl ethidium bromide or 0.75 µl of SYBR safe was added to the gel mixture. This was then poured into the gel rigs. 10x DNA loading dye was added to each sample and a ladder was run by the side of the samples. 10 µl of Thermo Scientific GeneRuler DNA Ladder mix at a concentration of 0.1 µg $µl^{-1}$ was used for this. 20-50 µl of sample was added to the wells and the gels were run for approximately 1 hour and 30 minutes at 80 V. Images of the gels were taken using the BioRad Gel Doc™ EZ Imaging System.

2. 6. 8 DNA extraction

The gels were viewed with ultraviolet light to make the bands visible and then physically cut out using a sterile scalpel. The DNA was extracted from the gel using an RBC Real genomics HiYield Gel/PCR fragments Extraction Kit. The slice of gel containing the DNA was dissolved in 500 µl of DF buffer and incubated at 55 ºC for 10 minutes. This was spun on the DF column at 10,000 xg followed by a wash and another centrifugation to dry. The final extracted DNA was eluted in 20 µl ddH_2O for 2 minutes at full speed.

2. 6. 9 DNA purification

The DNA was cleaned using a Monarch PCR & DNA clean-up kit. The sample was diluted in DNA clean-up buffer and centrifuged at 13,000 rpm for 1 minute, wash buffer added and the sample re-spun. The purified DNA was eluted in 6 µl ddH_2O spun for 1 minute at full speed.

2. 6. 10 PCR

Primers were supplied by Eurofins MWG in a freeze-dried form. These were diluted to 10 µM with ddH_2O. PCR reactions are described in in the Tables below (Tables 8, 9 and 10).

Table 8: Initial PCR reaction volumes for amplification of ALAS 1 fragments	
Components of PCR reaction	**Volume/ concentration required**
ALAS 1 WT template	20 ng µl
Forward primer	1 µM
Reverse primer	1 µM
REDTaq	25 µl
Distilled water	20
Total volume	50 µl

Table 9: PCR reaction conditions, showing number of cycles for each step, temperature and time.

PCR Step	Number of cycles	Temperature (°C)	Time (minutes)
Initial Denaturation	1	94	1
Denaturation	35	94	1
Annealing	35	55	2
Elongation	35	72	2
Final Elongation	1	72	10

Table 10: Primers used for each PCR reaction	
Primer name	**Sequence**
pET 28a ALAS1 197_F	5’-GCTAGCTTTCAGTATGATCGTTTCTTTGAG-3’
pET 28a ALAS1 197_R	5’-CCCAAGCTTGGGTCAGGCCTGAGCAGATACCAACT-3’
pET 21a ALAS1 197_F	5’-GCTAGCATGTTTCAGTATGATCGTTTCTTTGAG-3’
pET 21a ALAS1 197 &T_R	5’-CCCAAGCTTGGGGGCCTGAGCAGATACCAACT-3’
pET 21a ALAS1-T_F	5’-GCTAGCATGGCAGAGCAGTACACTACCAACAG-3’

2. 6. 11 Ligations of ALAS 1 truncation into pET21a and pET28a vectors

The insert and the plasmid were digested and cleaned using method in 2. 6. 9. FastAP Thermosensitive Alkaline Phosphatase (Thermo Fisher) was carried out on the pET vectors. 1X Thermo Scientific™ FastAP™ reaction buffer, 0.1 - 0.2 mg/mL of the phosphoprotein, 10 µl of FastAP Thermosensitive Alkaline Phosphatase was incubated at 37 °C for 1 hour. The inserts were ligated into the plasmids pET21a and pET28a using a Rapid Ligation Kit (Thermo Fisher). The components of the reaction are listed below in Table 11. The components were mixed and then incubated at 22 ºC for 10 minutes.

Table 11: Reaction volumes for ligation of the new ALAS constructs into different vectors.	
Components of ligation reaction	Volume/ concentration required
Plasmid (pET21a/pET28a)	50 ng µl
10x Buffer	2 µl
Insert DNA	0.5 µl
Ligase	0.2 µl
Distilled water	To make total volume
Total volume	**20 µl**

3. Chapter 3 results – Investigating heme synthesis as a viable treatment option for prostate cancer and mechanism of cell death caused.

3. 1. Targeting heme synthesis pathway

3. 1.1 The prostate cancer cell lines used in the study

PC3, DU145 and LNCaP cells were used for the following experiments. PC3 cells are representative of castrate resistant disease and were derived from bone metastases. The cells have the characteristics of prostatic small cell carcinoma. LNCaP cells were derived from metastatic lymph nodes and share characteristics with adenocarcinoma. They are sensitive to hormone treatment; it has been shown that they express androgen receptor (AR) and Prostate-specific antigen (PSA). DU145 cells provide a model of castration resistant prostate cancer that was originally a derivative of a central nervous system metastasis (Tai et al., 2011). These cells lines were used to represent multiple types of prostate cancer cells including fast growing and less aggressive forms of cancer and to also allow for analysis of both androgen dependant and androgen independent (castration resistant) cancer forms.

3. 1.2 Succinyl acetone inhibits prostate cancer growth

Heme synthesis has been identified as a potential novel therapeutic target for prostate cancer. To investigate this, the effect of the ALAD (the second step in heme synthesis) inhibitor succinyl acetone (SA) upon cell growth was quantified. Different prostate cancer cell lines were treated with 0 – 2 M SA and the effect upon proliferation was measured using crystal violent staining. The absorbance was measured and used to determine relative growth for each cell line at each concentration of drug. The proliferation of PC3, DU145 and LNCaP was inhibited by SA (Figure 5). From the dose response curves, the IC_{50} values for SA across the cell lines could be calculated. DU145 appear to be the most sensitive to SA, having an IC_{50} value of 32.4 mM (Table 12).

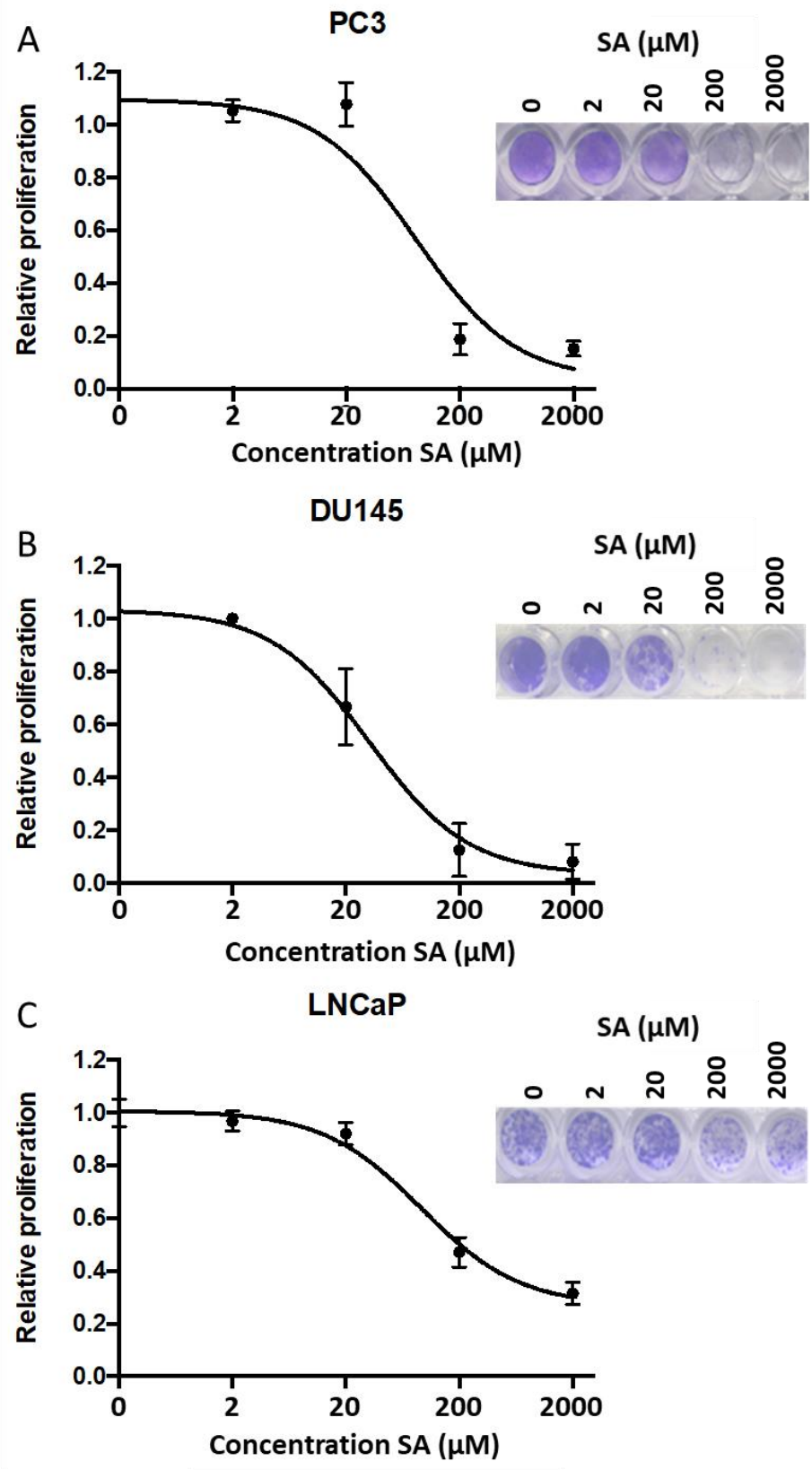

Figure 5 ***Succinyl acetone inhibits prostate cancer proliferation****. (A) PC3, (B) LNCAP and (C) DU145 were seeded in 96 well plates treated with 0 – 2000 µM SA for 7 days. Proliferation was quantified using crystal violet assays and normalised to the absorbance in the absence of SA. Mean of 3 independent repeats (6 replicates for each experiments) ± 1 SEM. Example crystal violet images of the plates are provided.*

Table 12: succinyl acetone inhibits prostate cancer proliferation. PC3, LNCaP and DU145 were seeded in 96 well plates treated with 0 – 2000 µM SA for 7 days. proliferation was quantified using crystal violet assays and normalized to the absorbance in the absence of SA. Mean of 3 independent repeats (6 replicates for each experiments) ± 1 SEM. IC_{50} values were calculated using graphpad prism.

Cell Line	IC_{50} (mM)
PC3	82.6
DU145	32.4
LNCaP	492.8

3. 1.3. Heme can reverse the inhibitory effects of succinyl acetone

To confirm that SA blocks proliferation via inhibition of heme synthesis, heme was added to the cells to see if the effect of the drug could be reversed. The prostate cell lines were treated in the same way as above ± heme. The cells were allowed to grow for 7 days and stained with crystal violet and relative growth calculated by measuring absorbance for each cell line at each concentration of drug, with and without the addition of heme. The proliferation of PC3, DU145 and LNCaP cells was inhibited by SA and this could be partially rescued by heme at 20 and 200 µM SA (Figure 6). Representative images of the crystal violet staining are also provided (Figure 6); here the inhibition in growth and partial heme rescue can be seen visually. This difference is most pronounced at 200 µM of SA treatment (Figure 6) showing the strongest rescue with heme. There appears to be no rescue at the highest concentration of SA (2 mM).

For comparison purposes, the heme rescue data for 200 µM SA was re-plotted separately (Figure 7). As described previously, SA inhibits the proliferation of all the cell lines but is most potent in DU145 cells which still has the lowest IC_{50} values with and without heme (Table 13). Heme was able to reverse the inhibitory effects of SA across all the cell lines at 200 µM SA as there significantly less growth inhibition in all three prostate cancer cell lines. The IC_{50} values also increased for all of the cell lines following the addition of heme (Table 13), demonstrating that heme can reduce the inhibitory action of SA.

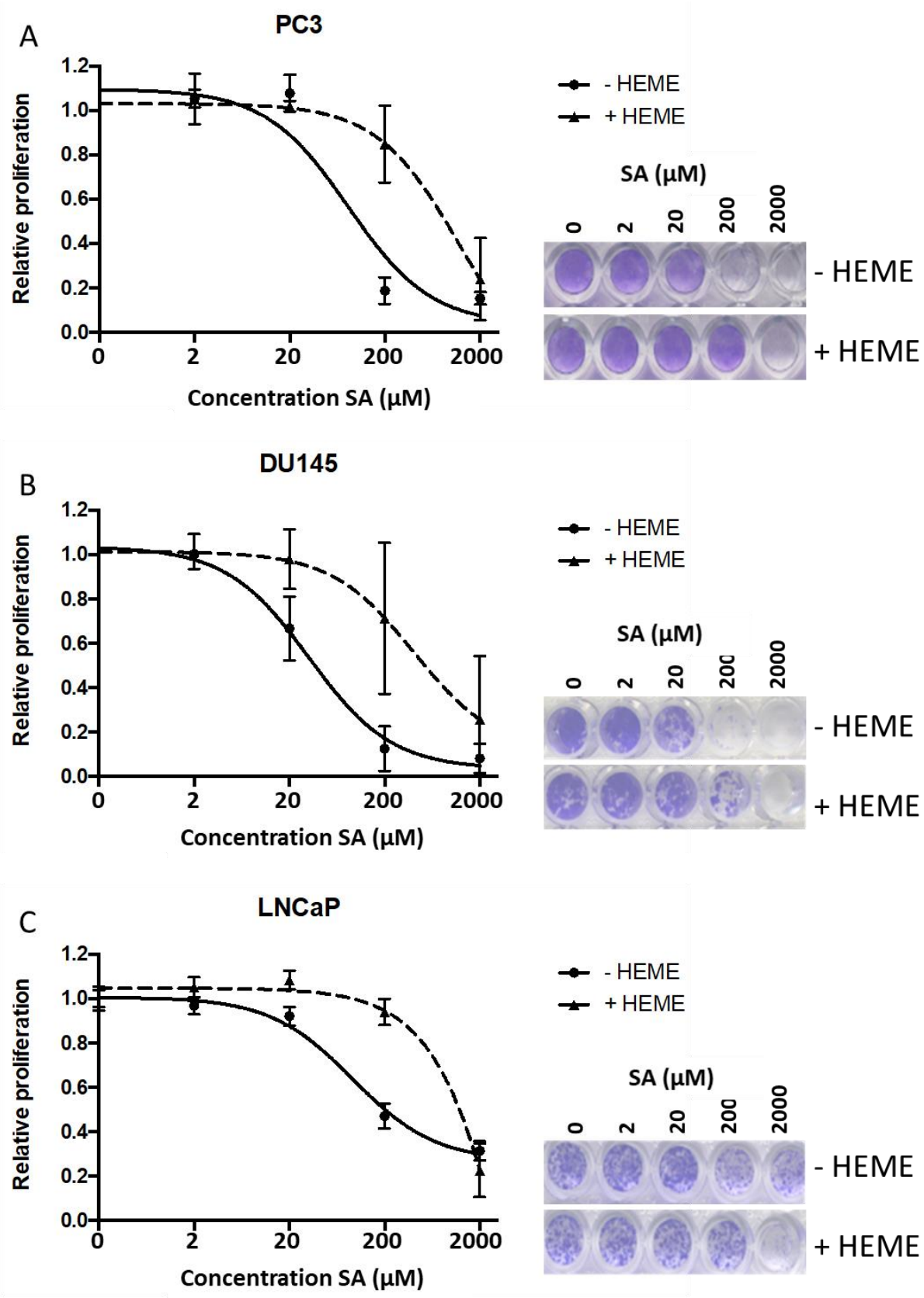

Figure 6 Prostate cancer proliferation is inhibited by succinyl acetone and rescued with the addition of heme *(A) DU145 (B) LNCAP (C) PC3 were seeded in 96 well plates, treated with 0 – 2000 µM SA and 10 µM heme for 7 days. Proliferation was quantified using crystal violet assays. Mean of 3 independent repeats (6 replicates for each experiments) ± 1 SEM. Representative images or the crystal violet staining are also provided.*

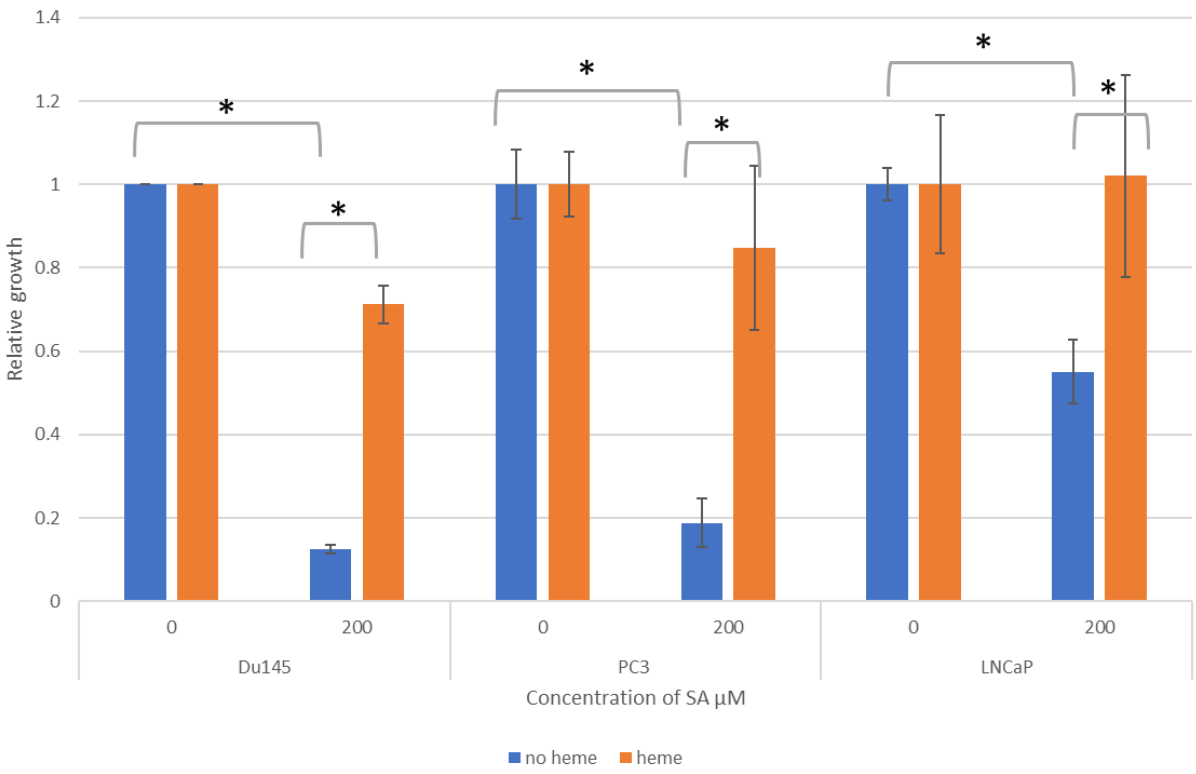

Figure 7 DU145, LNCaP and PC3 cell proliferation is inhibited by succinyl acetone and rescued by heme. *All cells were seeded in 96 well plates, treated with 0 – 2000 µM SA and 10 µM heme for 7 days and proliferation quantified using crystal violet assays. Mean of 3 independent repeats (6 replicates for each experiments) ± 1 SEM. ANOVA * p<0.05.*

Table 13: prostate cancer proliferation is inhibited by succinyl acetone and rescued with the addition of heme DU145, LNCaP PC3 all cells were seeded in 96 well plated, treated with 0 – 2000 µM SA and 10 µm heme for 7 days and proliferation quantified using crystal violet assays. Mean of 3 independent repeats (6 replicates for each experiments) ± 1 SEM. IC_{50} values were calculated using graphPad Prism.

	IC_{50} (mM)	
Cell Line	**- heme**	**+ heme**
PC3	82.6	1208.2
DU145	32.4	411.2
LNCaP	492.8	7343.8

3. 1. 4. Succinyl acetone depletes cellular heme content

In order to determine that SA inhibits the cells ability to produce heme to halt cell proliferation, the cellular heme content was determined by measurement of fluorescence of porphyrin. This was measured in cells that had been treated with differing concentrations of SA. A measurement of cellular heme content, normalised to total protein content, was taken after 7 days of growth. SA reduces the cellular heme content in PC3, DU145 and LNCaP cells at concentrations above 20 µM (Figure 8), although this was only found to be significant in DU145 and PC3 at the highest concentration tested. It therefore appears that SA inhibition of prostate cancer cell lines is as a result of the depletion of heme levels.

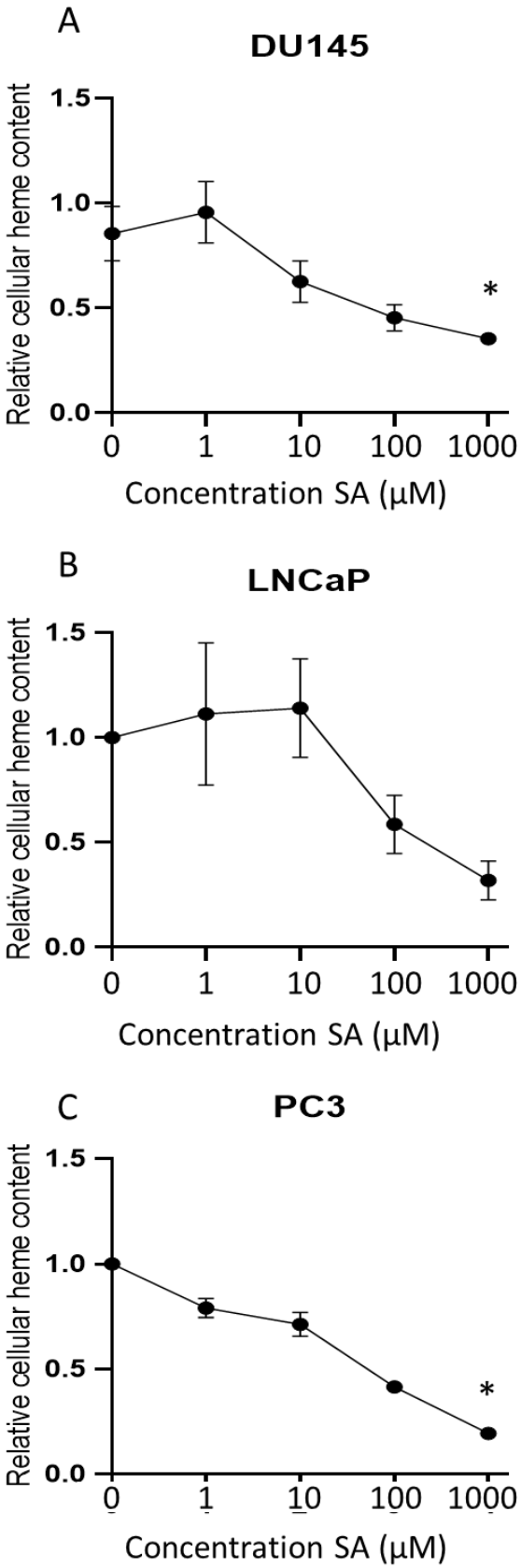

Figure 8 Cellular heme content is decreased by succinyl acetone treatment *(A) DU145 (B) LNCaP and (C) PC3 cells were seeded in 6 well plates, treated with 0 – 2000 µM SA for 7 days and heme content quantified by measurement of porphyrin fluorescence. Mean of 3 independent repeats ±1 SEM. ANOVA * p<0.05*

3. 1. 5. Effects of A-11554563 and MK2206 on cell growth in cotreatment with SA.

The drugs A-11554563 and MK2206 have been shown, alongside several anticancer agents, to synergistically inhibit cancer cell proliferation in various cell lines (Jong et al., 2018; Hirai et al., 2010; Narayan et al., 2017). These studies had shown a stronger tumour inhibition action than individual drugs when cells were treated with monotherapy.

A-1155463 is a selective inhibitor of BCL-XL proteins (abcam). BCL-XL is a member of the BCL-2 family. The BCL-2 family are a group of proteins that regulate apoptosis and can act as anti or pro-apoptotic regulators (NCBI BCL2L1). Cancer cells commonly increase expression of anti-apoptotic proteins like BCL-2 to make caspase activation more difficult and halting cell death. A-1155463 inhibits this pathway by binding and neutralizing BCL-XL members of the BCL-2 family that are pro-survival and inducing apoptosis via release of BAX and BAK proteins. BCL-XL over expression has been found to be involved in PC3 resistance to treatment-induced apoptosis. Apoptosis can be re-established in these PC3 cells when a BCL-XL is inhibited (Castilla et al., 2006). Over expression of BCL-XL in LNCaP cells protected them from the apoptosis induction. High levels of expression of BCL-XL made both PC3 cells and LNCaP cells resistant to this method of apoptosis induction (Shiau et al, 2006) making A-1155463 an attractive possibility for further increasing the effect of SA on LNCaP and PC3 cells.

MK2206 is an AKT inhibitor that allosterically inhibits a serine/threonine protein kinase within the P13K/AKT signalling pathway. This pathway promotes cell survival and growth. An AKT inhibitor could be of use for a tumour that has an increased AKT signalling and reduced sensitivity to cytotoxic agents. Hirai et al., (2010) found that combining MK2206 with several anticancer agents synergistically inhibited cancer cell proliferation in various cell lines. PTEN negatively regulates AKT signalling. It was found in the PC3 cells that there is a large *PTEN* gene deletions and frame shift *PTEN* mutations within LNCaP cells (Vlietstra et al., 1998). Changing or removing PTEN function of negatively regulating the AKT pathway results in increased survival of PC3 and LNCaP cells.

Because of these potential synergistic effects of A-11554563 and MK2206, they were used in co-treatment with SA to explore the combined effect of these drugs on proliferation. LNCaP and PC3 cells were treated with increasing concentrations (0 – 1 mM) of either A-11554563 or MK2206 and $\pm$ 200 µM of SA. A-11554563 and MK2206 inhibited LNCaP proliferation at concentrations $\geq$ 200 µM (Figure 9 A and B). The addition of SA did not enhance this inhibition. In contrast, PC3 were insensitive to A-11554563 and only sensitive to MK2206 at the highest concentration (Figure 9 C and D). Similar to LNCaP, the addition of SA did not enhance the activity of these inhibitors. It therefore appears that combination of SA with inhibitors of AKT and BCL-XL does not enhance therapy response.

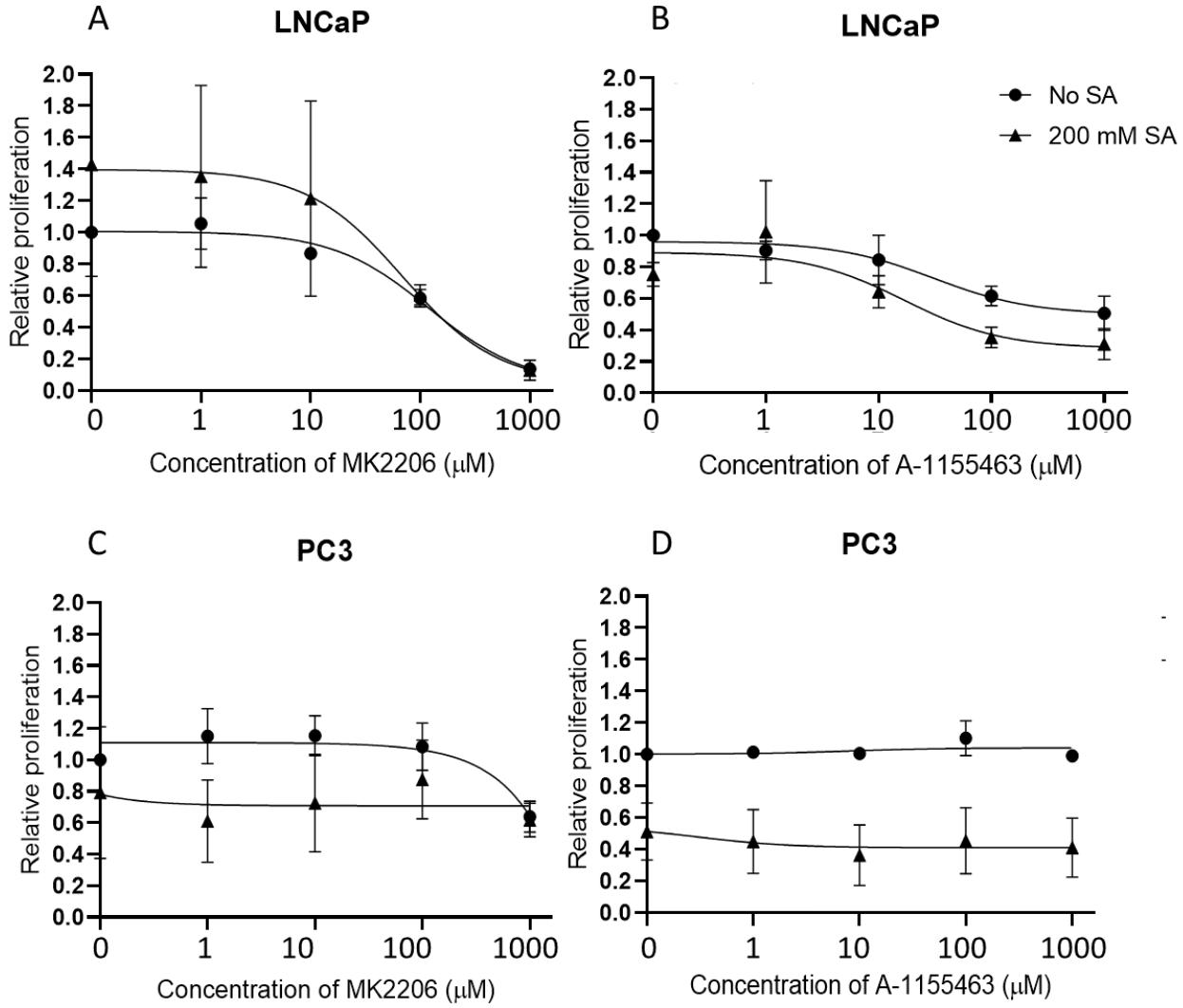

Figure 9 Co treatment proliferation assays of LNCaP and PC3 cells with SA and A-1155463/MK2206 shows no major decrease in proliferation of cancer cells *(A) LNCaP & MK2206 (B) LNCaP & A-1155463 (C) PC3 & MK2206 (D) PC3 & A-1155463. All cells were seeded in 96 well plates, treated with 0 – 1 mM MK2206 or A-1155463 and 200 μM SA for 7 days and proliferation quantified using crystal violet assays. Mean of 3 independent repeats (C, D) Mean of 2 independent repeats (A, B), (6 replicates for each experiment) ± 1 SEM.*

3. 2. Cell death mechanisms

3. 2. 1 Succinyl Acetone increases the level of CICD in DU145 cells.

The previous experiments demonstrated that SA inhibits prostate cancer proliferation. In order to determine if, and the method in which, the cells were dying after SA treatment, fluorescence-activated cell sorting (FACS) or flow cytometry was carried out on SA treated cells. The cells were treated with 200 µM SA and PI inclusion (% caspase independent cell death - CICD) and DNA hypodiploidy (apoptosis) assays were performed. An Accuri C6 flow cytometer was used to determine the % of cells undergoing apoptosis and CICD. There is very little cell death (less than 5%) without SA there is an increase in CICD in response to SA, but this was not found to be significant (Figure 10 A - C).

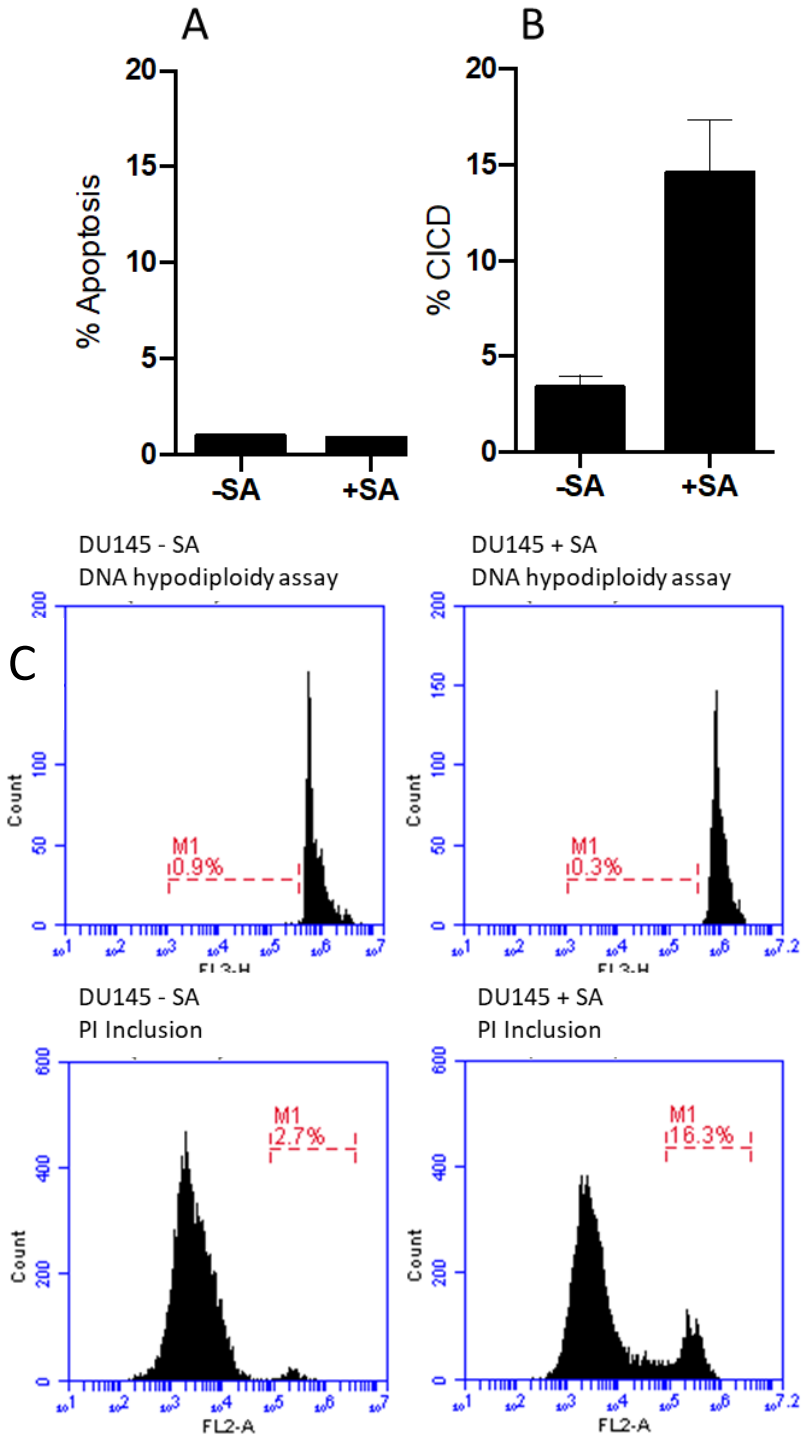

Figure 10 Treatment of DU145 cells with SA does induce cell death by caspase independent cell death (CICD) and not Apoptosis *(A) DNA hypodiploidy assay (B) PI inclusion assay. All cells were seeded in 6 well plates, treated with 200 µM SA for 7 days and % apoptosis was determined by DNA hypodiploidy assay and % caspase independent cell death (CICD) was determined by PI inclusion assay. Mean of 4 independent repeats ± 1 SEM. C) Raw data histograms showing % apoptosis and % CICD for each condition.*

3. 2. 2 TNF-α levels are not affected by SA treatment

TNF-α is a soluble cytokine, a part of the TNF-α ligand family binding to members of the TNF-α receptor (TNF-R) family signalling pathway. This signalling pathway goes on to induce expression of genes that can regulate inflammation. Under the correct condition's TNF-α can induce cell death (Sedger and McDermott 2014). TNF-α secretion has been described to be a feature of apoptosis and necroptosis (Chen and Goeddel 2002).

To further determine that SA is not inducing apoptosis and to investigate if necroptosis is taking place as the CICD, TNF-α levels secreted in the media and within the total cell lysate were measured using an ELISA after growth for 5 days with and without the treatment of 200 µM SA. To calculate the concentration of TNF-α expressed, a standard curve was generated using known concentrations of TNF-α (Figure 11 A). As expected, increasing concentrations of the standards resulted in an increase in absorbance in the colorimetric ELISA assay.

To isolate the secreted fraction, the conditioned media was passed through a syringe filter. Filtered and unfiltered cell solutions were measured to represent TNF-α contained within the cell (unfiltered) and the TNF-α that had been secreted (filtered). The raw data recorded from the ELISA analysis of TNF-α concentration from cells that had been treated with and without SA shows that there was little to no difference between the cellular concentration of TNF-α in the cells with and without SA (Figure 11 B). This suggests that when the prostate cancer cells are dying by inhibition of heme synthesis they are not producing any TNF-α protein, suggesting a mechanism of cell death that does not involve TNF-α production.

A

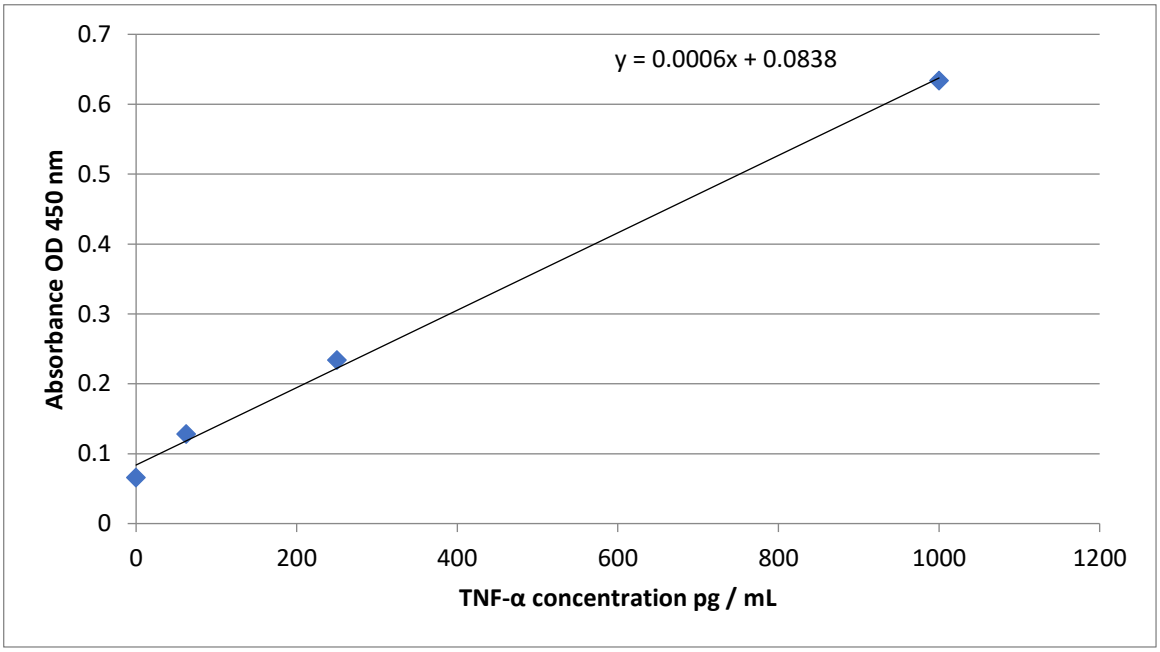

B

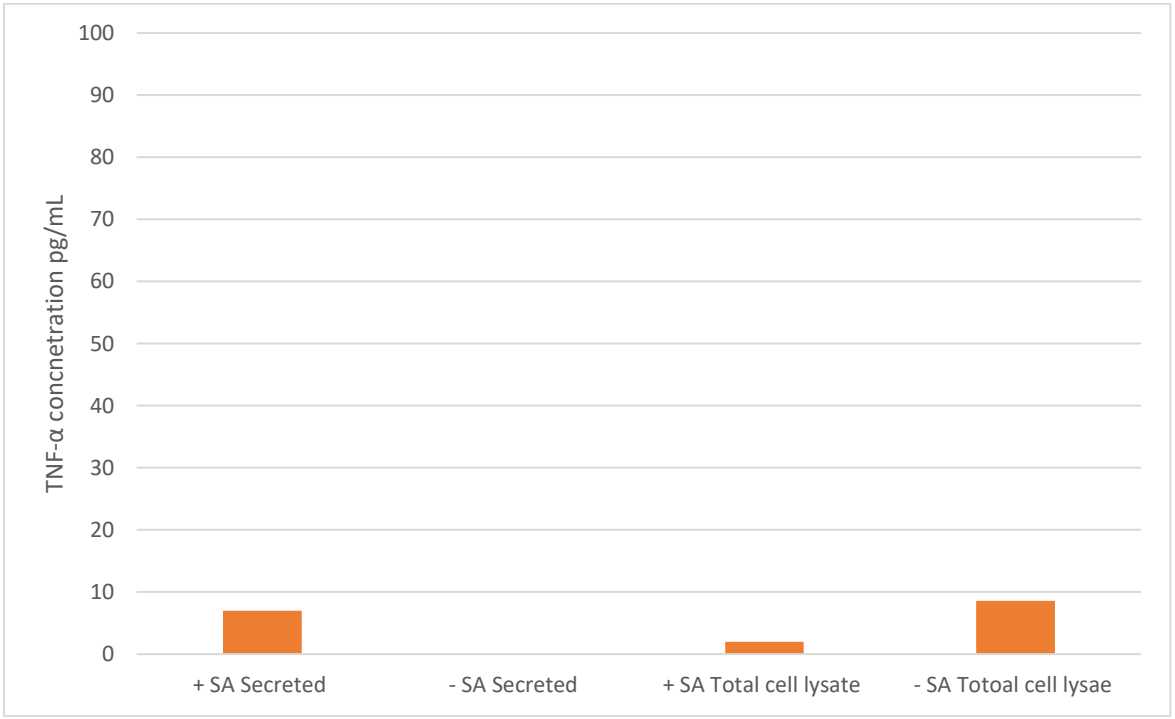

Figure 11 TNF-α protein levels within the PC3 cells does not increase with SA treatment. *(A) standard curve of known TNF-α concentrations to calculate TNF concentrations within PC3 cells. (B) Table showing the protein and TNF-α concentrations of SA treated cells.*

3. 2. 3 *TNF-α* gene expression levels are unaffected following SA treatment

To confirm the results of the ELISA assay, the effect of SA upon *TNF-α* gene expression was determined using qPCR. Cells were treated with increasing concentrations of SA (0 µM to 2000 µM) and left for 7 days. RNA was extracted and reverse transcribed into cDNA prior to quantification using qPCR. In agreement with the ELISA results, there is no significant change in *TNF-α* expression in response to SA treatment (Figure 12). This, therefore, alongside the flow cytometry data, demonstrates that when cells are treated with SA, cells are dying by a form of CICD that does not involve *TNF-α* production.

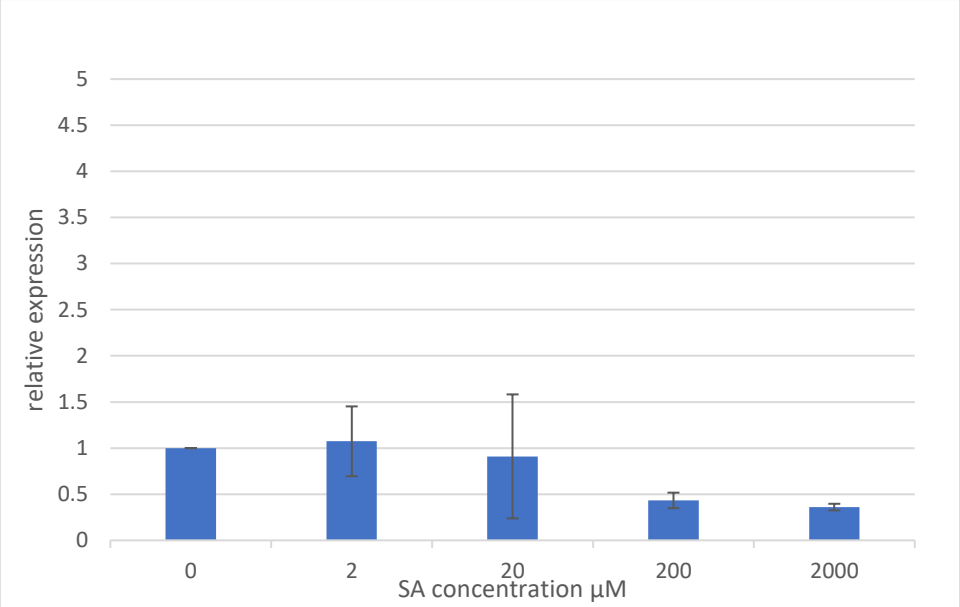

Figure 12 RNA TNF-α levels do not change within PC3 cells treated with succinyl acetone. *200,000 PC3 cells were seeded per well and incubated overnight prior to treatment with 0-2 mM SA. Cells were left for 6 days prior to harvesting. RNA was extracted and 250 ng RNA was reversed transcribed to make cDNA using the Luna kit (NEB), carried out using a T100 Thermal Cycler (Bio-Rad). qPCR was performed using primers specific for TNF-α and L19 (Table 1) was used for normalisation on a Roche LighCycler machine. qPCR data was analysed using the* $2^{-\Delta\Delta Ct}$ *method. mean of 2 repeats.*

3. 2. 4 SA depletes heme and so therefore increases prostate cancer cells sensitivity to ROS damage, causing death via CICD.

We have shown that SA does deplete cellular heme content (Figure 8). This heme depletion is expected to increase the cells sensitivity to ROS (reactive oxygen species) damage due to the limited heme for ROS protective proteins. For example, cytochrome c oxidase and cytoglobin. Cytochrome c oxidase does this by acting as a peroxynitrite reductase protecting the cell from peroxynitrite formed by the reaction of the superoxide anion radical with a nitric oxide radical (Musatov and Robinson 2012). Cytoglobin has been reported to have ROS scavenger functions (Zorov et al,. 2014).

H_2O_2 was added to the cells to introduce ROS damage to investigate the effect treatment of SA has on a cell sensitivity to ROS damage. H_2O_2 causes ROS damage by its downstream product the hydroxyl radical (OH). OH radical is highly reactive and can induce breaks within single strands of DNA and can cause lipid peroxidation. H_2O_2 is able to diffuse between membranes enabling it to cause ROS damage throughout cell. The % of cells undergoing apoptosis and CICD, in response to SA and H_2O_2, was quantified by flow cytometry. Treatment of cells with both H_2O_2 and SA showed no change in % apoptosis (Figure 13 A). Treatment of cells SA has been shown to increase the % of cells undergoing CICD. Interestingly, treatment with both H_2O_2 and SA further significantly increased the % of cells dying via CICD to approximately 50% (Figure 13 B). Representative histograms are provided, showing the increase in cell death as a result of CICD (Figure 13 C). The results therefore demonstrate that SA treatment increases cell sensitivity to ROS damage and these damaged cells are dying via CICD and not apoptosis.

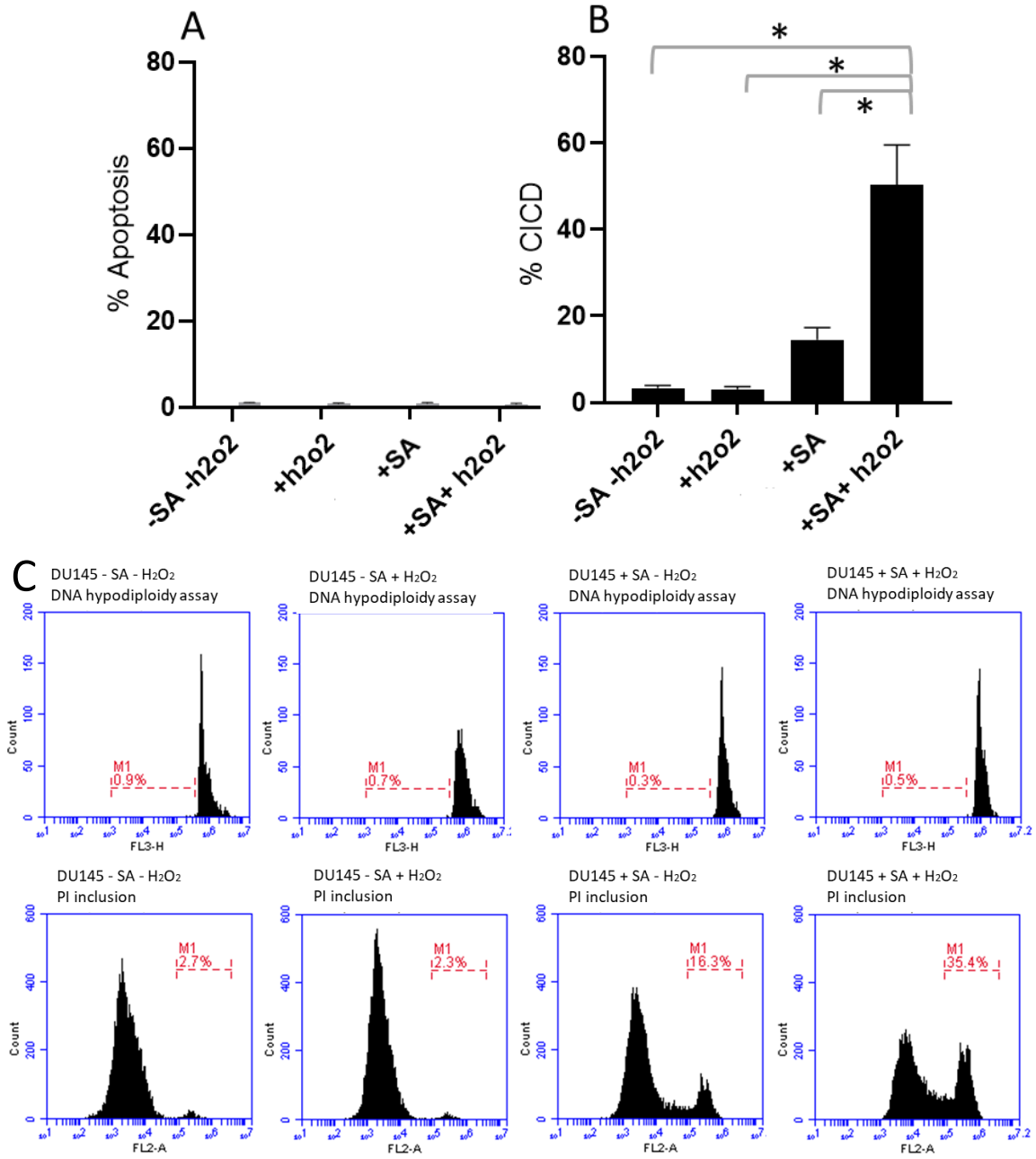

Figure 13 DU145 cells treated with both SA and H_2O_2 die by CICD*. (A) DNA hypodiploidy assay (B) Pi inclusion assay. All cells were seeded in 6 well plates, treated with 200 µM SA for 7 days and/or 200 µl H_2O_2 for 24 hours and % caspase independent cell death (CICD) was determined by PI inclusion assay and % apoptosis was determined by DNA hypodiploidy assay. Mean of 4 independent repeats ± 1 SEM. ANOVA * p<0.05. (C) Raw data histograms showing % apoptosis and % CICD for each condition.*

3. 2. 5. Cell death is not blocked by Z-VAD

Z-VAD (a pan caspase inhibitor) blocks caspase activity and apoptosis. It is a key compound for studies into apoptosis, originally developed for therapeutic uses but cytotoxicity of one of its derivatives made it unsuitable for use as a therapeutic drug (Van Noorden 2001). It was used in these studies to confirm that the cells were not dying via apoptosis.

The results show that there was no change in the low levels of apoptosis in both conditions with and without the addition of Z-VAD (Figure 14A and C). As before, the combination of SA and H_2O_2 significantly increased CICD (Figure 14B). This induction of cell death was not affected by the addition of Z-VAD (compare Figure 14B and D), confirming that cell death is caspase independent, supporting the hypothesis that the combination of SA and H_2O_2 promotes CICD.

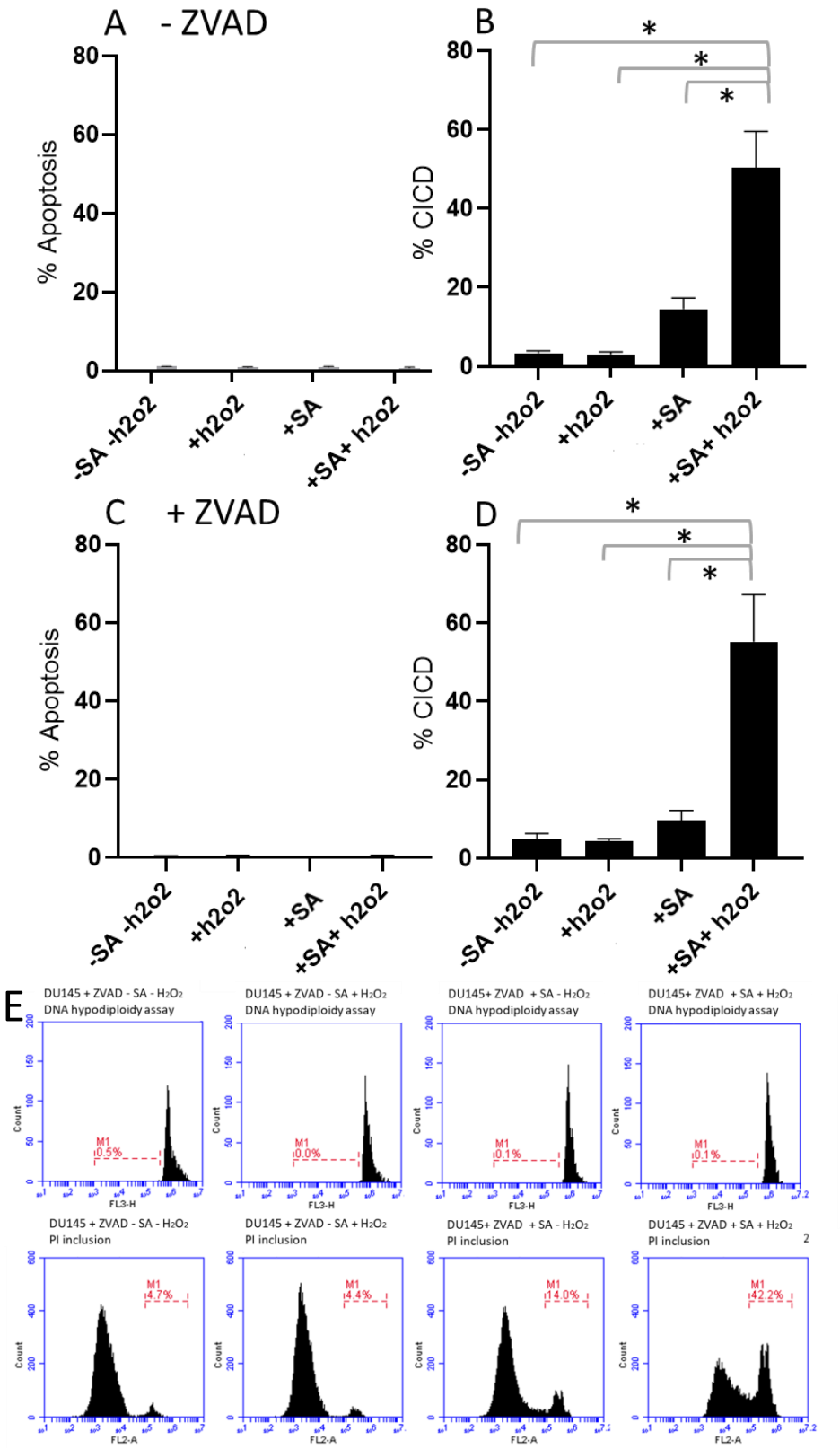

Figure 14 No change in the levels of apoptosis and necroptosis in DU145 cells treated with Z-VAD after death induced by SA and H_2O_2 *(A) DNA hypodiploidy assay no Z-VAD (B) PI inclusion assay no Z-VAD treatment. (C) DNA hypodiploidy assay treated with Z-VAD. (D) PI inclusion assay treated with Z-VAD. All cells were seeded in 6 well plates, treated with/without 20 µl Z-VAD and 200 µM SA for 7 days and/or 200 µl H_2O_2 for 24 hours and % apoptosis was measured by DNA hypodiploidy assay and % caspase independent cell death (CICD) was measured by PI inclusion assay. Mean of at least 3 independent repeats ± 1 SEM. ANOVA * p<0.05 (E) Raw data histograms showing % apoptosis and % CICD for each condition.*

3. 2. 6 Cell death is not blocked by Necrostatin

In order to further determine how the cells were dying; cells were treated with necrostatin alongside SA. Necrostatin acts as a small molecule inhibitor of necroptosis and has been found to act as a selective allosteric inhibitor of RIPK1 in vitro (Degterev et al., 2008). And so, to establish whether the H_2O_2 and SA treated cells were dying by necroptosis, they were treated with necrostatin to attempt to block the necroptotic death pathway. The percentage of cells undergoing apoptotic cell death and CICD was quantified by flow cytometry.

In agreement with the previous results, the combination of SA and H_2O_2 significantly increased cell death via necroptosis (Figure 15 B) and apoptosis levels remained unchanged (Figure 15 A). Surprisingly, the addition of necrostatin was unable to reverse the % of cells undergoing CICD (compare Figure 15 B and D). It is therefore possible that cells may be dying via a different mechanism of CICD.

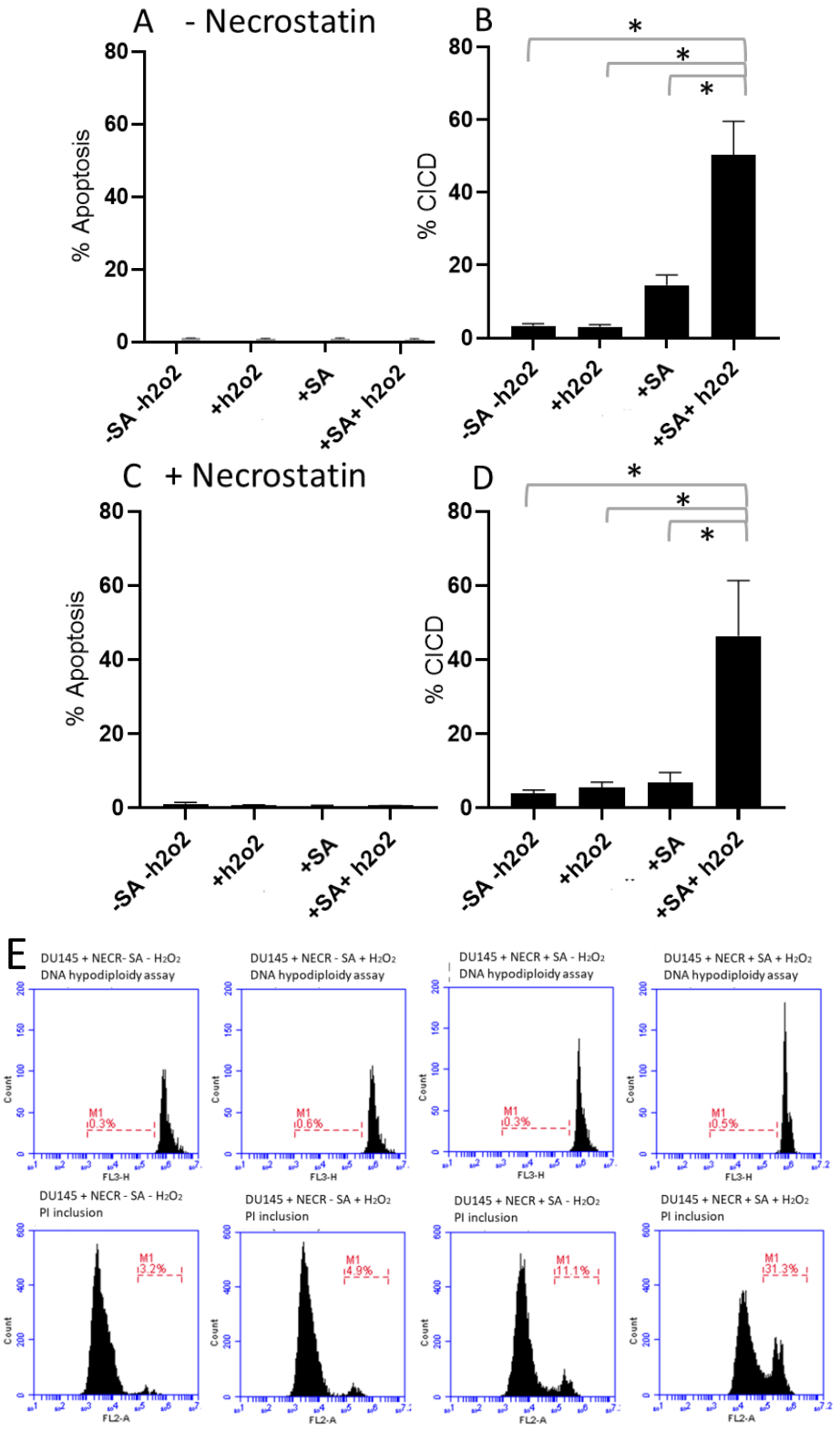

Figure 15 No change in the levels of apoptosis or % caspase independent cell death (CICD) after death induced by SA and H_2O_2 with necropstatin *(A) DNA hypodiploidy assay no necrostatin (B) Pi inclusion assay no necrostatin treatment. (C) DNA hypodiploidy assay treated with necrostatin. (D) PI inclusion assay DU145 treated with necrostatin. All cells were seeded in 6 well plates, treated with/without 40 mM necrostatin and 200 µM SA for 7 days and/or 200 µl H_2O_2 for 24 hours and % apoptosis was measured by DNA hypodiploidy assay and % CICD was measured by PI inclusion assay. Mean of 3 independent repeats (C, D) 4 independent repeats (A, B) ± 1 SEM. ANOVA * p<0.05, (E) Raw data histograms showing % apoptosis and % CICD for each condition.*

3. 2. 7 Cells experience the same levels of CICD and apoptotic cell death after treatment with ferrostatin

Since necrostatin was unable to block cell death, I was interested to see if cells could be dying of a related caspase-independent mechanism of cell death, namely ferroptosis. Ferroptosis is another form of regulated necrosis. Ferroptosis is associated with iron-dependant unchecked accumulation of lipid hydroperoxides (Zilka et al., 2017). High-throughput screening has identified the drug ferrostatin as an inhibitor of ferroptosis due to its ability to inhibit lipid hydroperoxides accumulation. Ferrostatins are able to specifically prevent ferroptosis in many conditions, however, the mechanism in which they work is still not fully understood (Michael et al., 2018).

To investigate this, cells were treated as before, with the ferroptosis inhibitor ferrostatin and again, cell death quantified using flow cytometry. The data shows there in no difference in % cell apoptosis and % CICD with and without the addition of ferrostatin (Figure 16). PC3 cells treated with SA and H_2O_2 death cannot be inhibited with ferrostatins.

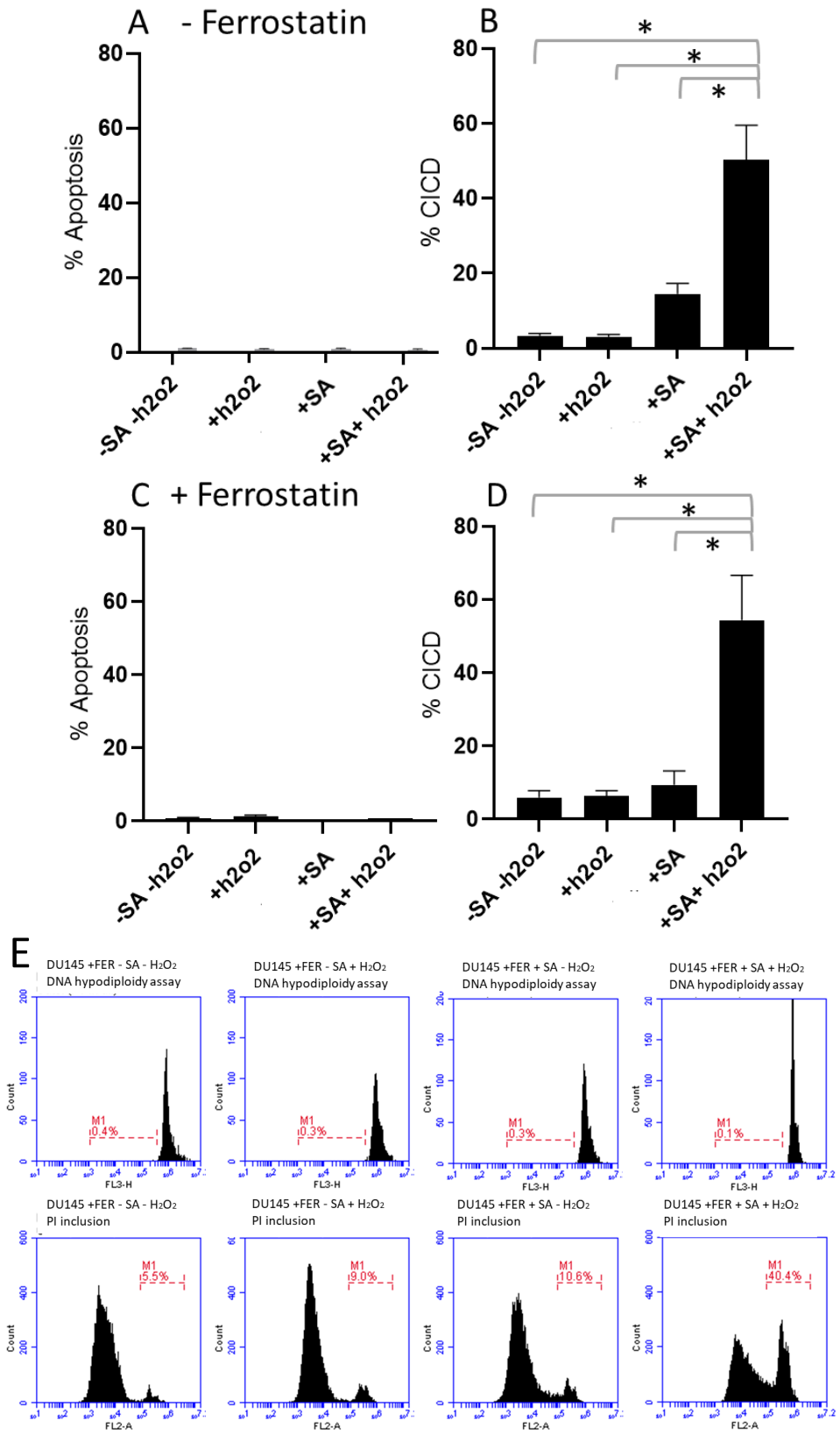

Figure 16 No change in the levels of apoptosis and necroptosis in DU145 cells treated with ferrostatin after death induced by SA and H_2O_2 *(A) DNA hypodiploidy assay DU145 cells no ferrostatin (B) Pi inclusion assay DU145 no ferrostatin treatment. (C) DNA hypodiploidy assay DU145 cells treated with ferrostatin. (D) PI inclusion assay DU145 cells treated with ferrostatin. All cells were seeded in 6 well plates, treated with/without 10 nM ferrostatin and 200 µM SA for 7 days and/or 200 µl H_2O_2 for 24 hours. % apoptosis was measured by DNA hypodiploidy assay and % % caspase independent cell death (CICD) was measured by PI inclusion assay. Mean of 3 independent repeats (C, D) 4 independent repeats (A, B) ± 1 SEM. ANOVA * p<0.05, (E) Raw data histograms showing % apoptosis and % CICD for each condition.*

3. 2. 8. Cells experience the same levels of CICD and apoptotic cell death after being knocked out for FADD

FADD is an adapter protein that helps to form the death inducing signalling complex involved in apoptosis. It has been suggested that FADD plays a role in RIPK1 and 3 dependant necroptosis (Lee et al., 2012) and caspase 8 activation requires FADD leading to RIPK1 and 3 cleavage preventing necroptosis. A FADD deficiency is thought to inhibit caspase 8 and therefore apoptosis and activate necroptosis. To investigate further the mechanism of cell death in DU145 cells treated with SA and H_2O_2 the requirement for FADD for their death was investigated. This was done via flow cytometry carried out on different DU145 FADD knock-out cell lines. These FADD knock-out cell lines named DU145 FADD 1b and DU145 FADD 2b.

SA and H_2O_2 has no effect upon the % of cells undergoing apoptosis in the parental or knock-out lines (Figures 17 A, C and E). As described previously, the % of CICD was significantly increased following SA and H_2O_2 treatment. Interestingly, this induction of cell death was similar in the FADD knock-out lines, suggesting that cell death is FADD independent. Representative histograms are provided in Figure 18.

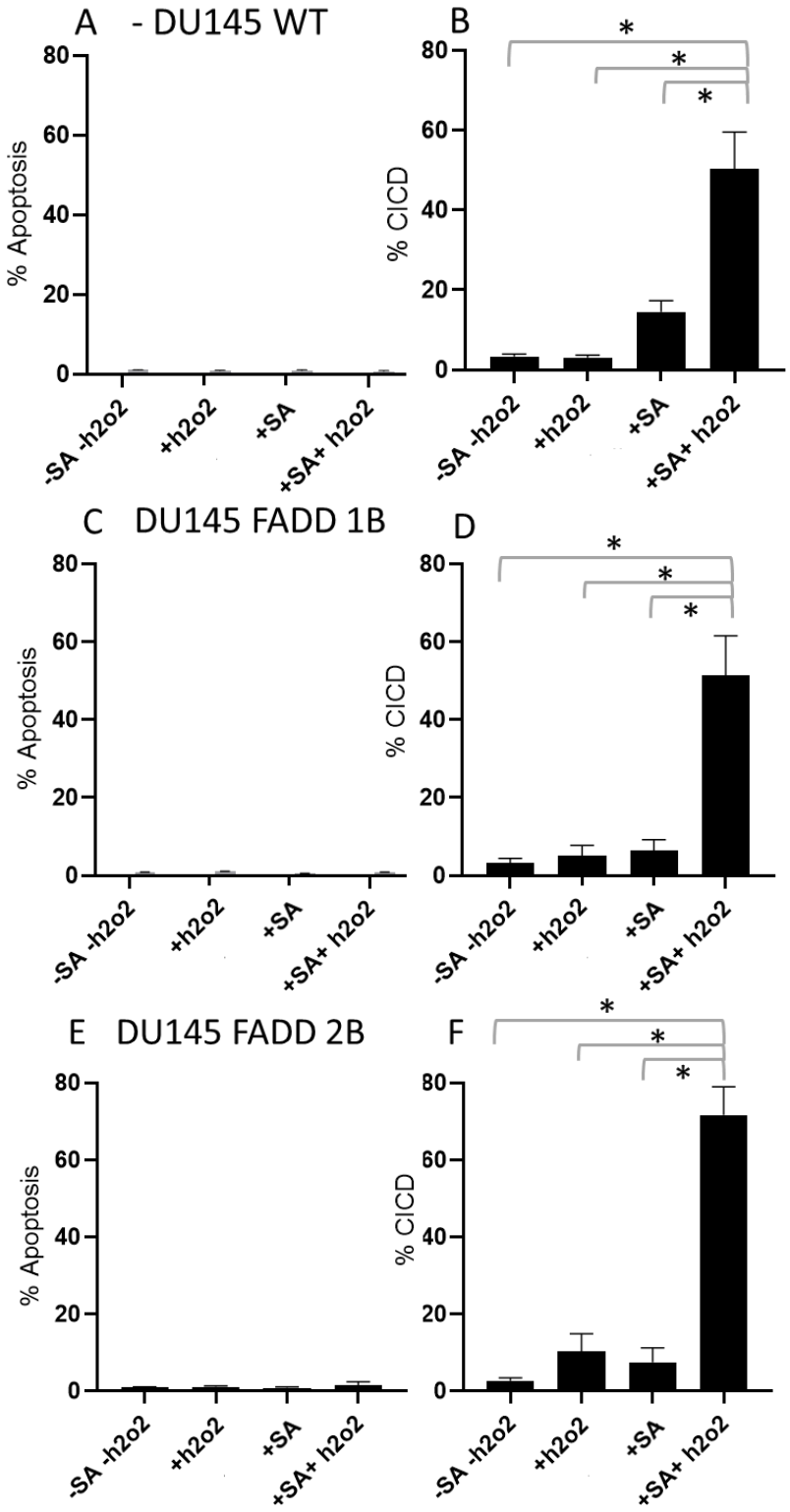

***Figure 17 Cell death induced by SA and H_2O_2 is FADD independent**. (A) DNA hypodiploidy assay DU145 WT cells (B) Pi inclusion assay DU145 WT cells (C) DNA hypodiploidy assay DU145 FADD 1b cells (D) PI inclusion assay DU145 FADD 1b cells (E) DNA hypodiploidy assay DU145 FADD 2b cells (F) PI Inclusion assay DU145 FADD 2b. All cells were seeded in 6 well plates, treated with 200 µM SA for 7 days and/or 200 µl H_2O_2 for 24 hours. % apoptosis was measured by DNA hypodiploidy assay and % CICD was measured by PI inclusion assay. Mean of 4 independent repeats (A, B) ± 1 SEM. ANOVA * p<0.05.*

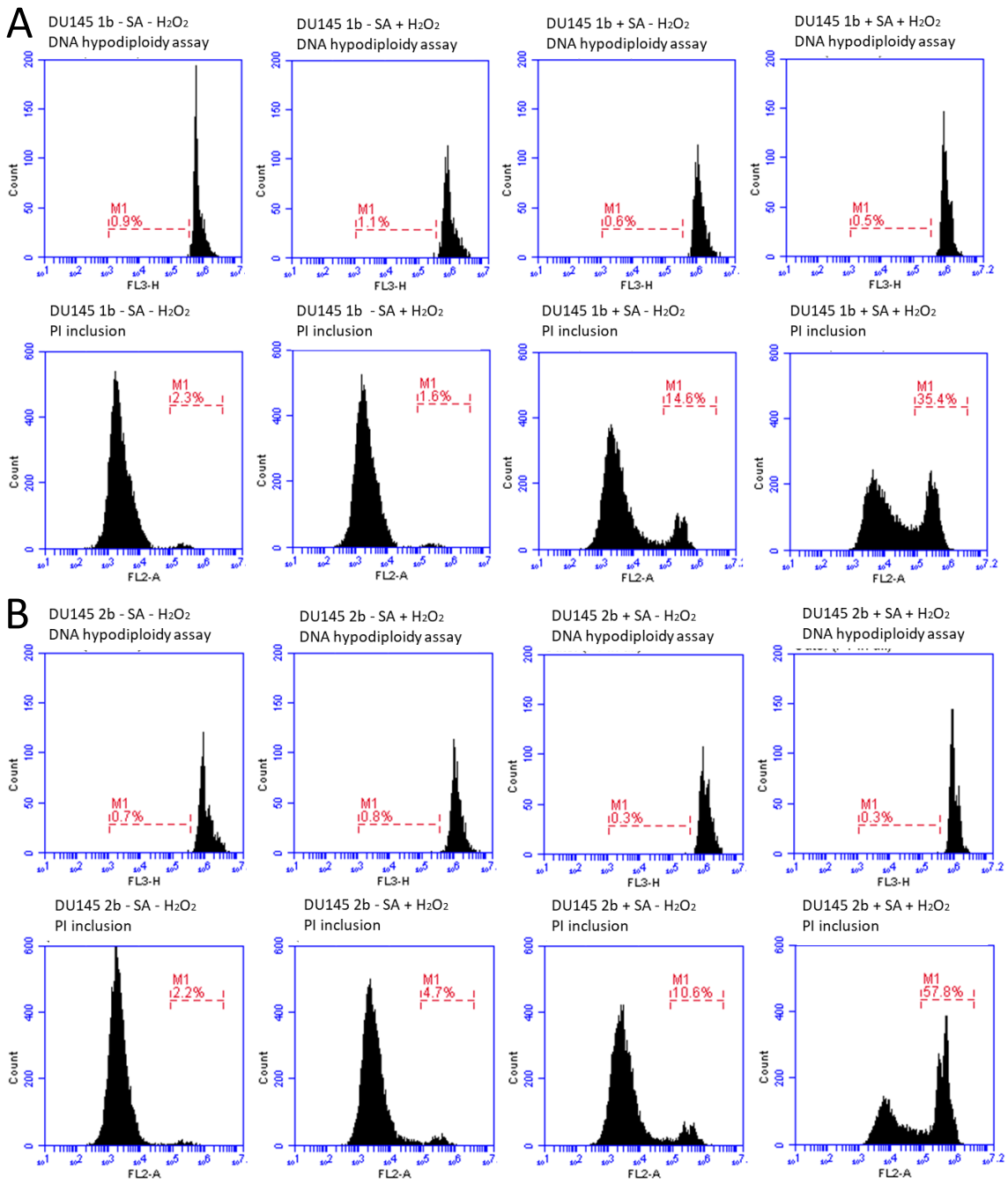

Figure 18 Cell death induced by SA and H_2O_2 is FADD independent, example of raw data histograms showing % apoptosis and % CICD of (A) DU145 FADD 1b and (B) DU145 FADD 2b cells*. All cells were seeded in 6 well plates, treated with 200 µM SA for 7 days and/or 200 µl H_2O_2 for 24 hours. % apoptosis was measured by DNA hypodiploidy assay and % CICD was measured by PI inclusion assay.*

4.0 CHAPTER four Results – Cloning, expression and purification of ALAS 1 and ALAS 2 in bacteria

The work presented here and from the Brooke Group (unpub) suggests that targeting heme synthesis may be a viable treatment option for prostate cancer. ALAS is the first enzyme of the heme synthesis pathway and it exists as two isoenzymes: ALAS 1 and ALAS 2. ALAS 1 is expressed in all cell types, and is overexpressed in prostate cancer, whereas ALAS 2 is produced only in developing erythrocytes. We therefore propose to target ALAS1. A crystal structure of ALAS 2 exists (RCSB PDB), whereas no structural information is available for ALAS 1. The aim of this part of the project was therefore to express ALAS 1 and ALAS 2 for future biochemical assays and crystallography studies.

Auto induction media was used for the expression in the following experiments. This media works by the bacteria consuming glucose during the first period of growth as the preferred source of carbon and therefore other carbon utilisation pathways, are inhibited. Once the glucose has been depleted the lac repressors are free to bind with lactose and are relieved from the operon causing the lac operon to be switched on. This also initiates the expression of the heterologous protein from the recombinant system. The import of lactose results in production of allolactose, which further promotes lac operon induction (Blommel et al., 2009).

At the beginning of this project there was no solved structure for human ALAS2. Just after purifying the protein (section 4. 1. 4) the structure was put onto the protein database (RSCB PBD 6HRH).

4. 1 ALAS 2 Expression

4. 1. 1 ALAS 2 T expression in BL-21 cells

In order to purify the ALAS 2 protein it was transformed into BL-21 and the lac operon was utilised to induce expression. The ALAS 2 sequence was truncated (termed ALAS2-T) to remove the

mitochondrial targeting peptide and was cloned into the pET28a vector (Appendix Figure 2). BL-21 cells were used as the standard starting expression host due to their OmpT protease and Lon protease deficiencies, helping recombinant proteins to accumulate and decrease the likelihood of them degrading during the purification process (Donahue and Bebee 1999).

ALAS2-T was transformed into BL-21 cells and grown in a starter culture overnight. A sample of this was taken as the "uninduced" fraction for later analysis. The starter culture was transferred to 2 L flasks containing auto induction media overnight. A fraction of this was kept as the "total lysate" fraction. The cells were lysed and passed through an emulsiflex. The lysate was centrifuged, and the soluble fraction was also collected for SDS PAGE analysis (Figure 20). There are no clear bands at the expected weight of 61.4 kDa for ALAS2-T in either the total lysate or soluble fraction lanes of the gel, suggesting that the protein was not expressed by the BL-21 cells in either a soluble or insoluble form (Figure 20).

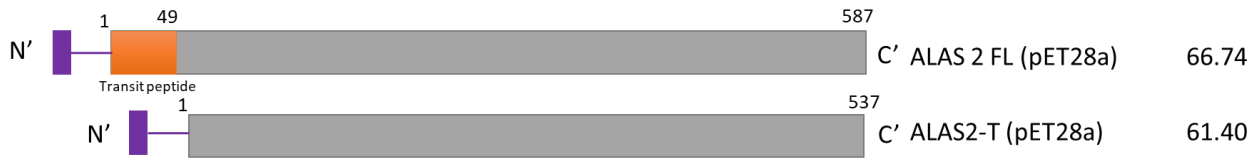

Figure 19 Schematic showing the sizes of the ALAS 2 protein and the ALAS2-T protein used for expression. *Purple box representing the 19 reside HIS-tag. Numbers to the right representing the expected kDa of the proteins once expressed.*

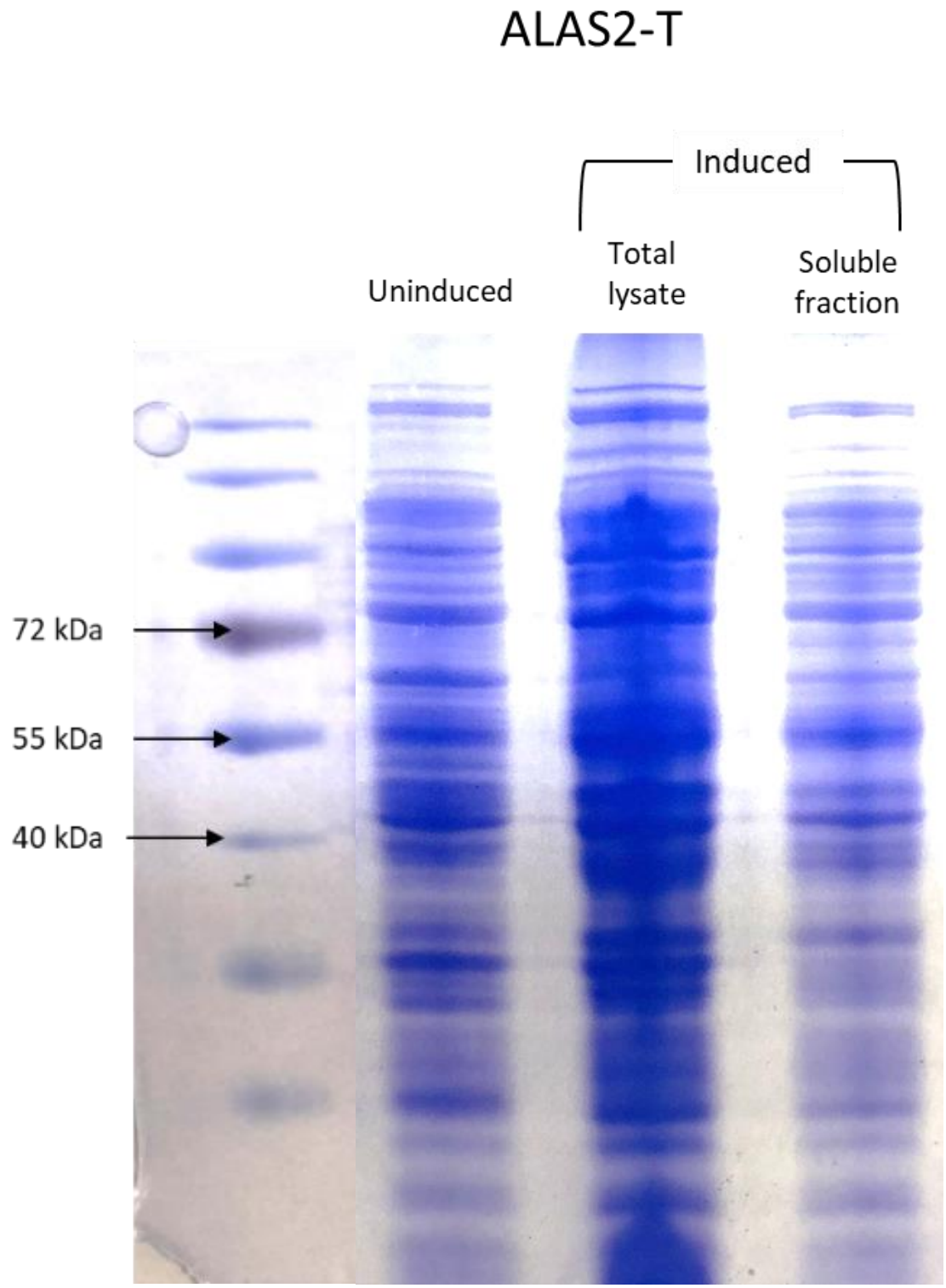

Figure 20 ALAS2-T expression was not induced in BL-21 cells. *ALAS2-T was transformed into BL-21 cells and grown in a starter culture 8 hours. A sample of this was taken as the "uninduced" fraction. The starter culture was transferred to 2 L flasks containing auto induction media grown at 37 °C for 1.5 hours and incubated overnight at 20 °C. A fraction of this was the "total lysate" fraction. The cells were lysed and passed through an emulsiflex. The lysate was centrifuged, and the soluble fraction was also collected for SDS PAGE analysis. Each fraction was boiled for 30 minutes with 6X loading dye at 85 °C before loading to SDS-PAGE (10 % acrylamide gel) ran at 125 V for 2 hours. The gel was stained with Coomassie stain and incubated at room temperature overnight before being photographed.*

4. 1. 2 Diagnostic digest to verify the pET-28A ALAS2-T plasmid

Expression of ALAS2-T in BL-21 was unsuccessful and hence I verified the plasmid using a diagnostic digest. The DNA construct containing ALAS 2 was digested with restriction enzyme *Bgl*II. The restriction enzyme digest of pET28a ALAS2-T should result in fragments of 68 bp, 328 bp and 6903 bp. The digested DNA was ran on a 1 % agarose gel (Figure 21) and visualised with UV light. There is a clear band of approximately 7 kb in the *Bgl*II cut plasmid, representing the 6903 bp fragment (Figure 21). The smaller fragments 68, 328 bp were barely visible on the gel, but were visible when the image was over-exposed (data not shown). The plasmid was also verified by Sanger sequencing.

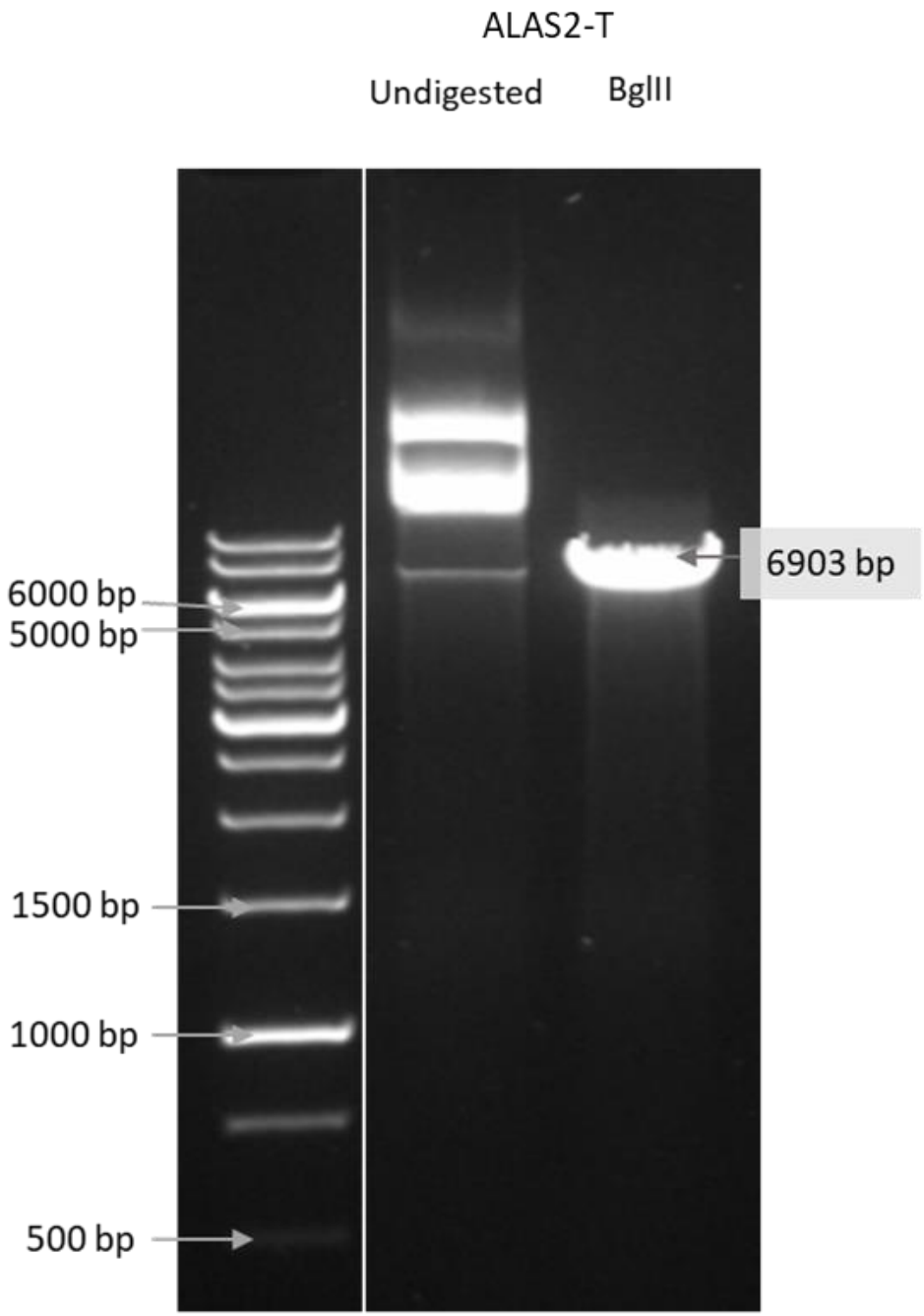

Figure 21 Successful digestion of p28a ALAS2-T*. 1 % agarose analytical gel of p28a ALAS2-T digestion with restriction enzyme Bgl*II*. Uncut p28a ALAS2-T was run alongside to allow comparison. DNA was digested with BglII and products separated using gel electrophoresis. The DNA fragments were visualised using a BioRad gel doc system. A 1 kb ladder (ThermoFisher) was run alongside the products to allow for sizing of the fragments. Significant bands and sizes are labelled with arrows.*

4. 1. 3 ALAS2-T was successfully expressed in Rosetta cells

Following verification of the plasmid, ALAS2-T was transformed into two different bacterial strains, namely Rosetta and pGro7. These strains possess different specifications that enhances their ability to express the protein in a soluble form. The transformed cells were grown in auto induction media and a small aliquot of each stage of the expression process was taken to be analysed on using SDS PAGE.

The expression of ALAS2-T in pGro7 cells showed weak expression of a protein at approximately 50 kDa (Figure 22 A). Expression was markedly higher in the Rosetta line, but the majority of the protein appeared to be insoluble since the amount in the soluble fraction was significantly less (Figure 22 A). To confirm that the band visualised was ALAS2-T, an immunoblot was performed. As expected, a clear band was evident for in the Rosetta lysate, predominantly in the total lysate, but also visible in the soluble fraction (Figure 22 B).

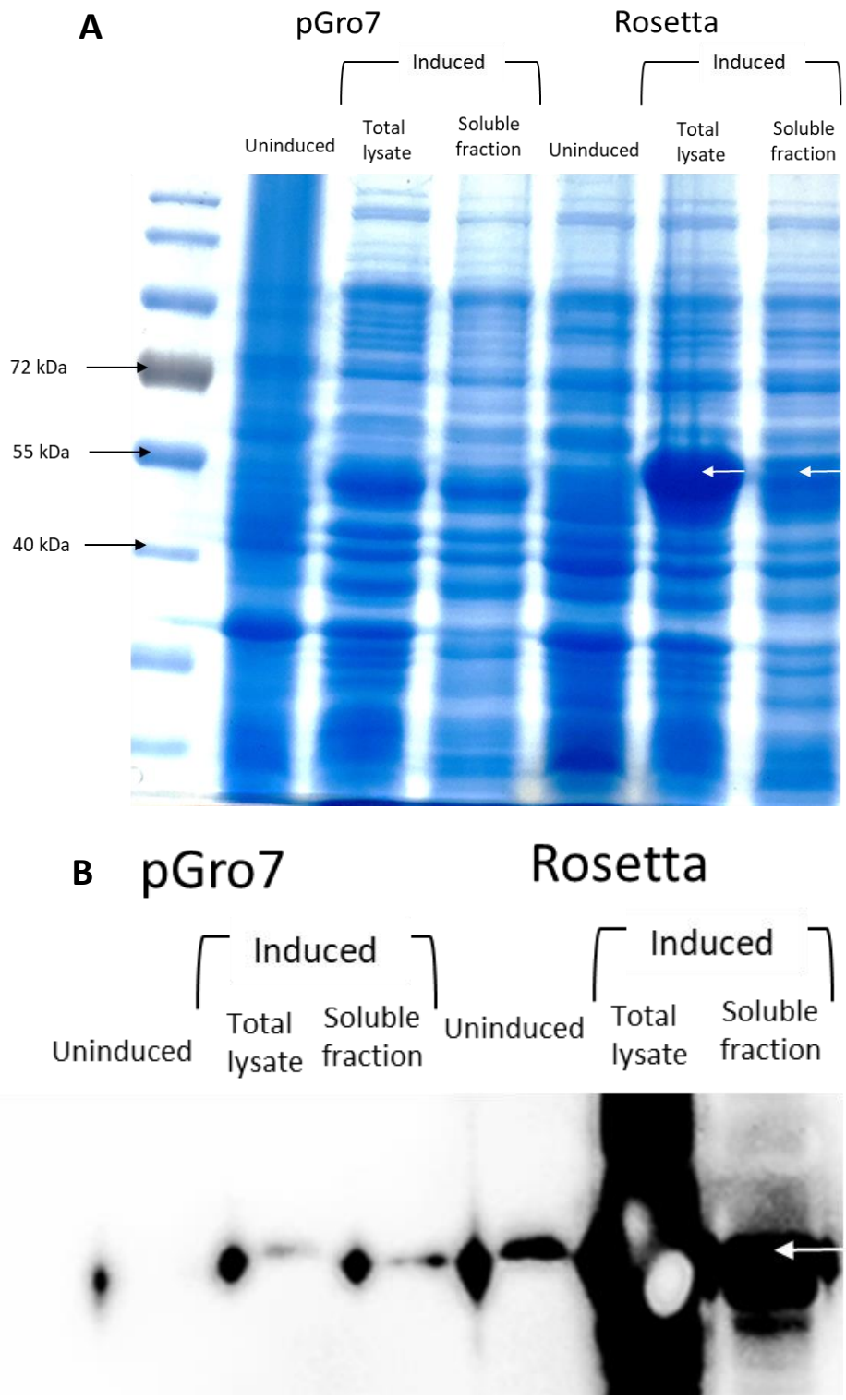

Figure 22 ALAS2-T was successfully epressed in Rosetta cells. ALAS2-T was transformed into Rosetta and pGro7 cells and *grown in a starter culture 8 hours. A sample of this was taken as the "uninduced" fraction. The starter culture was transferred to 2 L flasks containing auto induction media grown at 37 °C for 1.5 hours and incubated overnight at 20 °C. A fraction of this was the "total lysate" fraction. The cells were lysed and passed through an emulsiflex. The lysate was centrifuged, and the soluble fraction was also collected for SDS PAGE analysis. Each fraction was boiled for 30 minutes with 6X loading dye at 85 °C before loading to SDS-PAGE (10 % acrylamide gel) ran at 125 V for 2 hours. (A) The gel was stained with Coomassie stain and incubated at room temperature overnight before being photographed. (B) A western blot analysis was carried out using HIS-tag antibody 1° in 1:20,000 dilution and 2° goat anti-mouse, the image was detected using LuminataTM Forte Western HRP Substrate (Millipore) on a Fusion FX (VILBER LOURMAT).Significant bands indicated with arrows.*

4. 1. 4 ALAS2-T expression and purification in Rosetta cells

The ALAS 2 expressing Rosetta cells were on a larger scale (8 L) to facilitate a high yield of protein after purification. Each stage of the expression and purification process was aliquoted and used for analysis on an SDS page gel. i.e. a sample was taken of the flow through, wash and elution in addition to the uninduced, total lysate and soluble fraction parts taken previously. The results (Figure 23) show protein induction present at approximately 53 kDa in the total lysate, soluble fraction and elution fractions. ALAS2-T had there been successfully expressed and purified in preparation for future biochemical and crystallography assays.

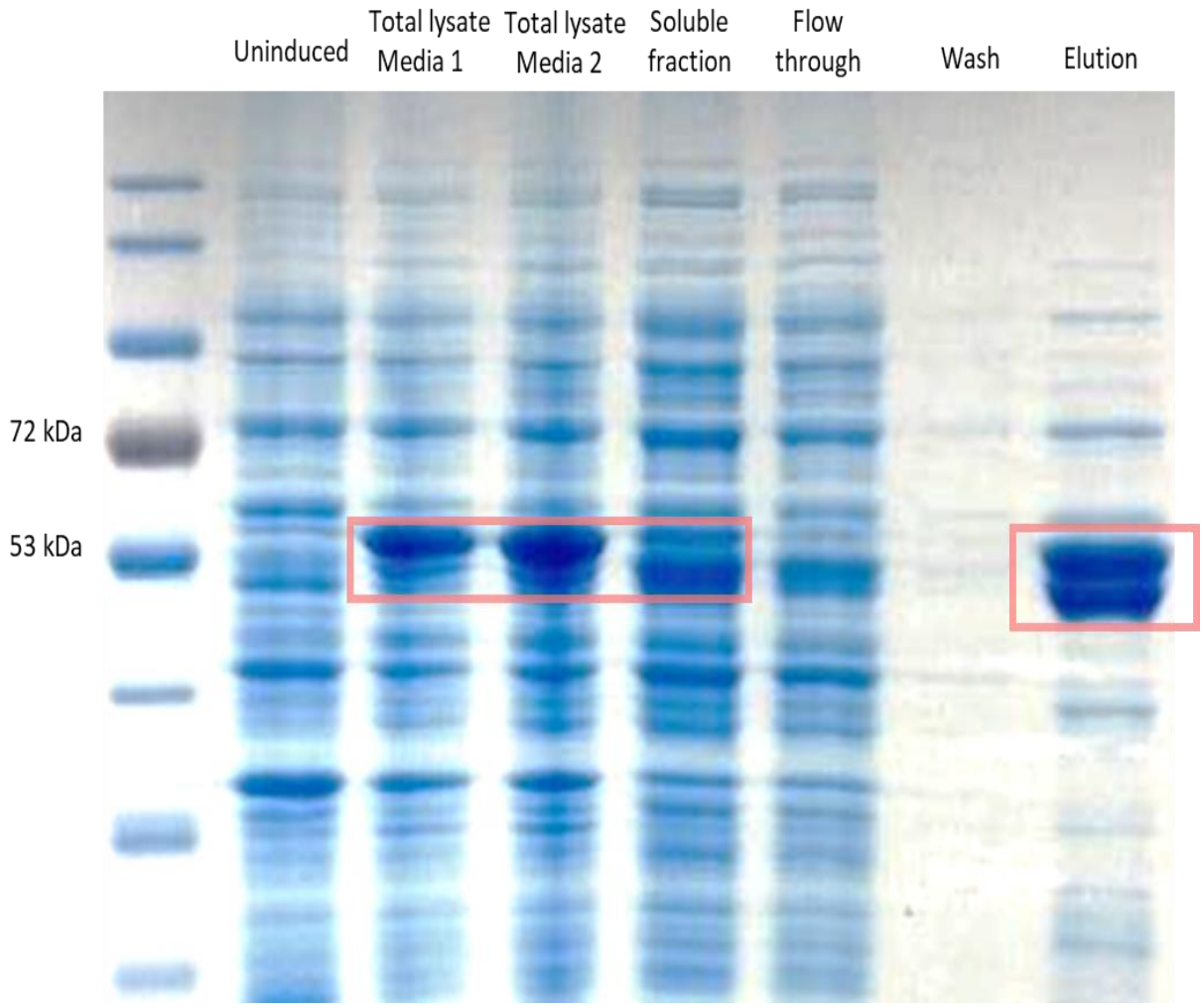

Figure 23 ALAS2-T is successfully expressed and purified in rossetta cells. *ALAS2-T was transformed into Rosetta cells and grown in a starter culture 8 hours. A sample of this was taken as the "uninduced" fraction. The starter culture was transferred to 2 L flasks containing auto induction media grown at 37 ºC for 1.5 hours and incubated overnight at 20 ºC. A fraction of this was the "total lysate" fraction. The cells were lysed and passed through an emulsiflex. The lysate was centrifuged, and the soluble fraction was also collected for SDS PAGE analysis. This was then ran through the HisTrap Ni Sepharose excel column followed by a wash with 50 ml lysis buffer. The purified protein was eluted in 20 ml lysis buffer with 300 mM imidazole added. The eluted sample along with samples of the flow through and was were visualised using SDS-PAGE. Each fraction was boiled for 30 minutes with 6X loading dye at 85 ºC before loading to SDS-PAGE (10 % acrylamide gel) ran at 125 V for 2 hours. (A) The gel was stained with Coomassie stain and incubated at room temperature overnight before being photographed. Significant bands are highlighted in red.*

4. 2 ALAS 1 Expression

4. 2. 1. ALAS1-T expression in BL-21 cells

As a therapeutic target for prostate cancer, ALAS 1 is of more interest due to tissue specific expression differences and since ALAS 1 is upregulated in prostate cancer cells (Brooke, unpub.) ALAS1-T contained within a pET28a vector was transformed into BL-21 to utilise their ability to express the protein. ALAS1-T was used as this removed the mitochondrial targeting sequence ensuring the expressed protein would resemble the final active protein (Figure 24). BL-21 cells were used for their deficiencies in Ompt and lon proteases that helps recombinant protein production by decreasing their likelihood to degrade during purification (Donahue and Bebee 1999).

ALAS1-T was transformed into BL-21 cells and grown in a starter culture overnight (this was run on the SDS page as the “uninduced” fraction). The culture was then grown in 2 L of auto induction media overnight. A fraction of this was then taken to be ran on the SDS PAGE as the “total lysate” fraction. Following this, the cells were lysed to release any protein contained. This lysate was then centrifuged to isolate the soluble fraction, and this was also separated using SDS PAGE and the gel was Coomassie stained. ALAS1-T is predicted to have a molecular weight of 67.20 kDa The Coomassie stained gel shows no clear bands in either the total lysate or soluble fraction lanes of the gel at the expected weigh (Figure 25), suggesting that the protein was not expressed by the BL-21 cells.

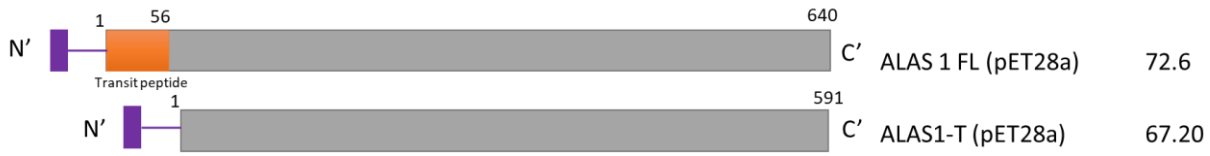

Figure 24 Schematic showing the sizes of the ALAS 1 protein and the ALAS1-T protein used for expression. Purple box representing the 19 reside HIS-tag. Numbers to the right representing the expected kDa of the proteins once expressed.

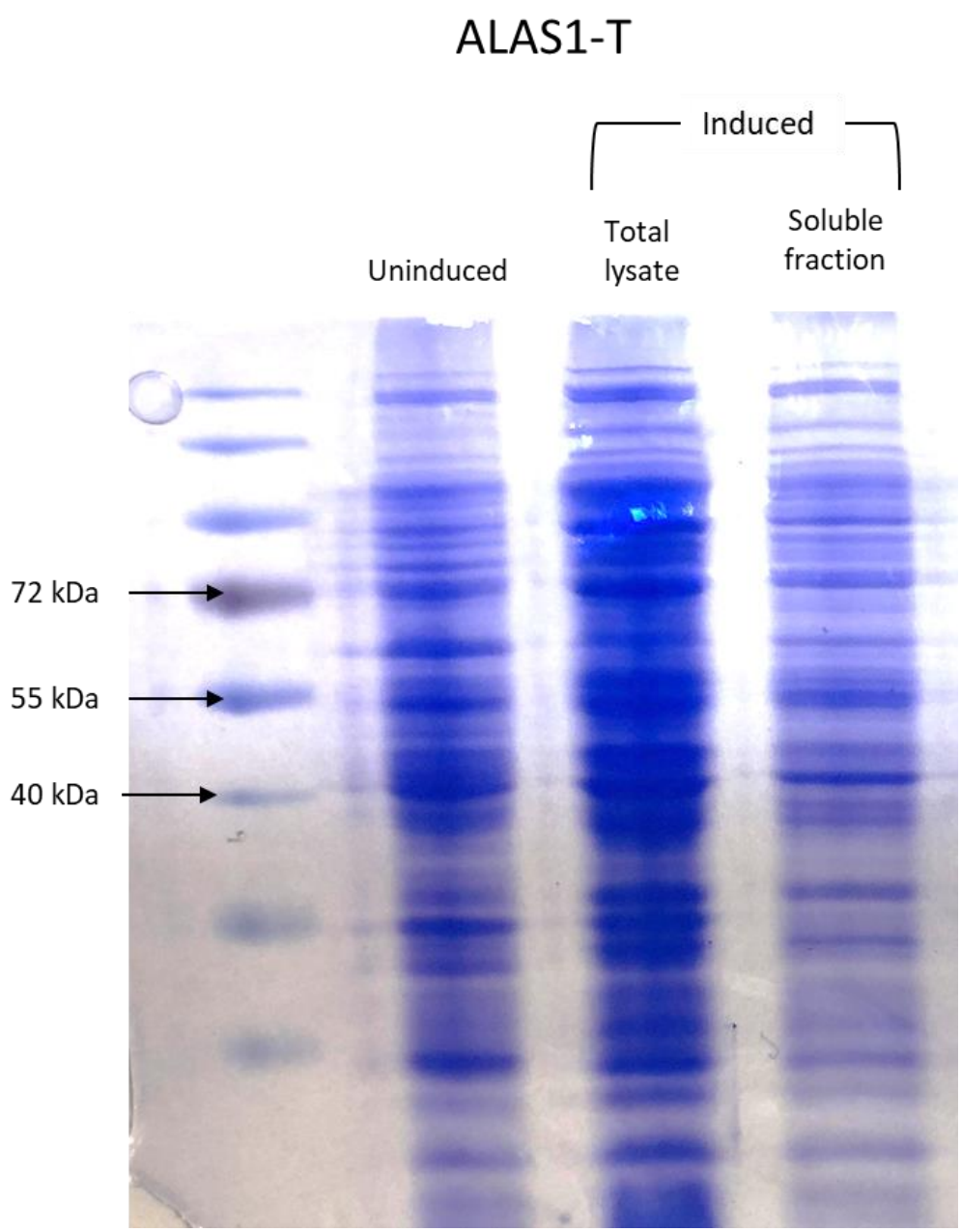

Figure 25 No successful expression of ALAS 1 T in BL-21 cells. *ALAS1-T was transformed into BL-21 cells and grown in a starter culture 8 hours. A sample of this was taken as the "uninduced" fraction. The starter culture was transferred to 2 L flasks containing auto induction media grown at 37 °C for 1.5 hours and incubated overnight at 20 °C. A fraction of this was the "total lysate" fraction. The cells were lysed and passed through an emulsiflex. The lysate was centrifuged, and the soluble fraction was also collected for SDS PAGE analysis. Each fraction was boiled for 30 minutes with 6X loading dye at 85 °C before loading to SDS-PAGE (10 % acrylamide gel) ran at 125 V for 2 hours. The gel was stained with Coomassie stain and incubated at room temperature overnight before being photographed.*

4. 2. 2 Diagnostic digests of pET28aALAS1-T

As there was no expression in the BL-21 cells, the ALAS1-T expression plasmid (pET28aALAS1-T) was digested with *Bgl*II and bands separated and visualised using gel electrophoresis. The restriction enzyme should cut pET28aALAS1-T into a 1136 bp fragment and a 6163 bp fragment (Appendix Figure 3). The gel shows that when pET28aALAS1-T was digested, bands of the expected size were visible. The plasmid was also verified using Sanger sequencing (Figure 26).

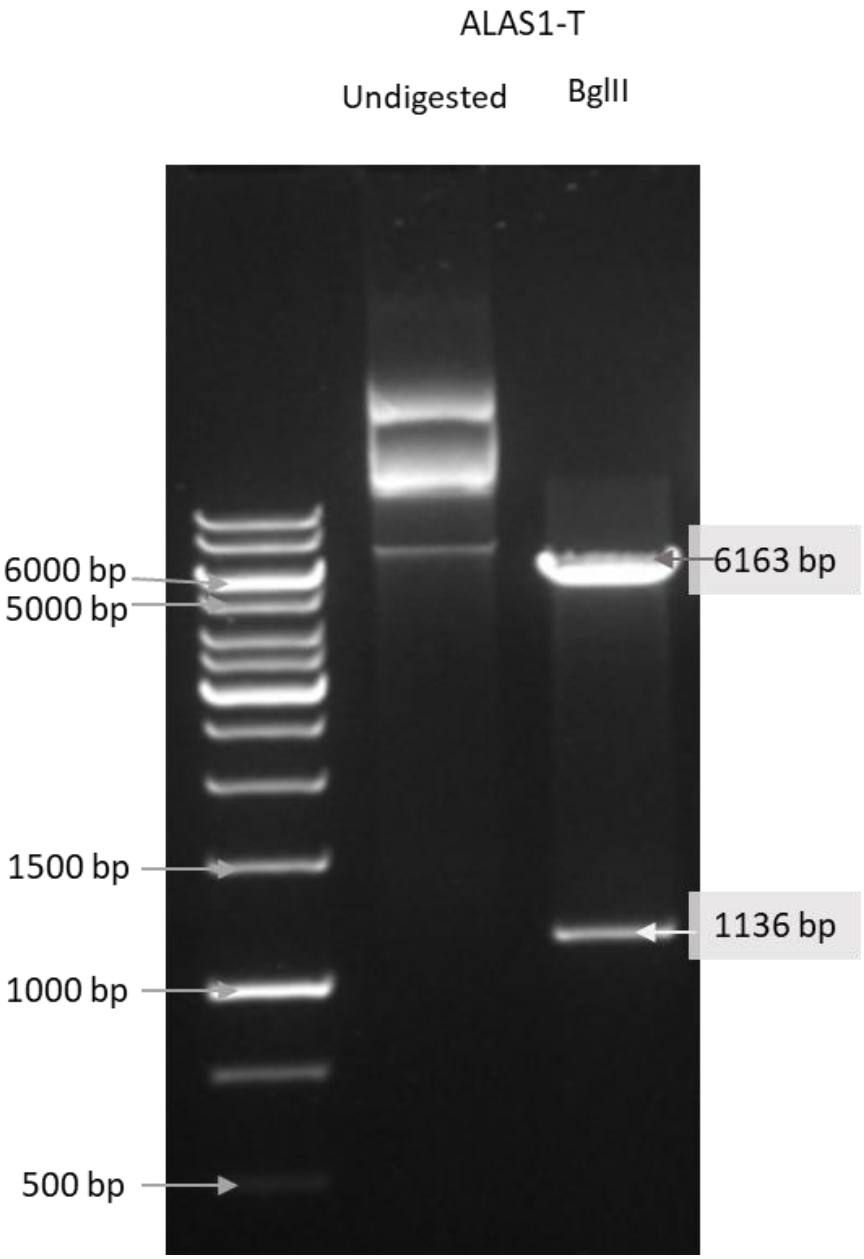

Figure 26 Successful digestion of p28a ALAS1-T*. 1 % agarose analytical gel of p28a ALAS1-T digestion with restriction enzyme BglII. Uncut p28a ALAS1-T was run alongside to allow comparison. DNA was digested with BglII and products separated using gel electrophoresis. The DNA fragments were visualised using a BioRad gel doc system. A 1 kb ladder (ThermoFisher) was run alongside the products to allow for sizing of the fragments. Significant bands labelled with arrows and approximate size.*

4. 2. 3 p28aALAS1-T expression in pGro7 and Rosetta cells

As the BL-21 cells were unable to express ALAS1-T, p28aALAS1-T was then transformed into two different bacterial cell types to investigate their different abilities to express the protein in a soluble form. These transformed cells were grown in auto induction media and a small aliquot of each stage of the expression process was taken to be analysed on an SDS PAGE.

pGro7 cells can produce chaperone proteins to help protein folding. The addition of 0.5 mg/ml arabinose during overnight growth promotes expression of these proteins. The pGro7 cells were therefore grown in two conditions; with and without the expression of chaperone proteins to investigate the effects of the chaperones on the expression of ALAS1-T.

There is some protein expression in pGro7 cells, both with and without chaperones (Figure 27 A and B). However, there appear at a lower weight then would be expected making it unlikely to be the ALAS1-T protein). This is supported by the absence of expression shown in the western blot using 6 X HIS-tag antibody. It confirms the bands shown in the pGro7 expression are expression of ALAS1-T (Figure 27 C).

The Rosetta cells show no clear protein expression in the Coomassie stain at the expected weight (Figure 27 A). Even though there is some protein expression within the total lysate fraction on the western blot (Figure 27 C) it is not present in the soluble fraction section. Suggesting any protein produced was insoluble and therefore not suitable for purification.

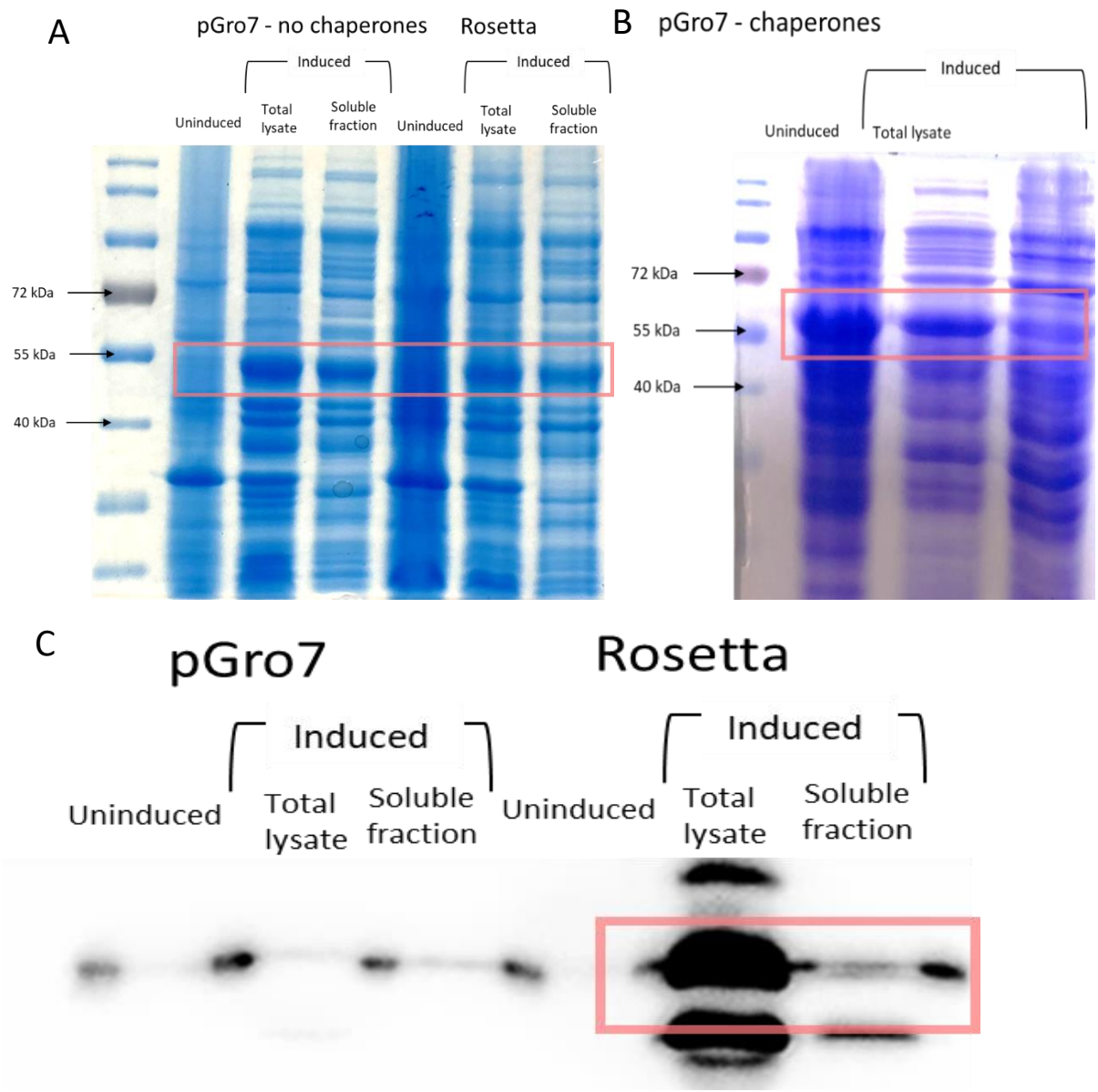

Figure 27 No protein expression of ALAS1-T in rossetta cells or pGro7 cells. *ALAS1-T was transformed into Rosetta and pGro7 cells and grown in a starter culture 8 hours. A sample of this was taken as the "uninduced" fraction. The starter culture was transferred to 2 L flasks containing auto induction media grown at 37 °C for 1.5 hours and incubated overnight at 20 °C (A). (B) Arabinose was added to the overnight growth of pGro7 cells. A fraction of this overnight growth was the "total lysate" fraction. The cells were lysed and passed through an emulsiflex. The lysate was centrifuged, and the soluble fraction was also collected for SDS PAGE analysis. Each fraction was boiled for 30 minutes with 6X loading dye at 85 °C before loading to SDS-PAGE (10 % acrylamide gel) ran at 125 V for 2 hours. (A) The gel was stained with Coomassie stain and incubated at room temperature overnight before being photographed. (C) A western blot analysis was carried out using HIS-tag antibody 1° in 1:20,000 dilution and 2° goat anti-mouse, the image was detected using LuminataTM Forte Western HRP Substrate (Millipore) on a Fusion FX (VILBER LOURMAT). Relevant bands indicated with red box.*

4. 2. 4 Site-directed mutagenesis of ALAS 1 heme regulatory motif does not improve expression.

A study by Munakatah *et al* (2004) discovered that the heme regulatory motif (HRM), a short amino acid sequence within ALAS 1, is important in ALAS 1 transportation within the cell. It was also found that mutagenesis of a cysteine residue within the third HRM to a serine improved the biological half-life of the protein significantly. Based on this knowledge, site-directed mutagenesis of the ALAS1-T protein was carried out to convert the cysteine residue 108 to a serine residue in order to improve the stability of the expressed protein and improve solubility (Figure 28). The sequence was checked using BLAST (Figure 29A) and through analysis of the chromatograms (Figure 29B). The results from the sequencing show the change from TGC (original sequence) to AGC – highlighted (Figure 29 A and B), showing successful insertion of the substitution into ALAS 1. The BLAST sequencing also identified non-aligning sequence at the start of the sequence, but upon analysis of the chromatograms it was deemed that this was due to errors in the Sanger sequencing.

p28a-ALAS1-T_{C108S} was transformed into BL-21 cells, grown in autoinduction media and protein expression investigated. This allowed it to be determined whether the mutation had made the protein more stable in its soluble form. The Coomassie stained gel shows no clear bands at the expected weight of 67.20 kDa in either of the induced columns; total lysate or soluble fraction (Figure 30) showing that no increased expression or solubility was achieved with this mutation.

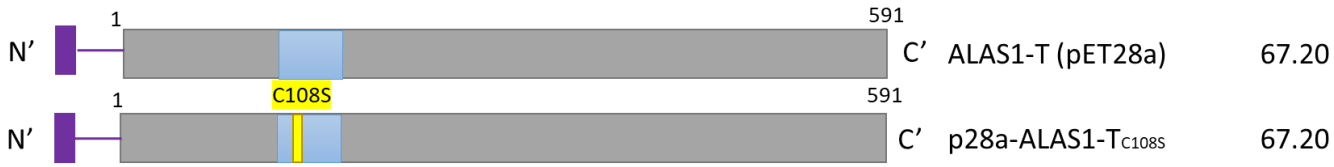

Figure 28 Schematic representing the sizes of the ALAS 1 T protein used for expression and the mutated ALAS1-T_{C108S}. *The yellow box at residue 108 representing the cys residue mutated to a ser. Purple box representing the 19 reside HIS-tag. Blue box representing the HRM residues 107-111. Numbers to the right representing the expected kDa of the proteins once expressed.*

A

PREDICTED: Homo sapiens 5'-aminolevulinate synthase 1 (ALAS1), transcript variant X1, mRNA

Sequence ID: XM_011533477.2 Length: 2370 Number of Matches: 1

Range 1: 434 to 1457 GenBank Graphics ▼ Next Match ▲ Previous Match

Score	Expect	Identities	Gaps	Strand
1724 bits(933)	0.0	996/1024(97%)	14/1024(1%)	Plus/Plus

```
Query  168  TCCATGGCAGCAGTACACTACCAACAGATCAAAGAAACCCCTCCGGCCAGTGAGAAAGAC  227
Sbjct  434  TCCACTGCAGCAGTACACTACCAACAGATCAAAGAAACCCCTCCGGCCAGTGAGAAAGAC  493

Query  228  AAAACTGCTAAGGCCAAGGTCCAACAGACTCCTGATGGATCCCAGCAGAGTCCAGATGGC  287
Sbjct  494  AAAACTGCTAAGGCCAAGGTCCAACAGACTCCTGATGGATCCCAGCAGAGTCCAGATGGC  553

Query  288  ACACAGCTTCCGTCTGGACACCCCTTGCCTGCCACAAGCCAGGGCACTGCAAGCAAAAGC  347
Sbjct  554  ACACAGCTTCCGTCTGGACACCCCTTGCCTGCCACAAGCCAGGGCACTGCAAGCAAATGC  613

Query  348  CCTTTCCTGGCAGCACAGATGAATCAGAGAGGCAGCAGTGTCTTCTGCAAAGCCAGTCTT  407
Sbjct  614  CCTTTCCTGGCAGCACAGATGAATCAGAGAGGCAGCAGTGTCTTCTGCAAAGCCAGTCTT  673
```

B

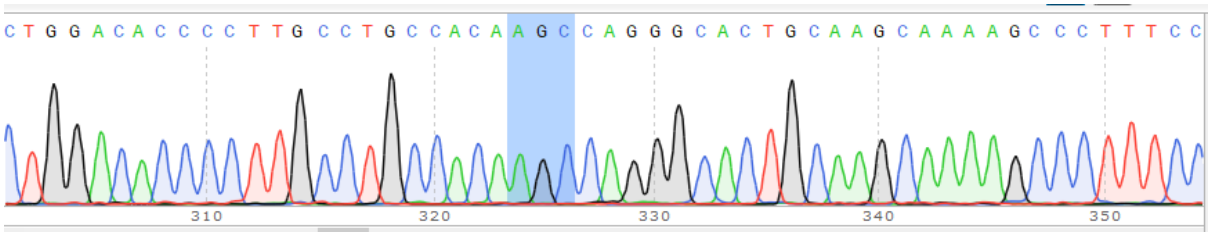

Figure 29 Site directed mutagenesis of ALAS1-T showing a successful mutation C108S. Sequencing carried out by EUROFINS. *Sequence change highlighted in blue on the chromatogram (below) and within a yellow box on the Blast sequence alignment (above). The pET28a ALAS1-T plasmid was mutated using site-directed mutagenesis and transformed into BL-21 cells. The plasmid was amplified and extracted using a mini-prep and sent for Sanger sequencing.*

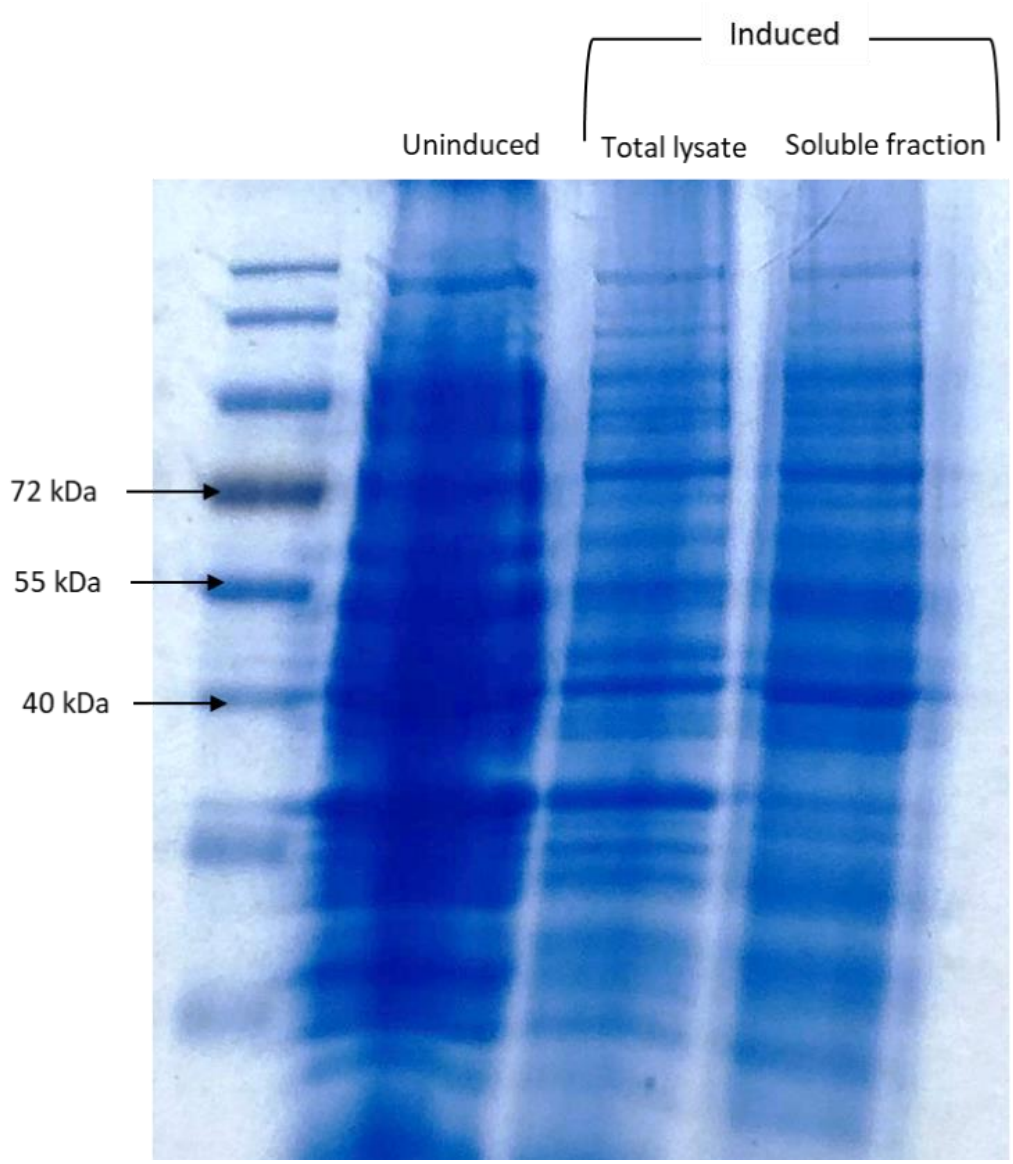

Figure 30 Mutation C108S did not improve stability of ALAS1-T_{C108S} when expressed in BL-21 cells. *ALAS1-T_{C108S} was transformed into BL-21 cells and grown in a starter culture 8 hours. A sample of this was taken as the "uninduced" fraction. The starter culture was transferred to 2 L flasks containing auto induction media grown at 37 °C for 1.5 hours and incubated overnight at 20 °C. A fraction of this was the "total lysate" fraction. The cells were lysed and passed through an emulsiflex. The lysate was centrifuged, and the soluble fraction was also collected for SDS PAGE analysis. Each fraction was boiled for 30 minutes with 6X loading dye at 85 °C before loading to SDS-PAGE (10 % acrylamide gel) ran at 125 V for 2 hours. The gel was stained with Coomassie stain and incubated at room temperature overnight before being photographed.*

4. 2. 5 HIS-tag manipulation from N-terminus to the C-terminus and further truncation of the ALAS1-T protein

After the mutated ALAS1-T did not show expression the ALAS 1 protein was further truncated to discover if this would increase the solubility of the protein. The structure of human ALAS 2 released on the PDB database (6HRH) had the N-terminus signal sequence plus an additional 87 residues cleaved from the WT structure. Theorising that this is the region of the protein causing expression and solubility issues, this principle was applied to ALAS 1. Through modelling (performed by M. Cowan) it was decided that 197 amino acids should be removed from the N-terminus of the protein (termed ALAS1-197). The 6X HIS-tag antibody was also moved from the N terminus to the C terminus (Figure 31) for this construct and the ALAS1-T construct to investigate the effect this would have on the stability and solubility of the protein.

Primers were designed to amplify ALAS1-T from amino acid 197 to 443 (Figure 31) with the addition of *NheI* and *HindIII* sites and PCR using these primers was carried out. After the PCR reaction, the fragment was purified using the monarch PCR & DNA clean up kit and the product was digested with restriction enzymes *NheI* and *HindIII*. The DNA was subsequently visualised using gel electrophoresis (Figure 32). The bands showed the correct sizes of ALAS1-T (1776 bp) and ALAS1-197 (1336 bp) (Figure 33). These fragments were cut out of the gel and each fragment extracted for ligation into either pET21a or pET28a. The final three DNA constructs were named: p28aALAS1-197, p21aALAS1-197 and p21aALAS1-T.

After ligation into the vectors and transformation unto BL-21 cells, colonies were picked and these were mini prepped, and the harvested plasmids cut with restriction enzymes *NheI* and *HindIII* and ran on an agarose gel to ensure the different ALAS 1 constructs had been successfully ligated into the vector. The diagnostic digest showed that one of each construct (p28aALAS1-197, p21aALAS1-197 and p21aALAS1-T) had been successfully created (Figure 33) showing bands at 1776 bp for p21a T and the rest of the plasmid of 5391 bp visible at approximately the correct size (colony A). The p28aALAS1-197

(colony B) was successfully cut to show ALAS1-197 of 1336 bp and the remaining 5319 bp plasmid. p21ALAS1-197 shows some uncut plasmid along the top of the band but the 1336 ALAS1-197 fragment is still visible showing successful ligation into the plasmid. All plasmids were subsequently verified by Sanger sequencing.

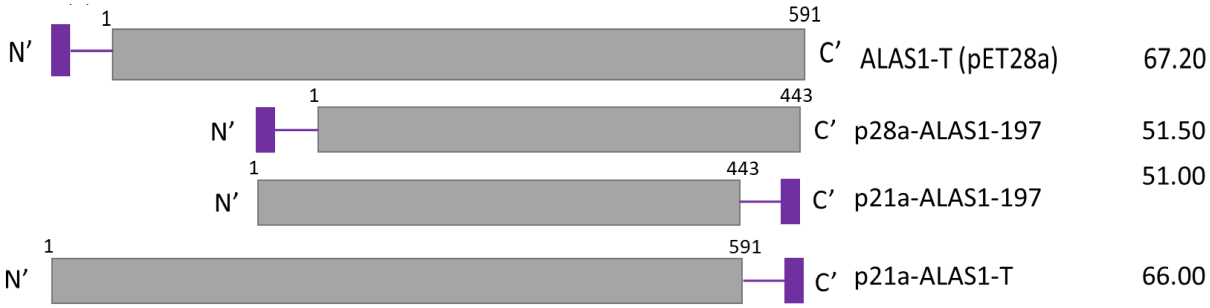

Figure 31 Schematic representing the sizes of the ALAS1-T protein and the new constructs p28aALAS1-197, p21aALAS1-197 and p21aALAS1-T*. Showing the further shortened ALAS 1 and with the HIS-tag moved from the N term to the C term. Purple box at the N' term represents the 19 reside HIS-tag, the C' term HIS-tag is 12 residues.*

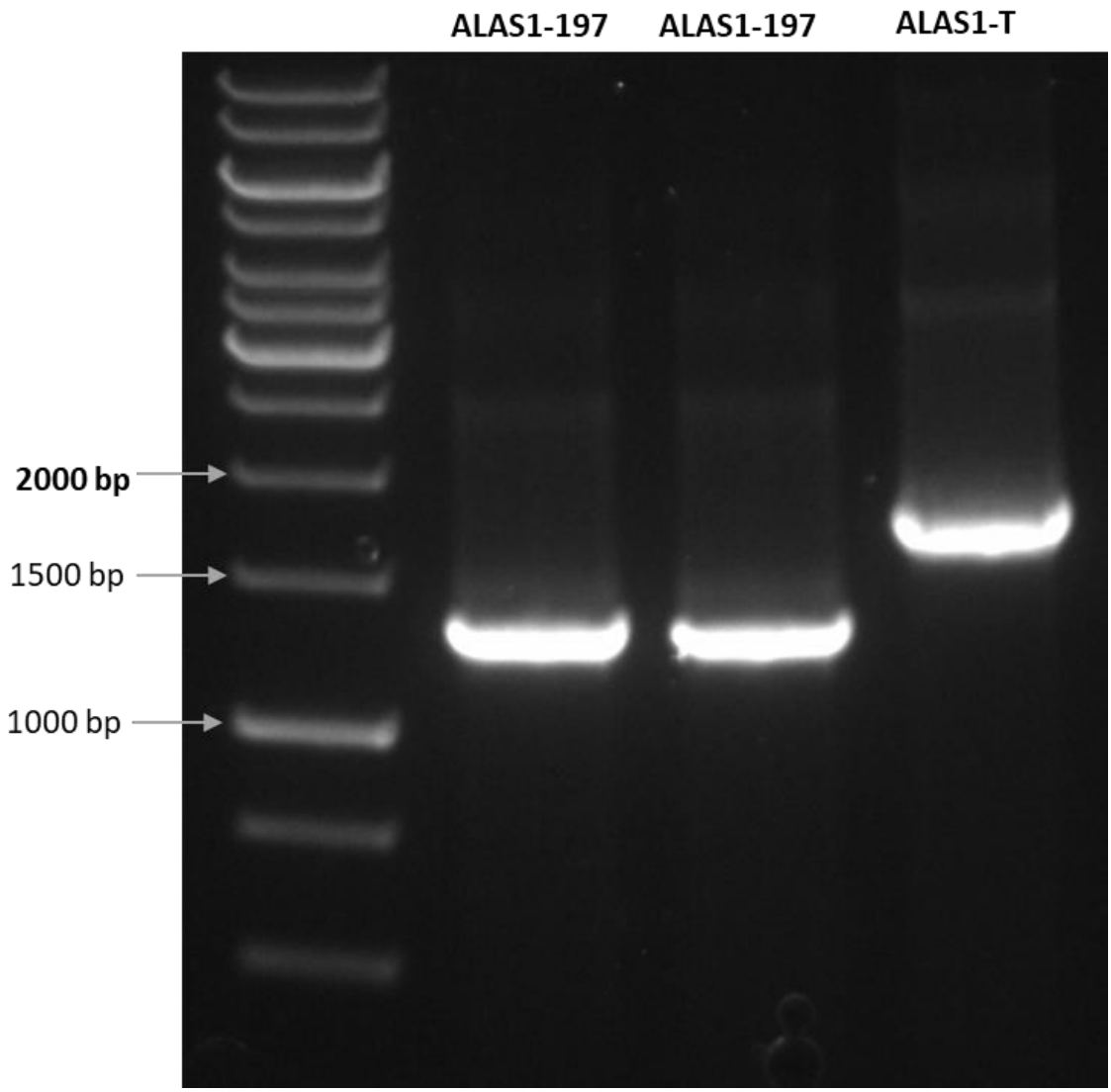

Figure 32 Successful digestion of ALAS1-T and ALAS1-197*. 1 % agarose gel of ALAS1-T and ALAS1-197 digestion with restriction enzyme NheI and HindIII to produce fragments for ligation. DNA was digested with NheI and HindIII and products separated using gel electrophoresis. The DNA fragments were visualised using a BioRad gel doc system. A 1 kb ladder (ThermoFisher) was run alongside the products to allow for sizing of the fragments. Significant bands labelled with arrows and size.*

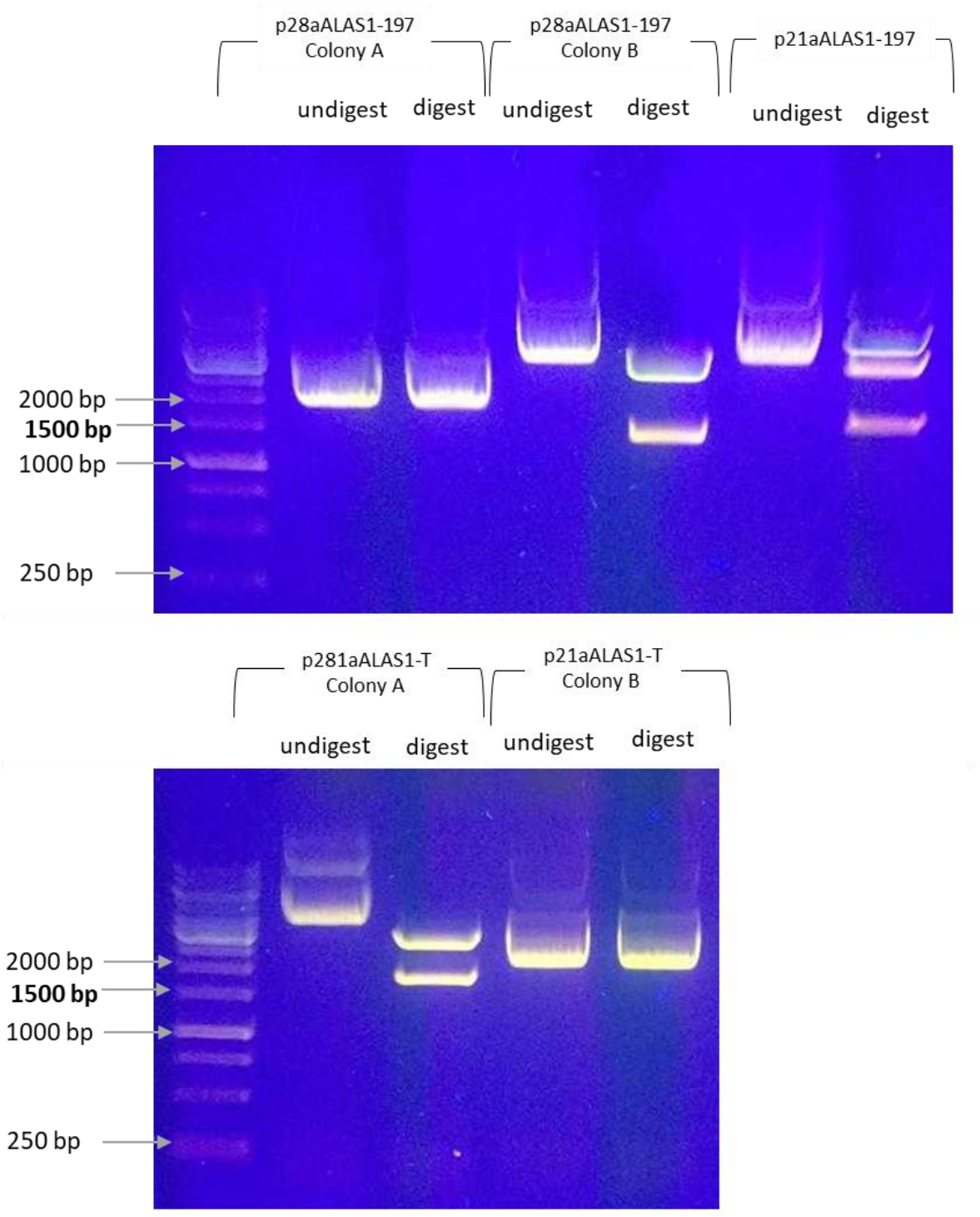

Figure 33 Successful digestion of pET28aALAS1-197, pET21aALAS1-197 and pET21aALAS1-T*. 1 % agarose analytical gel of pET28aALAS1-197, pET21aALAS1-197 and pET21aALAS1-T digestion with restriction enzymes NheI and HindIII.. DNA was digested with NheI and HindIII and products separated using gel electrophoresis. The DNA fragments were visualised using a BioRad gel doc system. A 1 kb ladder (ThermoFisher) was run alongside the products to allow for sizing of the fragments.*

After the plasmids had been verified, the expression vectors were transformed into two cell types; T7 shuffle and BL-21 which were then grown in auto induction media. The uninduced and induced total lysate were analysed by SDS-PAGE without the soluble fraction to screen for any successful protein expression, soluble or not. p28aALAS1-197 and p21aALAS1-197 should produce a shortened ALAS 1 protein with a molecular weight of 51.50/51.00 kDa and the p21aALAS1-T protein have an expected molecular weight of 66.00 kDa. The gel shows bands for all three constructs in the total lysate at approximately the correct weights in both cell types (Figure 34) suggesting that the proteins had been successfully expressed. Some of the band was present in the uninduced and induced fractions; p28aALAS1-197 in T7 shuffle and p21aALAS1-T BL-21. This may suggest leaky expression.

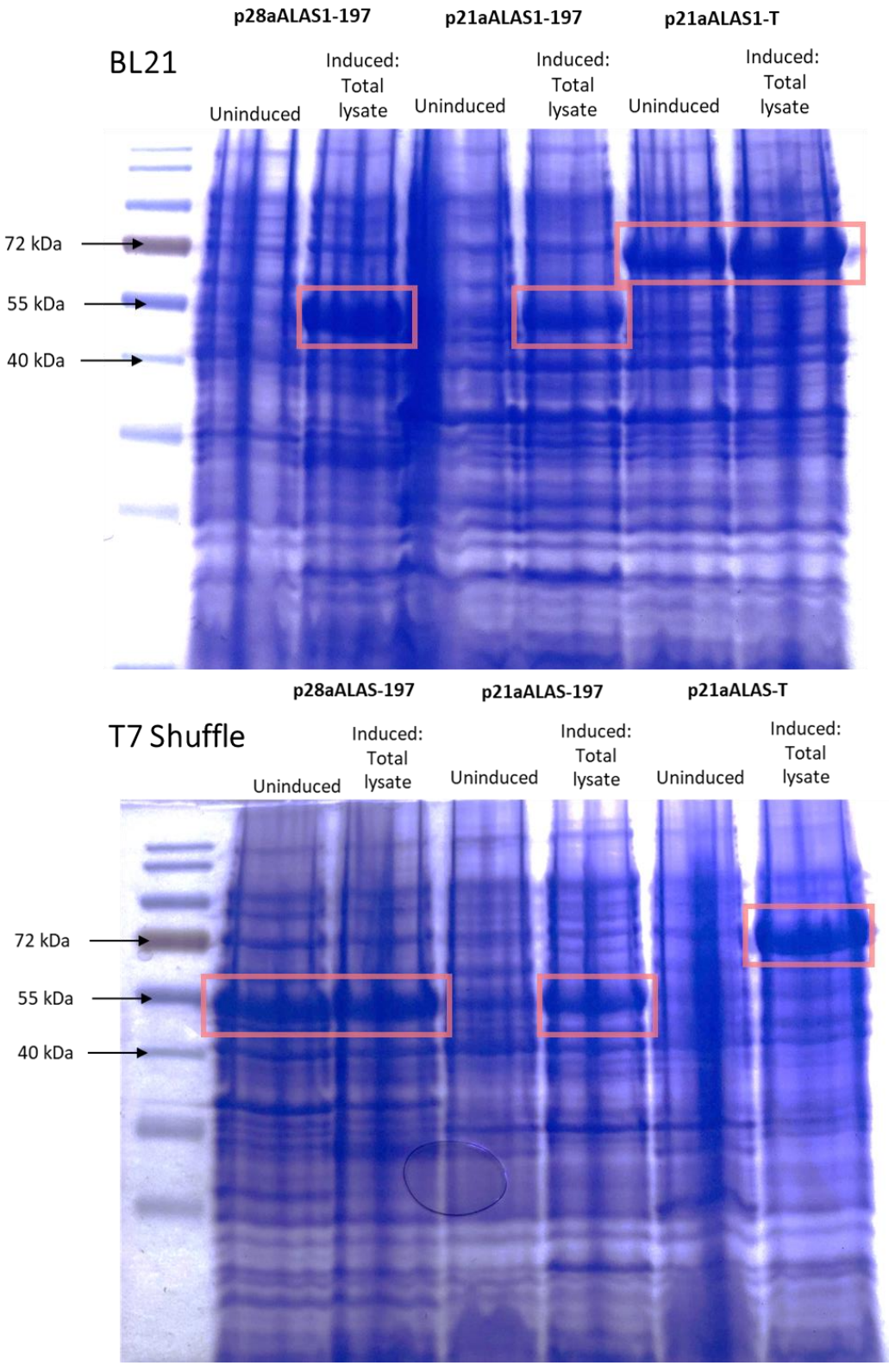

Figure 34 p28aALAS1-197, p21aALAS1-197 and p21aALAS1-T expressed in BL-21 cells (top) and T7 shuffle cells (bottom). *p28aALAS1-197, p21aALAS1-197 and p21aALAS1-T were transformed into BL-21 and T7 shuffle cells and grown in a starter culture 8 hours. A sample of this was taken as the "uninduced" fraction. The starter culture was transferred to 2 L flasks containing auto induction media grown at 37 °C for 1.5 hours and incubated overnight at 20 °C. A fraction of this was the "total lysate" fraction collected for SDS PAGE analysis. Each fraction was boiled for 30 minutes with 6X loading dye at 85 °C before loading to SDS-PAGE (10 % acrylamide gel) ran at 125 V for 2 hours. The gel was stained with Coomassie stain and incubated at room temperature overnight before being photographed. Showing only total lysate to screen for any successful protein expression. Relevant bands are highlighted with a red box.*

p21aALAS1-197, p21aALAS1-T, p28aALAS1-197 within T7 shuffle cells were taken forward for further analysis. These were emulsiflexed and centrifuged to obtain the soluble fraction. This was then separated and visualised using SDS-PAGE and Coomassie staining. The results of the SDS-PAGE analysis for p28aALAS1-197 shows no bands in the soluble fraction section at the expected weight of 51 kDa (Figure 35). This suggests that p28aALAS1-197 vector had not expressed in a soluble form (Figure 35). The other construct p21aALAS1-T with a C-terminal HIS-tag also does not show soluble expression but the p21aALAS1-T (also with the C-terminal HIS-tag) was able to express a soluble form of the protein shown by a band visible at 51 kDa. In future work the p21aALAS1-197 will be used within T7 shuffle cells as the best option for expression using a C-terminal HIS-tag.

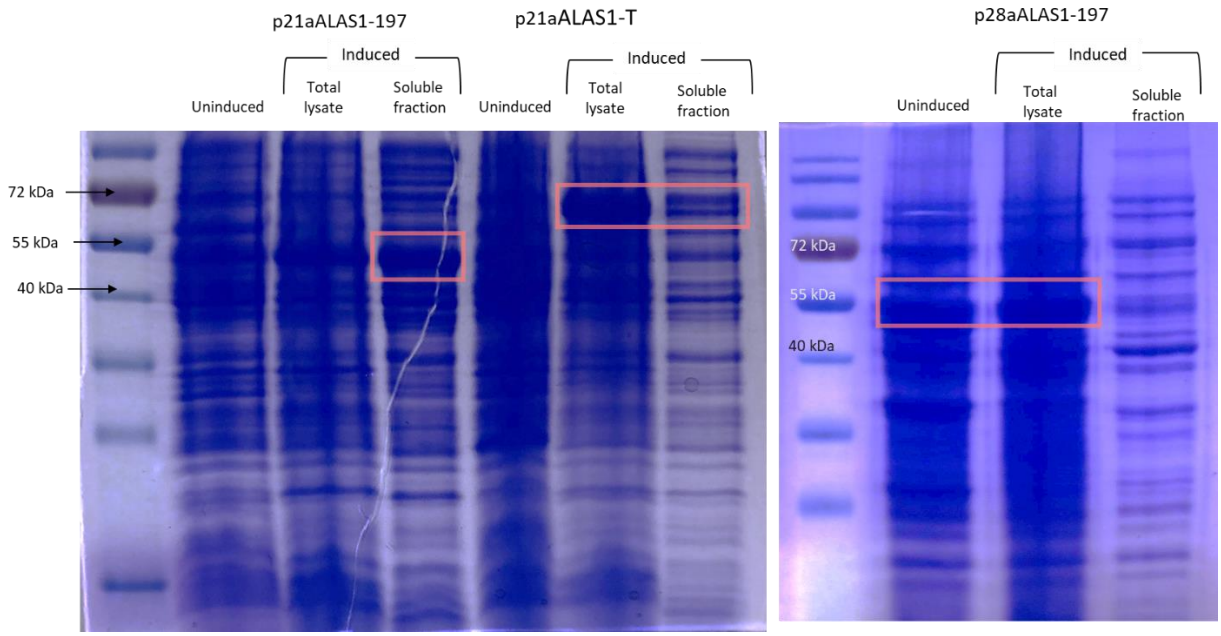

Figure 35 Successful expression of p21aALAS1-197 within T7 shuffle cells*. p28aALAS1-197, p21aALAS1-197 and p21aALAS1-T were transformed into T7 shuffle cells and grown in a starter culture 8 hours. A sample of this was taken as the "uninduced" fraction. The starter culture was transferred to 2 L flasks containing auto induction media grown at 37 ºC for 1.5 hours and incubated overnight at 20 ºC. A fraction of this was the "total lysate" fraction. The cells were lysed and passed through an emulsiflex. The lysate was centrifuged, and the soluble fraction was also collected for SDS PAGE analysis. Each fraction was boiled for 30 minutes with 6X loading dye at 85 ºC before loading to SDS-PAGE (10 % acrylamide gel) ran at 125 V for 2 hours. The gel was stained with Coomassie stain and incubated at room temperature overnight before being photographed.*

5.0 Chapter five Discussion

5. 1 Investigating heme synthesis as a treatment option for prostate cancer

The prostate cancer cell lines used were LNCaP, PC3 and DU145 cells and represent different stages of the disease. LNCaP cells were originally derived from lymph nodes (Horoszewicz et al., 1983). LNCaP cells express androgen receptor and prostate specific antigen (PSA), are androgen dependent and tend to grow at a slower rate relative to other prostate cancer cells lines (Tai et al., 2011). PC3 cells were originally derived from bone metastases. These cells do not express androgen receptor and have characteristics of castrate resistant disease and are considered to be a model of aggressive PC (Tai et al., 2011). DU145 cells also provide a model of castration resistant PC that was originally a derivative of a central nervous system metastasis (Scaccianoce et al., 2003).

A number of enzymes within the heme synthesis pathway have been found to be up regulated in prostate cancer (Brooke et al. unpub). SA has been used in many studies to investigate the effect of heme synthesis pathway on cancer by targeting ALAD (ALA dehydrogenase), the second enzyme in the pathway (Lee et al,. 2019). ALAD acts when ALA moves into the cytoplasm where ALAD condenses and cyclizes two molecules of ALA (Del and Batlle 1993). SA was used in this study to determine if heme synthesis is a viable target for prostate cancer treatment. The results of the growth assays showed that the addition of SA decreased the proliferation of all three cell lines in a dose dependent manner. DU145 appear to be the most sensitive to SA, having an IC_{50} value of 16.2 mM. This data suggests that the targeting of this pathway can effectively inhibit PC proliferation. This has also been shown in previous studies, such as Weinbacha and Elbert (1985), where SA was found to be a potent suppresser of growth and heme synthesis in L1210 leukemia cells. Another study found SA was able to induce cell cycle arrest in HeLa cells, drastically reducing their growth (Ye and Zhang 2004). A similar decrease in growth was found in NSCLC cells also treated with SA (Hooda et al,. 2015).

To show that SA was inhibiting PC proliferation by interrupting the heme synthesis pathway and not via another mechanism, heme was added to the cells treated with SA to see if this would rescue the phenotype. Partial heme rescue was shown in all the cell lines, at a concentration of 200 μM of SA, showing that SA does block heme synthesis. This is supported by studies such as Ye and Zhang (2004) that show SA inhibition of HeLa proliferation can be partially rescued with the addition of heme. Further, cell death induced by SA treatment could be reversed by heme added 6 days before SA treatment. The heme content of cells treated with varying concentrations of SA was measured to further investigate the effects of SA on inhibiting the heme synthesis pathway. The results support the findings that heme production is being stunted as all three cell lines show a reduction in heme content as the concentrations of SA increases. PC3 and DU145 cells showing a significant decrease in heme content when cells were treated with 2 M SA. This therefore suggests that the heme synthesis pathway could be a suitable novel treatment option for prostate cancer. However, the effect of SA should also be assessed on non-tumorigenic cell lines (e.g. PNT1A) to see if the effects are cancer specific.

It has been shown that inhibition of the heme synthesis pathway can sensitise cancer cells to other existing therapies. A study that depleted UROD (uroporphyrinogen decarboxylase, the last enzyme in the heme synthesis pathway) levels in head and neck cancer cells found that radiation induced cell death increased. The group also demonstrated that depletion of UROD stunted the tumour formatting abilities of the cells and delayed tumour growth in mouse models (Ito et al,. 2011). They found that this increase in radiation sensitivity was due to the interruption of the heme synthesis via the lack of UROD and an increase in ROS damage. This method of downregulation of UROD also sensitised other human tumour cells to other agents currently used in chemotherapy (Ito et al,. 2011). For this reason, SA drug combinations, namely MK2206 and A-1155463, were investigated in this study.

The MK2206 drug is an AKT (protein Kinase B) inhibitor that allosterically inhibits the serine/threonine protein kinase (AKT) within the phosphoinositide 3-kinase (P13K) signalling pathway, appearing at a

signalling node downstream of P13K (Carnero et al,. 2008). Because of its role in cell proliferation and inhibition of apoptosis, an unregulated P13K/AKT signalling pathway can become a factor in a tumorigenesis and progression to treatment resistance (Hirai et al., 2010). This means that an AKT inhibitor could be of use for a tumour that has increased P13K/AKT signalling and reduced sensitivity to cytotoxic agents.

PTEN is a protein that can negatively regulate this AKT signalling pathway (Vlietstra et al., 1998). There are many studies to support the idea that the P13K/AKT pathway and/or the *PTEN* gene is altered in prostate cancer cells lines. Sarker et al,. (2009) found that deregulation of the P13K pathway is being increasingly found in prostate cancer patients, with 30 % of castration resistant patients having one form of mutated *PTEN* gene. Abnormal P13K/AKT signalling has been detected in PC cell lines as well as in 30-50 % of primary prostate cancer tissues within humans (Morgan et al,. 2009). It has also been found that there are alterations in 42 % of primary prostate cancer cells within the P13K/AKT pathway and within metastatic tumours 100 % had P13K/AKT mutations (Taylor et al,. 2010). An increased growth was displayed in embryonic stem cells that were lacking the function of the *PTEN* gene even in absence of serum. PTEN mutated embryonic stem cells also presented an advanced entrance to S phase, accelerating progression through the cell cycle (Sun et al., 1999). It was found in the PC3 cell line that there is a large *PTEN* homozygous deletions. In the LNCaP cell line, it has been found that there is a frame shift in *PTEN* (Vlietstra et al., 1998).

It has been found that combining MK2206 with anticancer agents can synergistically inhibit cancer cell proliferation in various cell lines (Hirai et al., 2010). MK2206 has been used in combination with agents such as epidermal growth factor receptor inhibitors, antimetabolites, anti-microtubule agents (such as docetaxel) and DNA cross linkers. All of these combinations showed a substantially stronger tumour inhibition action than each drug individually (Hirai et al., 2010). This therefore demonstrates that MK2206 can improve the efficiency of existing therapies for cancer patients receiving other targeted treatments.

A study (Narayan et al., 2017) found MK2206 to reduce phosphorylation of thr308 and ser473 of AKT and were able to show a difference in sensitivity to irradiation when glioma cells were co treated with MK2206. Because of the potential synergistic effects of MK2206 and due to this pathway often being mutated or deleted in LNCaP and PC3 cells (Vlietstra et al,. 1998), MK2206 was tested with these two cells lines as a co-treatment alongside SA. It would be expected that MK2206 would have an effect on the growth of the LNCaP and PC3 cells due to their *PTEN* mutations and the treatment of these two cell lines with MK2206 has been proven to inhibit the AKT pathway (Floc'h et al,. 2012). It has been shown that MK2206 can inhibit growth, induce apoptosis and encourage cell cycle arrest (Al-Saffa et al,. 2018) by the AKT inhibition of PC3 cells. A reduction in the proliferation of LNCaP cells has also been demonstrated with MK2206 treatment (Floc'h et al,. 2012). However, in my hands, there was minimal decrease in growth at the highest concentrations of MK2206 tested and it was found that there were no significant synergistic effects of this drug combined with SA. Higher concentrations of MK2206 may therefore need to be tested in future.

The studies showing MK2206 did have synergistic effects used drugs that target cell DNA synthesis for cell division or the cell division itself (Hirai et al., 2010) or radiation (Ito et al,. 2011). These therapies work in a very different way to SA's inhibition of heme synthesis as SA does not target the cell cycle specifically, potentially being a reason for MK2206 inability to work synergistically against cell growth in these cells.

As well as the P13K/AKT mutations, *BCL-XL* over expression has been found in PC3 and LNCaP cells (Castilla et al., 2006). A-1155463 is a highly potent and selective inhibitor of BCL-XL (B-cell lymphoma) proteins (Tao et al,. 2014). BCL-XL is a member of the BCL-2 family. The BCL-2 family are a group of proteins that regulate apoptosis and can act as anti or pro-apoptotic regulators (NCBI BCL2L1), they share at least 1 of the 4 domains; BH1, BH2, BH3 and/or BH4. BCL-XL acts as a potent antiapoptotic protein. BCL-2 proteins are involved heavily in the mitochondrial apoptosis pathway. The proapoptotic modulators BAX and BAK are needed for this pathway. BCL-2 and BCL-XL inhibit the release of these

proapoptotic molecules from the mitochondria. When under stress BH3-only proteins inhibit anti-apoptotic BCL-XL proteins causing BAX and BAK oligomerization, further activating a caspase cascade causing cell death (Jong et al., 2018).

Cancer cells commonly increase expression of anti-apoptotic proteins like BCL-2 to make caspase activation more difficult and thus halting cell death. A chemotherapy treatment usually requires an ability to cause cell death and so BCL-2 increase can create chemotherapy resistance. This results in an intertest to develop drugs to inhibit BCL-2 proteins that is allow cancer cells to evade death and become resistant to treatment (Leverson et al., 2015). A-1155463 is a drug that can inhibit this mechanism of resistance by binding and neutralizing BCL-XL members that are pro-survival and inducing apoptosis via release of BAX and BAK proteins. As high *BCL-XL* expression is needed for apoptosis inhibition in response to cellular stresses, BCL-XL acts to inhibit BAK and this inhibition contributes to the progression and androgen resistance of prostate cancer cells via its over expression (Castilla et al,. 2006).

The results of the proliferation assays showed that there was very little to no benefit to using A-1155463 alongside SA in both PC3 cells and LNCaPs. The LNCaP cells do show a slight response to the A-1155463 drug but the PC3 cells showed no decrease or any change in proliferation with the addition of A-1155463. As discussed later, the mechanism of cell death induced by SA does not appear to be apoptosis, and hence inhibition of the anti-apoptotic protein BCL-2 may not enhance cell death.

5. 2 SA appears to promote CICD

Death is essential for many developmental functions and for homeostasis within adult tissue. Necroptosis is best described as a regulated form of necrosis. During apoptosis a cell shrinks, blebs, chromatic condensed and phagocytosis is performed by adjacent cells (Nagasaka et al,. 2010). This means that during apoptosis, the cellular contents are not released, and this does not trigger an

immune reaction (Linkermann and Green 2014). Necroptosis, however, initiates an immune reaction as the cellular contents are released. Damage related pattern molecules (DAMPs), for example mitochondrial DNA and HMGB1, are recognised by cells of the immune system (Linkermann and Green 2014). Although the vast majority of current anti-cancer therapeutics promote cell death via apoptosis, cell death via necroptosis has been proposed to be a more effective way to kill tumours, due to engagement of the hosts immune system (Giampazolias et al,. 2017). There is therefore great interest in the identification of therapies that promote necroptosis. It was determined whether the PC cells used in this study were dying due to necroptosis or apoptosis in response to SA. The inhibition of heme synthesis in PC cells does not induce cell death by apoptosis but does induce a low level of CICD.

Reactive oxygen species (ROS) are natural by-products of normal respiration within the mitochondria, particularly the electron transport chain, and other oxygen involving biochemical reactions. ROS is toxic to cells at too high levels but can be reduced by antioxidant defences (Oberley 2002). Hemo-proteins downstream of heme synthesis, for example cytoglobin, are important in protecting cells from ROS damage. Cytoglobin has also been found to significantly reduce ROS induction within a cell to protect ROS induced DNA damage (Hodges et al,. 2008) and has been reported to have ROS scavenger functions (Zorov et al,. 2014). Cytoglobin can protect from chemically induced ROS DNA damage when over expressed in cancer cell lines, downregulation of cytoglobin also was found to sensitise the cancer cells to ROS damage (McRonald et al,. 2012).

Hydrogen peroxide (H_2O_2) can be used to induce ROS damage within cells as it can be converted to 2 hydroxyl radicals ($2OH^{\bullet}$) (Indo et al., 2007). H_2O_2 causes ROS damage by its downstream product the hydroxyl radical (OH). OH radicals are highly reactive and can induce breaks within single strands of DNA and can cause lipid peroxidation (Bandyopadhyay et al,. 1999). Indo et al., (2007) demonstrated that H_2O_2 treatment results in high levels of ROS and an increase in the expression of associated stress protein HO-1 (heme oxygenase-1). The increase in ROS and HO-1 was followed by an increase in cell

death (Indo et al., 2007). HO-1 is a regulatory enzyme that cleaves heme to form the potent antioxidant biliverdin (converted to bilirubin reductase) which protects the cell from ROS damage and therefore ROS damage induced death (Wang etal., 2018).

SA inhibits heme synthesis and so would deplete the cell of ROS scavengers, leaving the cell vulnerable to ROS. This, alongside the addition of H_2O_2 will offset the ROS production/antioxidant capacity balance causing the cells to die from ROS damage. This was shown to be true in the flow cytometry experiments within this study H_2O_2 was used to induce ROS damage in cancer cells treated with SA. When the cells were treated with SA and H_2O_2 there was a significant increase of CICD.

To investigate if the CICD was necroptosis, the cells were treated with the caspase inhibitor Z-VAD, the necroptosis inhibitor necrostatin and the ferroptosis inhibitor ferrostatin. Z-VAD is an interleukin-1β converting enzyme-like (ICE-like) protease inhibitor and is a broad-spectrum caspase inhibitor that can modulate three types of cell death. Necrostatin acts as a small molecule inhibitor of necroptosis and has been found to act as a selective allosteric inhibitor of RIPK1 in vitro (Degterev et al., 2008). Ferroptosis is associated with iron-dependant unchecked accumulation of lipid hydroperoxides (Zilka et al., 2017). Ferrostatin had been determined by High-throughput screening to inhibit the ferroptosis mechanism.

As expected, Z-VAD had no effect on the amount of cell death by apoptosis or CICD when treated with SA and H_2O_2. Confirming that caspases are not required for the method of cell death. It was theorised that necroptosis was taking place, so it was surprising that the addition of necrostatin did not affect the amount of CICD taking place with SA and H_2O_2 treatment. Ferrostatin also had no impact on the levels of CICD. The DU145 cells could therefore be dying via another unknown form of CICD and this requires further investigation.

Cytokines such as tumour necrosis factor (TNF) have also been shown to be important regulators of necroptosis (Linkermann and Green 2014). TNF-α is a soluble cytokine, a part of the TNF ligand family, with many cellular targets. Production of TNF-α is activated by the immune system. Produced

predominantly by macrophages, TNF-α is also produced by a wide collection of tissues and cell types (Wajant et al., 2003). It has a significant role in regulating injury or infection caused inflammation via TNF-α. This is done through their cognate membrane receptor the TNF receptor (TNF-R) family, mainly by TNFR1. This signalling pathway goes on to induce expression of genes that can regulate inflammation. Under the correct condition's TNF-α can induce cell death and therefore is able to have a cytotoxic effect on tumour cells in some animal models (Wajant et al., 2003). In agreement with the necrostatin experiments, *TNF-α* expression was not induced by SA.

The different methods of cell death can regulate one another. For example, the inactivation of caspases causes cell death to move from apoptosis to a death expressing necrotic and apoptotic features (Galluzzi and Kroemer 2008). Necrosis has many initiators, modulators and effectors described and so the mechanism is intricate and difficult to reach a consensus (Jouan-Lanhouet et al., 2012). Necroptosis signalling pathway involves RIPK3 (receptor interacting protein kinase 3) and RIPK3 can act as a cellular regulation of necroptosis and RIPK1 is also involved in triggering or inhibiting necroptosis and apoptosis (Pasparakis and Vandenabeele 2015). RIPK1 actually is a regulator of many signalling pathways such as the caspase-8-dependant apoptotic pathway, NF-κB pathway and the MAP kinase cascade (Pasparakis and Vandenabeele 2015).

FADD is a Fas-associated protein that works as an adaptor to bridge death receptor signalling to the caspase cascade. It is required for the extrinsic activation of apoptotic cell death (Osborn et al,. 2010). The adaptor protein FADD is critical for death receptor mediated apoptosis (DR-). FADD is made up of two domains: the death domain (DD) and the death effector domain (DED). The FADD DD binds to death receptors DD causing FADD to use its DED to interact with procaspase-8 DED to form a signalling complex (DISC). Procaspase 8 self cleaves and becomes active and cleaves downstream effector caspases causing induction of apoptosis (Lee et al., 2012).

There has been some evidence from *in vivo* mice studies that suggest FADD plays a negative role in RIP1 & 3 dependent necroptosis. The DR mediated apoptosis required FADD causing prevention of

necroptosis via cleavage of RIPK 1 & 3. A FADD deficiency can inhibit apoptosis and activate necroptosis (Lee et al., 2012). Because of these potential effects on the cell death flow cytometry was then used to further investigate how FADD will affect the method of cell death. Three cell lines were used; DU145, DU145 FADD 1b, DU145 FADD 2b. 1b and 2b had been modified using CRISPR to create FADD knock-out clones. There was no difference in cell death found in either of the knocked-out cell lines. Suggesting a FADD independent cell death.

6.0 Chapter six – ALAS expression

The first part of this project demonstrated that heme synthesis could be a viable treatment option for prostate cancer. To improve specificity, it is proposed that the first and rate-limiting step of heme synthesis, carried out by ALAS, should be targeted. ALAS was first discovered by Shemin and Neuberger (Shemin 1958; Gibson 1958) and exists as two isoenzymes: ALAS 1 and ALAS 2. ALAS 1 is expressed in all cell types and ALAS 2 is produced only in developing erythrocytes (Riddle 1989). Research by the Brooke group (unpub) has shown that ALAS 1 is upregulated in prostate cancer cells. This makes ALAS1 a much more attractive target for heme synthesis inhibition as a prostate cancer therapy. It. ALAS works via an ordered kinetic mechanism whereby glycine binds first then followed by succinyl-CoA and aminolevulinate being released last, after CoA and CO_2 (Zhang and Ferreira 2002). This process follows a three steps kinetic reaction as there is a formation of an intermediate Michaelis complex. The crystal structure of ALAS 2 has been solved (PDB), however no structural information exists for ALAS 1. To facilitate a future drug discovery program, and to generate recombinant protein for biochemical assays, this project aimed to express and purify the 2 isozymes.

E. coli is a fast and robust system for protein expression and can perform post-translational modifications carried out in a eukaryotic cell. However, the rapid speed in which it expressed proteins often results in misfolded/unfolded protein, especially heterologous proteins that, to fold correctly, require longer fold times or molecular chaperones to assist correct folding. Combined with the reductive environment of the bacterial cytosol this often results in insoluble expression of proteins (Francis and Page 2010). BL-21, and its derivatives, are the most popular strain of bacteria used for protein expression studies. BL-21 cells are deficient in OmpT protease and Lon protease, which facilitates the recombinant proteins to accumulate and decrease their likelihood to degrade during purification (Donahue and Bebee 1999). For these reasons BL-21 cells were used for initial protein expression experiments. The overexpression of a recombinant protein can have a toxic effect on *E. coli* cells, but this was minimised by cloning the gene into a vector with the lac operon that is

controllable with auto induction media. This allowed for a high density of culture to be grown before ALAS expression was induced. BL-21 cells were unable to express ALAS2-T, ALAS1-T or ALAS1-T_{C108S} but were able to produce ALAS1 protein in the total lysate from the plasmids p28aALAS1-197, p21aALAS1-197 and p21aALAS1-T. In future work these constructs could be investigated for how well they can purify from this strain.

T7 shuffle cells are designed to produce disulphide bonded active proteins that are correctly formed, to accumulate high yield of protein within cytoplasm. The shuffle strain is based on the trxB gor suppressor strain SMG96. In these strains cytoplasmic reductive pathways are depleted to ensure correct formation of disulphide bonds (Lobstein et al., 2012). Rosetta cells are derivatives of BL-21 cells and were designed to improve expression of eukaryotic proteins that contain codons that are not often found within *E.Coli.* Because of this the ALAS2-T and ALAS1-T were expressed within both T7 shuffle and Rosetta cells. ALAS2-T was able to be expressed and purified in Rosetta cells, however ALAS1-T was unable to be expressed. Purified ALAS 2 produced in Rosetta cells will be used in the future for biological assays and crystallography studies to provide insight into the structure of the ALAS protein and help to investigate the possibly of targeting ALAS 1 for a PC therapy.

Modelling carried out by Megan Cowan suggested that the core and C-terminal of ALAS 1 is structured (Cowan uppub.). In comparison, the N – terminus is unstructured and was therefore predicted to be unlikely to be suitable for crystallisation studies. For expression analysis, ALAS1 was therefore truncated at amino acid 197 to remove the unstructured region. The 3 new proteins created were expressed in T7 shuffle cells and BL-21 cells. pET28 a and pET21a were used for this due to their placement of HIS-tags. Each have a HIS-tag placement at different positions of the heterologous protein (C- terminal his tag for pET28 a and N-terminal pET21a). The movement of the HIS tag was intended to improve the solubility and correct folding of ALAS1 once expressed. All three constructs were produced in BL-21 and T7 shuffle cells but p21aALAS1-197, p21aALAS1-T, p28aALAS1-197 within T7 shuffle cells were taken forward for further analysis. This demonstrated that ALAS1 could be

successfully expressed under these conditions and therefore provides a resource for future biochemical assays and crystallography studies.

7.0 Conclusion and future work

This study aimed to validate porphyrin synthesis as a therapeutic target for PC. It was found that SA does reduce the growth of LNCaP, PC3 and DU145 cells by inhibition of their heme synthesis pathway therefore validating it as a target. However, future work should be done on other non-cancerous cell lines, such as PNT1A to investigate if this effect is cancer specific. This will provide important information on the potential side-effects of such a therapeutic strategy. SA was found to promote CICD in the DU145 cells and not apoptosis. This effect was increased dramatically with the introduction of ROS damage, displaying that heme inhibition sensitises PC cells to ROS damage. The CICD was found not to be necroptosis or ferroptosis and was FADD independent, suggesting another, potentially new, form of CICD. Further analysis should be done to further investigate alternative cell death mechanisms. *TNF-α* expression was not induced by SA, but this should be repeated on cells treated with SA and H_2O_2.

For future drug discovery studies, the project aimed to express ALAS1 and ALAS2 in bacteria. ALAS2-T was successfully purified from Rosetta cells. ALAS1-T was also able successfully expressed in a soluble form in T7 shuffle cells. The expression and purification of these isozymes can now be scaled up to provide sufficient material for crystallography and biochemical assays to facilitate the identification of ALAS1 specific inhibitors.

8.0 Project pros and Cons.

This project was successfully able to validate the porphyrin synthesis pathway as a potential target for prostate cancer treatment. The purification of ALAS 2 and expression of ALAS 1 were also successfully carried out. There were some drawbacks however that are to be noted. These include the TNF-a protein and gene expression measurement experiments. These only show the TNF-α protein levels and expression when the cells are treated with SA alone. Cell death assays carried out later in this study showed that SA induced a low level of cell death and that the drug was cytostatic. It therefore fits that these experiments did not show an increase in TNF-α expression. The flow cytometry studies did however show that with the combination of SA with H_2O_2 induced cell death and so the TNF-α protein and expression level study should be repeated with this combinatorial treatment.

The flow cytometry experiments also had some limitations. They were unable to show exactly how the cells are dying when exposed to H_2O_2 and SA. Controls that are known to induce apoptosis, necroptosis and ferroptosis could have been used to determine if the cells are able to die by these methods and to confirm that the respective inhibitors were active. These controls could have also been used alongside the inhibitors, for example, an apoptosis inducing drug such as TRAIL (tumour necrosis factor (TNF)-related apoptosis inducing ligand) could be used to induce apoptosis in the cells also treated with Z-VAD. This would demonstrate if the action of Z-VAD is working and inhibiting the apoptosis caused by TRAIL. Using the cell death inhibitors Z-VAD, Necrostatin and ferrostatin in varying combinations could also have been carried out to investigate if the cells were switching between different methods of cell death when only one was inhibited.

APPENDIX

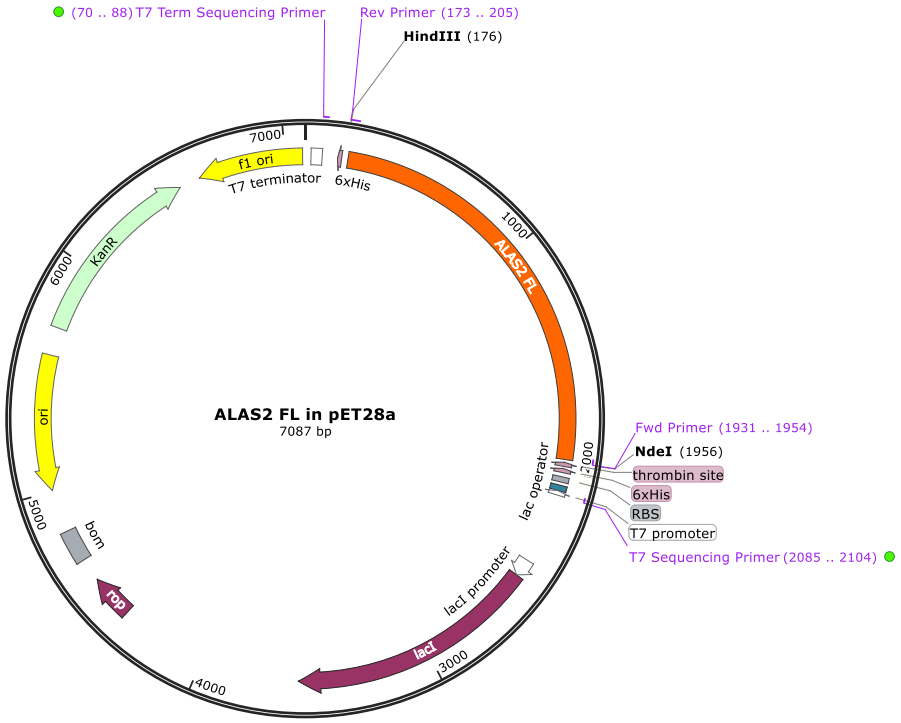

Appendix Figure 1 ALAS 2 full length cloned into pET28a vector. Plasmid map generated using SnapGene

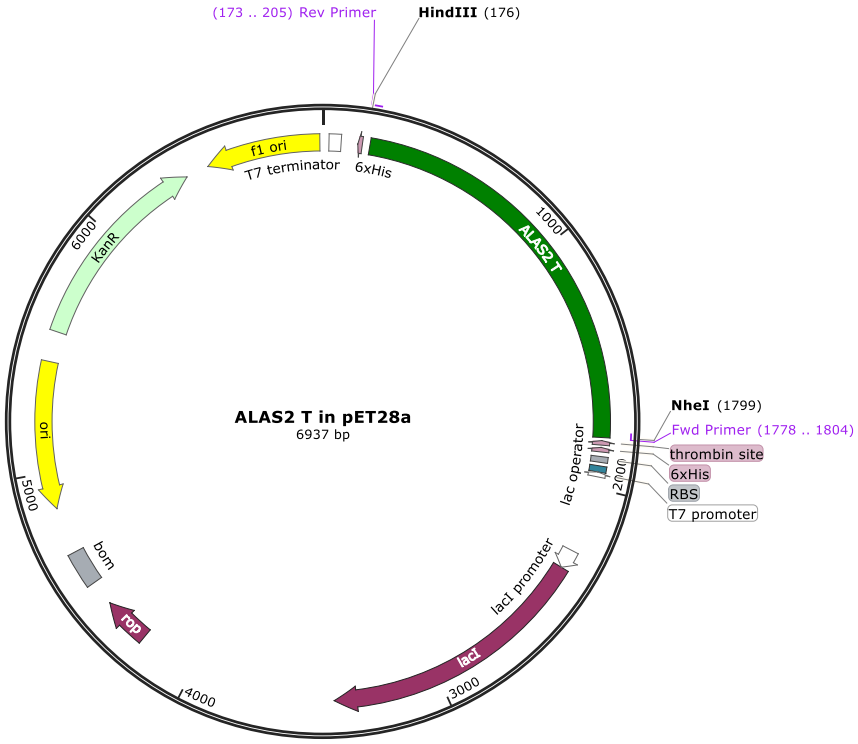

Appendix Figure 2 ALAS2 T cloned into pET28a vector. Plasmid map generated using SnapGene

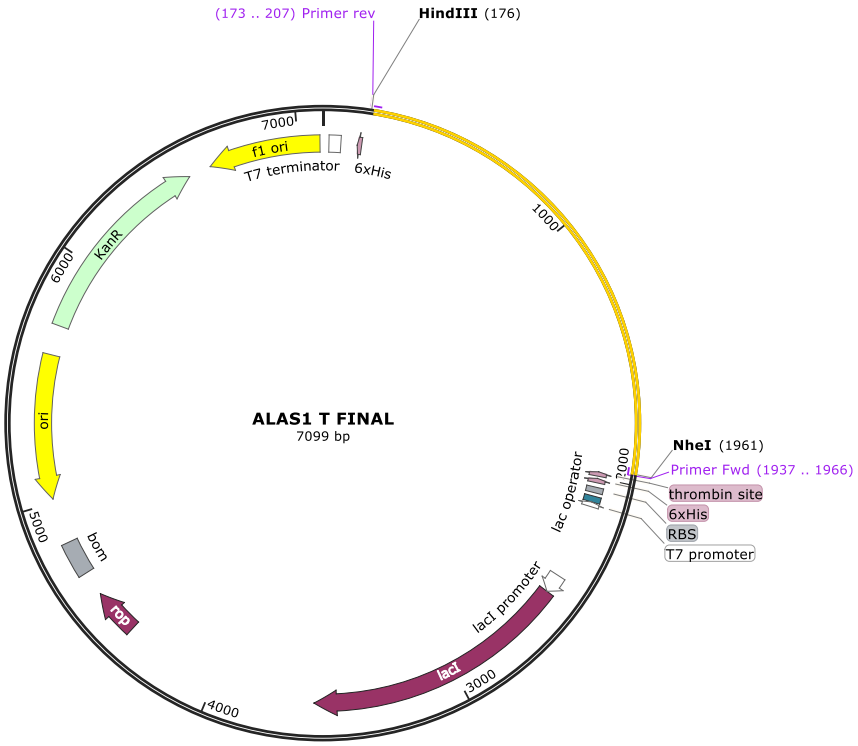

Appendix Figure 3 ALAS1 -T cloned into pET28a vector. Plasmid map generated using SnapGene

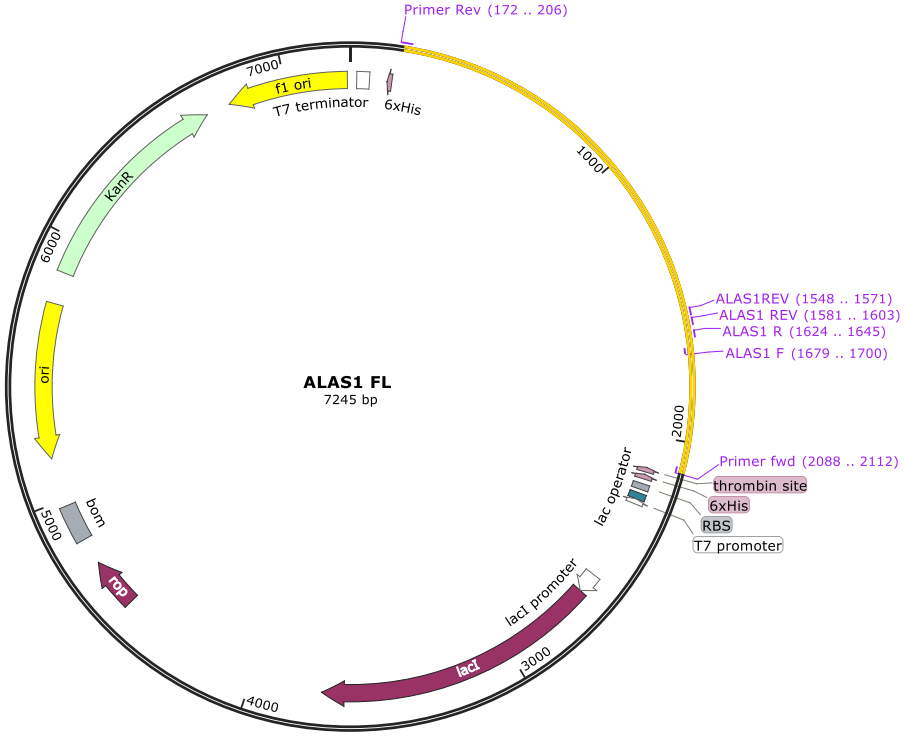

Appendix Figure 4 ALAS 1 full length cloned into pET28a vector. Plasmid map generated using SnapGene

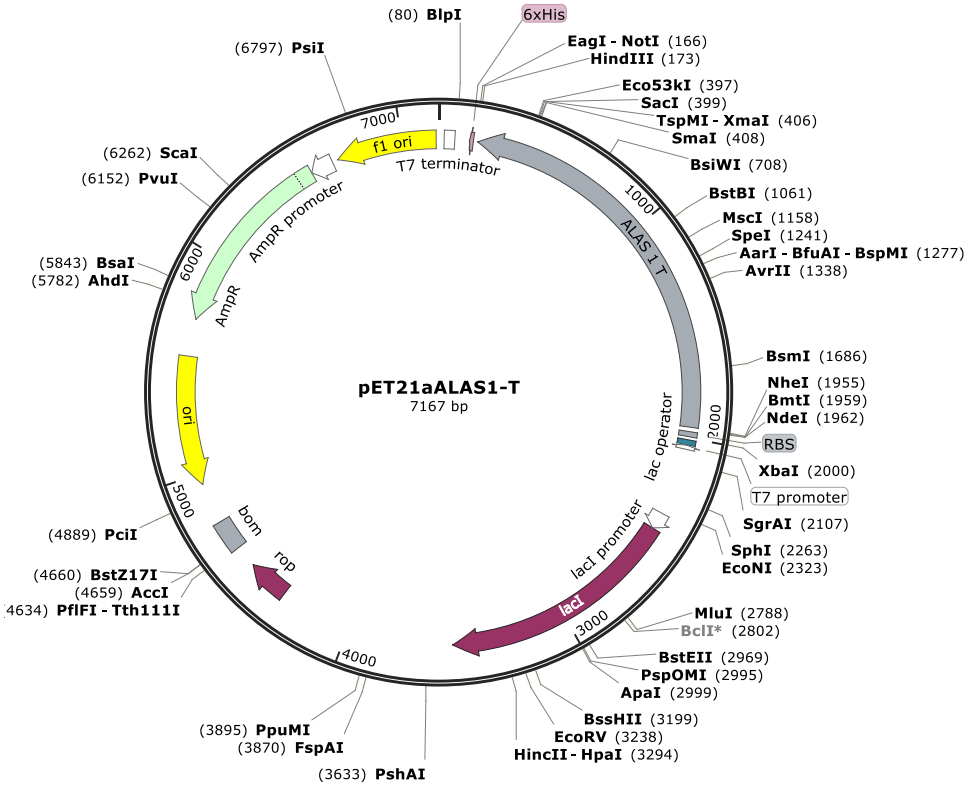

Appendix Figure 5 ALAS1-T cloned into a pET21a vector. Plasmid map generated using SnapGene

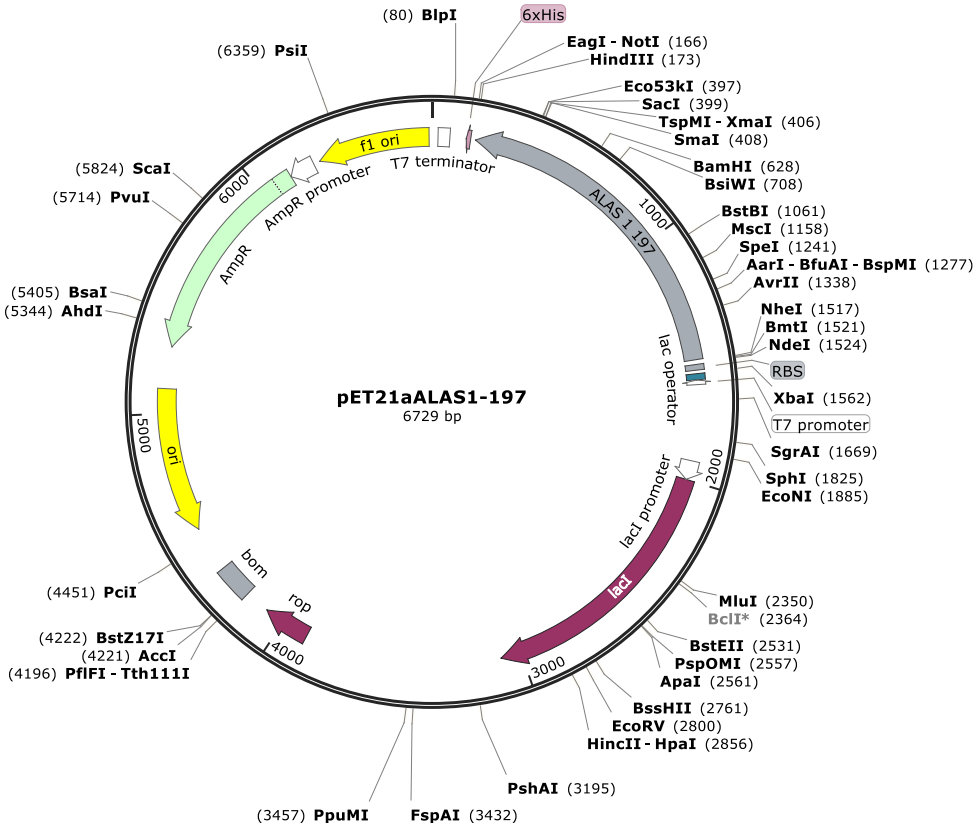

Appendix Figure 6 ALAS1-197 cloned into pET21a vector Plasmid map generated using SnapGene

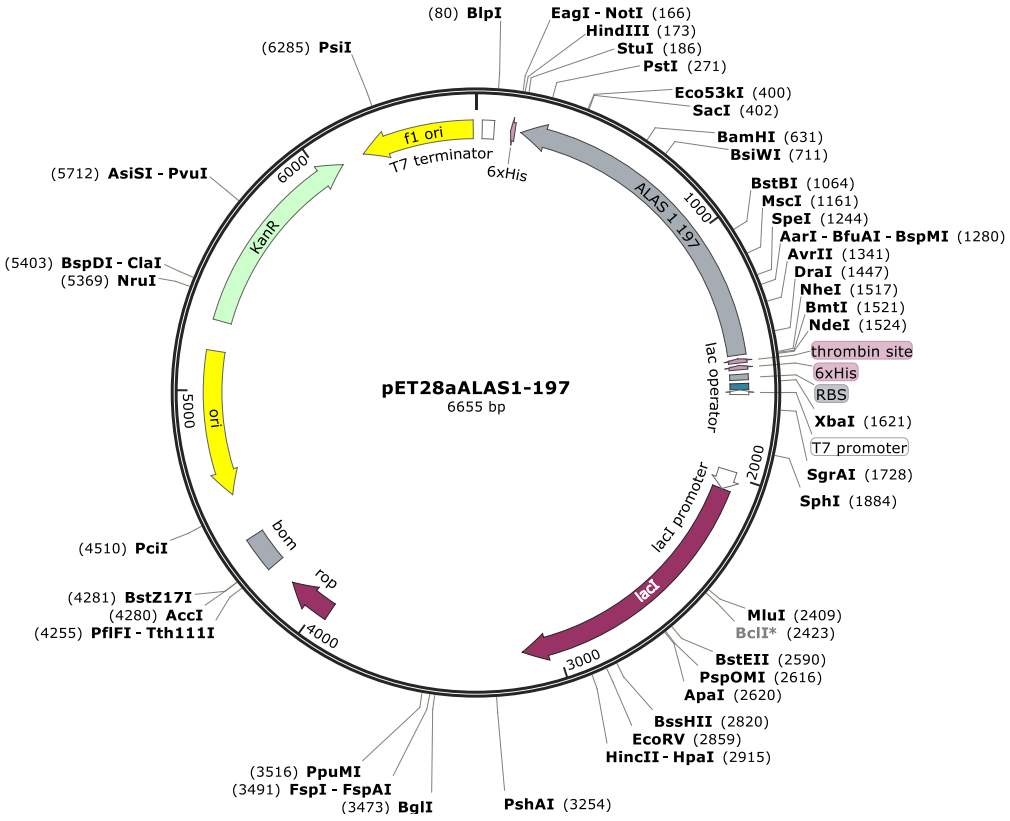

Appendix Figure 7 ALAS1-197 cloned into pET28a vector. Plasmid map generated using SnapGene.

References

ACS (2019) https://www.cancer.org/cancer/prostate-cancer/about/what-is-prostate-cancer.html last accessed 15/01/19

Al-Saffa, N, M,. Troy, H,. Wong, A,. Fong, T,. Paravati, R,. Jackson, E,. Gowan, S,. Boult, J, K, R,. Robinson, S, P,. Eccles, S, A,. Yap, T, A,. Leach, M, O,. and Chung, Y,. (2018) Metabolic biomarkers of response to the AKT inhibitor MK-2206 in pre-clinical models of human colorectal and prostate carcinoma. *British Journal of Cancer*. **119**, 1118–1128

Angeli, J, P, J,. Shah, R,. Pratt, D, A,. Conrad, M,. (2017) Ferroptosis Inhibition: Mechanisms and Opportunities. *Trends in Pharmacological Sciences*. **38,** 489-498

Astner, I,. Schulze, J, O,. Heuvel, J, V,. Jahn, D,. Schubert, W,. and Heinz, D, K,. (2005) Crystal structure of 5-aminolevulinate synthase, the first enzyme of heme biosynthesis, and its link to XLSA in humans. *The EMBO journal*. **24,** 3166–3177

Bailey, H.J., Shrestha, L., Rembeza, E., Newman, J., Kupinska, K., Diaz-saez, L., Kennedy, E., Burgess-Brown, N., von Delft, F., Arrowsmith, C., Edwards, A., Bountra, C., Yue, W.W. (2018) Structure of human erythroid-specific 5'-aminolevulinate synthase, ALAS2 **To be published**.

Bandyopadhyay, U,. Das, D,. and Banerjee, R, K,. (1999) Reactive oxygen species: Oxidative damage and pathogenesis. *Current science.* **77,** 658-666

Ben-Shlomo, Y,. Evans, S,. Ibrahim, F,. Patel, B,. Anson, K,. Chinegwundoh, F,. Corbishley, C,. Dorling, D,. Thomas, B,. Gillatt, D,. Kirby, R,. Muir, G,. Nargund, V,. Popert, R,. Metcalfe, C,. and Persad, R,. (2008) The risk of prostate cancer amongst black men in the United Kingdom: the PROCESS cohort study. *European urology.* **53** 99-105

Birsoy, K,. Sabatini, D, M,. and Possemato, R,. (2012) Untuning the tumor metabolic machine: Targeting cancer metabolism: a bedside lesson. *Nature Medicine.* **18,** 1022–3.

Blommel, P, G,. Becker, K, J,. Duvnjak, P,. Fox, B, G,. (2009) Enhanced Bacterial Protein Expression During Auto-induction Obtained by Alteration of Lac Repressor Dosage and Medium Composition. *Biotechnology progress.* **23**, 585–598

Bratt, O,. and Lamb, A, D,. (2018). Genetic Reasons to Walk the Extra Mile to Prevent Prostate Cancer. *European Urology*. **76,** 41–42

Carnero, A,. Blanco-Aparicio, C,. Renner, O,. Link, W,. Leal, J, F,. (2008) The PTEN/PI3K/AKT signalling pathway in cancer, therapeutic implications. *Current cancer drug targets*. **8**, 187-98.

Castilla, C,. Congregado, B,. Chinchón, D,. Torrubia, F, J,. Japón, M, A,. Sáez, C,. (2006) Bcl-xL Is Overexpressed in Hormone-Resistant Prostate Cancer and Promotes Survival of LNCaP Cells via Interaction with Proapoptotic Bak. *Endocrinology*, **147,** 4960–4967

Chen, G,. and Goeddel, D, V,. (2002) TNF-R1 Signaling: A Beautiful Pathway. *SCIENCE*. **296**, 1634-1635

Costello, L. C., and Franklin, R. B. (2000). The intermediary metabolism of the prostate: a key to understanding the pathogenesis and progression of prostate malignancy. *Oncology*. **59,** 269-82.

Degterev, A,. Hitomi, J,. Germscheid, M,. Ch'en, I, L,. Korkina, O,. Teng, X,. Abbott, D,. Cuny, G, D,. Yuan, C,. Wagner, G,. Hedrick, S, M,. Gerber, S, A., Lugovskoy, A,. and Yuan, J,. (2008). Identification of RIP1 kinase as a specific cellular target of necrostatins. *Nature chemical biology.* **4**, 313–321.

Del, C,. and Batlle, A, M,. (1993). Porphyrins, porphyrias, cancer and photodynamic therapy — a model for carcinogenesis. Journal of Photochemistry and Photobiology *B: Biology*. **20,** 5–22.

Donahue, R, A,. and Bebee, R, L,. (1999) BL21-SI ™ Competent Cells for Protein Expression in E.coli, *Life Technologies, Inc.* **21**, 49-51

Ebert, P, S,. Hess, R, A,. Frykholm, B, C,. and Tschudy, D, P,. (1979) Succinylacetone, a potent inhibitor of heme biosynthesis: Effect on cell growth, heme content and δ-aminolevulinic acid

dehydratase activity of malignant murine erythroleukemia cell. *Biochemical and Biophysical Research Communications*. **88,** 1382-1390

Elkahwaji, J, E,. Zhong, W,. Hopkins, W, J,. and Bushman, W,. (2007) Chronic bacterial infection and inflammation incite reactive hyperplasia in a mouse model of chronic prostatitis. *The prostate.* **67**, 14-21

Evans, S,. Metcalfe, C,. Ibrahim, F,. Persad, R,. and Ben-Shlomo, Y,. (2008) Investigating Black-White differences in prostate cancer prognosis: A systematic review and meta-analysis. *International journal of cancer.* **123,** 430-435

Ferreira, G, C,. Neame, P, J,. and Dailey, H, A,. (1993) Heme biosynthesis in mammalian systems: evidence of a Schiff base linkage between the pyridoxal 5'-phosphate cofactor and a lysine residue un 5-aminolevulinate synthase. *Protein Science.* **2,** 1959-1965

Ficarra, V,. Rossanese, M,. Zazzara, M,. Giannarini, G,. Abbinante, M,. Bartoletti, R,. Mirone, V,. and Scaglione, F,. (2014) The role of inflammation in lower urinary tract symptoms (LUTS) due to benign prostatic hyperplasia (BPH) and its potential impact on medical therapy. *Current urology reports*. **14,** 463-469

Floc'h, N,. Kinkade, C, W,. Kobayashi, T,. Aytes, A,. Lefebvre, C,. Mitrofanova, A,. Cardiff, R, D,. Califano, A,. Shen, M, M,. and Abate-Shen, C,. (2012) Dual Targeting of the Akt/mTOR Signaling Pathway Inhibits Castration-Resistant Prostate Cancer in a Genetically Engineered Mouse Model. *American association for cancer research.* **72**, 4483-4493

Francis, D, M,. and Page, R,. (2010) Strategies to Optimize Protein Expression in E. coli. *Current protocols in protein science.* **61,** 5.24.1-5.24.29

Galluzzi, L,. Kroemer, G,. (2008) Necroptosis: A Specialized Pathway of Programmed Necrosis. *Cell*. **135,** 1311-1323

Giampazolias, E,. Zunino, B,. Dhayade, S,. Bock, F,. Cloix, C,. Cao, K,. Roca, A,. Lopez, J,. Ichim, G,. Proïcs, E,. Rubio-Patiño, C,. Fort, L,. Yatim, N,. Woodham, E,. Orozco, S,. Taraborrelli, L,. Peltzer, N,. Lecis, D,. Machesky, L,. Walczak, H,. Albert, M, L,. Milling, S,. Oberst, A,. Ricci, J, E,. Ryan, K, M,. Blyth, K,. and Tait, S, W, G,. (2017) Mitochondrial permeabilization engages NF-κB-dependent anti-tumour activity under caspase deficiency. *Natural Cell Biology*. **19**, 1116-1129

Gibson, K, D,. Laver, W, G,. and Neuberger, A,. (1958) Initial stages in the biosynthesis of porphyrins. 2. The formation of delta-aminolaevulic acid from glycine and succinyl-coenzyme A by particles from chicken erythrocytes*. Biochemical Journal*. **70** 71-81

Grabski, A,. Mehler, M,. and Drott, D,. (2005) The Overnight Express Autoinduction System: High-density cell growth and protein expression while you sleep, *Nature methods.* **2,** 233–235

Grell, M,. Zimmermann, G., Gottfried, E,. Chen, C,. Grünwald, U,. Huang, D, C, S,. Lee, Y, W,. Dürkop, H,. Engelmann, H,. Scheurich, P,. Wajant, H,. and Strasser, A,. (1999) Induction of cell death by tumour necrosis factor (TNF) receptor 2, CD40 and CD30: a role for TNF-R1 activation by endogenous membrane-anchored TNF. *The Embo journal*. **18**, 3034-3043

Han, W., Gao, S., Barrett, D., Ahmed, M., Han, D., Macoska, J. A., He, H. H., Cai, C,. (2017). Reactivation of androgen receptor-regulated lipid biosynthesis drives the progression of castration-resistant prostate cancer. *Oncogene*. ***37*,** 710-721.

Heijink, D. M., Kleibeuker, J. H., Jalving, M., Boersma-van Ek, W., Koornstra, J. J., Wesseling, J., and de Jong, S. (2007). Independent induction of caspase-8 and cFLIP expression during colorectal carcinogenesis in sporadic and HNPCC adenomas and carcinomas. *Cellular oncology: the official journal of the International Society for Cellular Oncology.* **29,** 409–419

Hirai, H,. Sootome, H,. Nakatsuru, Y,. Miyama, K,. Taguchi, S,. Tsujioka, K,. Ueno, Y,. Hatch, H,. Majumder, P, K,. Pan, B,. and Kotani, H,. (2010) MK-2206, an Allosteric Akt Inhibitor, Enhances

Antitumor Efficacy by Standard Chemotherapeutic Agents or Molecular Targeted Drugs In vitro and In vivo. *Molecular Cancer Therapeutics.* **9,** 1956-1967

Hitomi, J., Christofferson, D. E., Ng, A., Yao, J., Degterev, A., Xavier, R. J., & Yuan, J. (2008). Identification of a molecular signaling network that regulates a cellular necrotic cell death pathway. *Cell*. **135**, 1311–1323.

Hodges, N, J,. Innocent, N,. Dhanda, S,. Graham, M,.(2008) Cellular protection from oxidative DNA damage by over-expression of the novel globin cytoglobin in vitro. *Mutagenesis*. **23,** 293–298

Hooda, J,. Alam, M, M,. and Zhang, L,. (2015) Evaluating the Association of Heme and Heme Metabolites with Lung Cancer Bioenergetics and Progression. *Metabolomics*. **5**, 150

Hooda, J,. Cadinu, D,. Alam, M, M,. Shah, A,. Cao, T, M,. Sullivan, L, A,. Brekken, R,. Zhang, L,. (2013) Enhanced heme function and mitochondrial respiration promote the progression of lung cancer cells. *PLOS one*. **8** e63402

Hoover, P,. and Naz, R, K,. (2012) Do men with prostate abnormalities (prostatitis/benign prostatic hyperplasia/prostate cancer) develop immunity to spermatozoa or seminal plasma? *International journal of andrology.* **35,** 608-615

Horoszewicz, j, S,. Leong, S, S,. Kawinski, E,. Karr, J, P,. Rosenthal, H,. Chu, T, M,. Mirand, E, A,. and Murphy, G, P,. (1983) LNCaP Model of Human Prostatic Carcinoma. *Cancer research*. **43**, 1809-1818

https://www.cancerresearchuk.org/health-professional/cancer-statistics/statistics-by-cancer-type/prostate-cancer/incidence accessed 15/12/18

Huggins, C,. Scott, W, W,. and Heinen, H, J,. (1942) Chemical composition of human semen and of the secretions of the prostate and seminal vesicles. *American journal of physiology*. **136,** 467-473

Hunter, G, A,. and Ferreira, G, C,. (2009) 5-aminolevulinate synthase: catalysis of the first step of heme biosynthesis. *Cellular and molecular biology*. **55,** 102–110.

Indo, H, P,. Davidson, M,. Yen, H,. Suenaga, S,. Tomita, K,. Nishii, T,. Higuchi, M., Koga, Y,. Ozawa, T,. Majima, H, J,. (2007) Evidence of ROS generation by mitochondria in cells with impaired electron transport chain and mitochondrial DNA damage. *Mitochondrion*. **7,** 106-18

Ito, E,. Yue, S,. Moriyama, E, H,. Hui, A, B,. Kim, I,. Shi, W,. Alajez, N, M,. Bhogal, N,. Li, G,. Datti, A,. Schimmer, A, D,. Wilson, B, C,. Liu, P, P,. Durocher, D,. Neel, B, G,. O'Sullivan, B,. Cummings, B,. Bristow, R,. and Wrana, J,. Liu, F, F,. (2011) Uroporphyrinogen decarboxylase is a radiosensitizing target for head and neck cancer. *Science translational medicine.* **3**, 67ra7–67ra7.

Jack, R, H,. Davies, E, A,. and Møller, H,. (2010) Prostate cancer incidence, stage at diagnosis, treatment and survival in ethnic groups in South-East England. *BJU international.* **105,** 1226-30.

Jong, Y, D,. Monderer, D,. Brandinelli, E,. Monchanin, M,. Akker, B, V,. Oosterwijk, J, V,. Blay, J, Y,. Dutour, A,. & Bovée, J, V, M,. (2018) Bcl-xl as the most promising Bcl-2 family member in targeted treatment of chondrosarcoma. *Oncogenesis.* **7**, 74

Jouan-Lanhouet, S,. Arshad, M, I,. Piquet-Pellorce, C,. Martin-Chouly, C,. Le Moigne-Muller, G,. Van Herreweghe, F,. Takahashi, N,. Sergent, O,. Lagadic-Gossmann, D,. Vandenabeele, P,. Samson, M,. and Dimanche-Boitrel, M, T,. (2012). TRAIL induces necroptosis involving RIPK1/RIPK3-dependent PARP-1 activation. *Cell death and differentiation.* **19,** 2003–2014.

Kaambre, T,. Chekulayev, V,. Shevchuk, I,. Karu-Varikmaa, M,. and Timohhina, N,. (2012) Metabolic control analysis of cellular respiration in situ in intraoperational samples of human breast cancer. *Journal Bioenergenetics*. **44,** 539–58.

Kalainayakan, S, P,. FitzGerald, K, E,. Konduri, P, C,. Vidal, C,. and Zhang, L,. (2018) Essential roles of mitochondrial and heme function in lung cancer bioenergetics and tumorigenesis. *Cell and bioscience.* **8,** 56

Lee, E., Seo. J., Jeong, M,. Lee, S,. Song, J,. (2012) The roles of FADD in extrinsic apoptosis and necroptosis. *BMB Reports.* **45,** 496-508

Lee, P, J,. Woo, S, J,. Yoo, H, M,. Cho, N,. and Kim, H, P,. (2019) Differential Mechanism of ATP Production Occurs in Response to Succinylacetone in Colon Cancer Cells. *Molecules*. **24,** 3575-3581

Leverson, J, D,. Phillips, D, C,. Mitten, M, J,. Boghaert, E, R,. Diaz, D,. Tahir, S, K,. Belmont, L, D,. Nimmer, P,. Xiao, Y,. Ma, X, M,. Lowes, K, N,. Kovar, P,. Chen, J,. Jin, S,. Smith, M,. Xue, J, Zhang, H,. Oleksijew, A,. Magoc, T, J,. Vaidya, K, S,. Albert, D, H,. Tarrant, J, M,. La, N,. Wang, L,. Tao, Z, F,. Wendt, M, D,. Sampath, D,. Rosenberg, S, H,. Tse, C,. Huang, D, C,. Fairbrother, W, J,. Elmore, S, W,. Souers, A, J,. (2015) Exploiting selective BCL-2 family inhibitors to dissect cell survival dependencies and define improved strategies for cancer therapy. *Science translational medicine*. **7**, 279-40

Lin, W, W,. (2016) Z-VAD-induced necroptosis in TLR3/4-stimulated macrophages involves TRIF-dependent interferon signaling pathway and ROS-dependent autophagy. *The journal of immunology.* **1**, 203

Linkermann, A., and Green, D, R. (2014). Necroptosis. *The New England journal of medicine.* **370,** 455–465.

Liu, Z,. Lin, H,. Ye, S,. Liu, Q,. Meng, Z,. Zhang, C,. Xia, Y,. Margoliash, E,. Rao, Z,. Liu, X,.(2006) Remarkably high activities of testicular cytochrome c in destroying reactive oxygen species and in triggering apoptosis*. PNAS.* **103**, 8965–8970

Lloyd, T., Hounsome, L., Mehay, A., Mee, S., Verne, J., & Cooper, A. (2015). Lifetime risk of being diagnosed with, or dying from, prostate cancer by major ethnic group in England 2008-2010. *BMC medicine.* **13,** 171

Lobstein, J,. Emrich, C, A,. Jeans, C,. Faulkner, M,. Riggs, P,. Berkmen, M,. (2012) SHuffle, a novel Escherichia coli protein expression strain capable of correctly folding disulfide bonded proteins in its cytoplasm. *Microbial Cell Factories.* **11**, 1-16

Mann, T,. (1974) secretory function of the prostate, seminal vesicle and other male accessory organs of reproduction. *Journal of reproductive fertility.* **37,** 179-188

Martinez-Outschoorn, U, E,. Peiris-Pages, M,. Pestell, R, G,. Sotgia, F,. and Lisanti, M, P,. (2017) Cancer metabolism: a therapeutic perspective. *Nature reviews Clinical oncology.* **14,** 11-31

McRonald, F, E,. Risk, J, M,. J. Hodges, N, J,.(2012) Protection from Intracellular Oxidative Stress by Cytoglobin in Normal and Cancerous Oesophageal Cells. *PLoSONE.* **7,** e30587

Meeks, J, J,. and Schaeffer, E, M,. (2013) Genetic Regulation of Prostate Development. *Journal of andrology.* **32,** 210-217

Michael, M,. Hu, G,. Feng, H,. Linkermann, A,. Min, W,. Stockwell, B, R,. (2018) Determination of the Subcellular Localization and Mechanism of Action of Ferrostatins in Suppressing Ferroptosis. *ACS chemical biology*. **13**, 1013-1020

Morgan, T, M,. Koreckij, T, D,. and Corey, E,. (2009) Targeted therapy for advanced prostate cancer: inhibition of the PI3K/Akt/mTOR pathway. *Current cancer drug targets*. **9**, 237-49.

Mottet, N,. Bellmunt, J,. Briers, E,. Bolla, M,. Cornford, P,. De Santis, M,. Henry, A, M,. Joniau, S,. Lam, T, B,. Mason, M, D,. Vander poel, H, G,. (2016) Guidelines on prostate cancer. European Association of Urology.

Munakatah, H,. Sun, J,. Yoshida, K,. Nakatani, T,. Honda, E,. Hayakawai, S,. Furuyama, K,. and Hayashi, N,. (2004) Role of the Heme Regulatory Motif in the Heme-Mediated Inhibition of Mitochondrial Import of 5-Aminolevulinate Synthase. *Journal of Biochemistry*. **136,** 233-238

Musatov , A,. Robinson, N, C,.(2012) Susceptibility of mitochondrial electron-transport complexes to oxidative damage. Focus on cytochrome c oxidase. *Free radical research.* **46**, 1313-26

Nagasaka, A,. Kawane, K,. Yoshida, H,. and Nagata, S. (2010) Apaf-1-independent programmed cell death in mouse development. *Cell Death and differentiation.* **17,** 931–41.

Narayan, R, S,. Fedrigo, C, A,. Brands, E,. Dik, R,. Stalpers, L, J,. Baumert, B, G,. Slotman, B, J,. Westerman, B, A,. Peters, G, J,. and Sminia, P,. (2017). The allosteric AKT inhibitor MK2206 shows a

synergistic interaction with chemotherapy and radiotherapy in glioblastoma spheroid cultures. *BMC cancer*. ***17***, 204.

Navone, N, M,. Polo, C, F,. Frisardi, A, L,. Andrade, N, E,. and Battle, A, M,. (1990) Heme biosynthesis in human breast cancer--mimetic "in vitro" studies and some heme enzymic activity levels. *The International journal of biochemistry.* **22,** 1407-11

NCBI BCL2L1 (2019) https://www.ncbi.nlm.nih.gov/gene/598 last accessed 18/09/19

Newton, K,. Dugger, D, L,. Wickliffe, K, E,. Kapoor, N,. De Almagro, C, M,. Vucic, D,. Komuves, L,. Ferrando, R, E,. French, F, M,. Webster, J,. Roose-Girma, M,. Warming, S,. Dixit V, M,. (2014) Activity of Protein Kinase RIPK3 Determines Whether Cells Die by Necroptosis or Apoptosis. *SCIENCE.* **343,** 1357-1360

Oberley, T, D,. (2002). Oxidative damage and cancer. *The American journal of pathology*. **160,** 403–408.

Orozco, S,. Yatim, N,. Werner, M, R,. Tran, H,. Gunja, S, Y,. Tait, S, W,. Albert, M, L,. Green, D, R,. and Oberst, A,. (2014). RIPK1 both positively and negatively regulates RIPK3 oligomerization and necroptosis. *Cell death and differentiation***. 21,** 1511–1521

Osborn, S, L,. Diehl, G,. Han, S,. Xue, L,. Kurd, N,. Hsieh, K,. Cado, D,. Robey, E, A,. and Winoto, A,. (2010) Fas-associated death domain (FADD) is a negative regulator of T-cell receptor–mediated necroptosis. *PNAS.* **107,** 13034–13039

Parsons, J, K,. Carter, H, B,. Partin, A,. W,. Windham, B, G,. Metter, E, J,. Ferrucci, L,. Landis, P,. and Platz, E, A,. (2006) Metabolic Factors Associated with Benign Prostatic Hyperplasia. *The Journal of Clinical Endocrinology & Metabolism.* **91,** 2562–2568

Pasparakis, M,. and Vandenabeele, P,. (2015) Necroptosis and its role in inflammation. *Nature*. **517** 311.

PCUK (2019) https://prostatecanceruk.org/prostate-information/treatments last accessed 15/07/18

Peng, Q,. Berg, K,. Moan, J,. Kongshaug, M,. and Nesland, J, M,. (2008) 5-Aminolevulinic Acid-Based Photodynamic Therapy: Principles and Experimental Research. *Photochemistry Photobiology.* **65,** 235-51

Pomerantz, M, M,. Li, F., Takeda, D, Y,. Lenci, R,. Chonkar, A,. Chabot, M,. Cejas, P,. Vazquez, F,. Cook, J,. Shivdasani, R, A,. Bowden, M,. Lis, R,. Hahn, W, C,. Kantoff, P, W,. Brown, M,. Loda, M,. Long H, W,. and Freedman, M, L,. (2015). The androgen receptor cistrome is extensively reprogrammed in human prostate tumorigenesis. *Nature genetics.* **47,** 1346-51.

Ponka, P,. (1997) Tissue-Specific Regulation of Iron Metabolism and Heme Synthesis: Distinct Control Mechanisms in Erythroid Cells. *Blood*. **89,** 1-25

Riddle, R, D,. Yamamoto, M,. And Engel, J, D,. (1989) Expression of delta-aminolevulinate synthase in avian cells: separate genes encode erthroid-specific and non-specific isoenzymes. *PNAS*. **85,** 792-796

Ryter, S, W,. and Tyrrell, R, M,. (2000) The heme synthesis and degradation pathways: role in oxidant sensitivity: Heme oxygenase has both pro- and antioxidant properties. *Free Radical Biology and Medicine*. **28,** 289-309

Sadeghi, M,. Enferadi, M,. and Shirazi, A,. (2010). External and internal radiation therapy: past and future directions. *Journal of cancer research and therapeutics*. **6,** 239–248.

Sarker, D,. Reid, A, H, M,. Yap, T, A,. and de Bono, J, S,. (2009) Targeting the PI3K/AKT Pathway for the Treatment of Prostate Cancer. *Clinical cancer research.* **15**, 4799- 4805

Sassa, S,. and Kappas, A,. (1983) Hereditary Tyrosinemia and the Heme Biosynthetic Pathway: profound inhibition of 8-aminolevulinic acid dehydratase activity by succinylacetone. *Journal of Clinical Investigation*. **71,** 625-634

Scaccianoce ,E., Festuccia, C,. Dondi, D,. Guerini, V., Bologna, M,. Motta, M,. and Poletti, A. (2003) Fzation of prostate cancer DU145 cells expressing the recombinant androgen receptor. *Oncology research*. **14,** 101-12.

Sedger, L, M,. and McDermott, M, F,. (2014) TNF and TNF-receptors: From mediators of cell death and inflammation to therapeutic giants – past, present and future. *Cytokine & Growth Factor Reviews.* **25,** 453-472

Shemin, D,. and Kikuchi, G,. (1958) Enzymatic synthesis of sigma-aminolevulinic acid. *Annals of the New York Academy of science*. **75,** 122-128

Shiau, C,. Huang, J,. Wang, D,. Weng, J,. Yang, C,. Lin, C,. Li, C,. Chen, C,.(2006) Tocopheryl Succinate Induces Apoptosis in Prostate Cancer Cells in Part through Inhibition of Bcl-xL/Bcl-2 Function. *The journal of biological chemistry*. **281**, 11819 –11825

Slee, E, A,. Zhu, H,. Chow, S, C,. Macfarlane, M,. Nicholson, D, W,. Cohen. G, M,. (1996) Benzyloxycarbonyl-Val-Ala-Asp (OMe) fluoromethylketone (Z-VAD.FMK) inhibits apoptosis by blocking the processing of CPP32. *Biochemical Journal.* **315,** 21-24

Sun, H,. Da-Ming Li, R, D, Liliental, J,. Zhang, H,. Gao, J,. Gavrilova, N,. Mueller, B,. Liu, X,. and Wu, H,.(1999) PTEN modulates cell cycle progression and cell survival by regulating phosphatidylinositol 3,4,5,-trisphosphate and Akt/protein kinase B signalling pathway. *PNAS*. **96.** 6199-6204

Tai, S., Sun, Y., Squires, J. M., Zhang, H., Oh, W. K., Liang, C. Z., and Huang, J. (2011). PC3 is a cell line characteristic of prostatic small cell carcinoma. *The Prostate.* **71,** 1668–1679.

Tao, Z, F,. Hasvold, L,. Wang, L,. Wang, X,. Petros, A, M,. Park, C, H,. Boghaert, E, R,. Catron, N, D,. Chen, J,. Colman, P, M,. Czabotar, P, E,. Deshayes, K,. Fairbrother, W, J,. Flygare, J, A,. Hymowitz, S, G,. Jin, S,. Judge, R, A,. Koehler, M, F,. Kovar, P, J,. Lessene, G,. Mitten, M, J,. Ndubaku, C, O,. Nimmer, P,. Purkey, H, E,. Oleksijew, A,. Phillips, D, C,. Sleebs, B, E,. Smith, B, J,. Smith, M, L,. Tahir, S, K,. Watson, K, G,. Xiao, Y,. Xue, J,. Zhang, H,. Zobel, K,. Rosenberg, S, H,. Tse, C,. Leverson, J, D,. Elmore,

S, W,. and Souers, A, J. (2014) Discovery of a Potent and Selective BCL-XL Inhibitor with in Vivo Activity. *ACS Medicinal Chemistry Letters*. **5**, 1088-93

Taylor, B, S,. Schultz, N,. Hieronymus, H,. Gopalan, A,. Xiao, Y,. Carver, B, S,. Arora, V, K,. Kaushik, P,. Cerami, E,. Reva, B,. Antipin, Y,. Mitsiades, N,. Landers, T,. Dolgalev, I,. Major, J, E,. Wilson, M,. Socci, N, D,. Lash, A, E,. Heguy, A,. Eastham, J, A,. Scher, H, I,. Reuter, V, E,. Scardino, P, T,. Sander, C,. Sawyers, C, L,. and Gerald, W, L,. (2010) Integrative genomic profiling of human prostate cancer. *Cancer Cell.* **18,** 11-22.

Van Noorden, C, J, F,. (2001) The history of Z-VAD-FMK, a tool for understanding the significance of caspase inhibition. *Acta Histochemica*. **103**, 241-251

Vandenabeele, P,. Berghe, T, V,. and Festjens, N,. (2006) Caspase Inhibitors Promote Alternative Cell Death Pathways, *Cell biology*. **358,** 44

Vander Heiden, M, G,. Cantly, L, C,. and Thompson, C, B,. (2010) Understanding the Warburg Effect: The Metabolic Requirements of Cell Proliferation. *Science.* **324,** 1029-1033

Vasaitis, T, S,. Bruno, R, D,. and Njar, V, C,. (2010). CYP17 inhibitors for prostate cancer therapy. *The Journal of steroid biochemistry and molecular biology.* **125,** 23-31.

Verze, P,. Cai, T,. and Lorenzerri, S,. (2016) The role of the prostate in male fertility, health and disease. *Nature Reviews Urology.* **13,** 379-86

Vlietstra, R, J,. Alewijk, D, C, J, G,. Herman, K, G,. Steenbrugge, G, J,. and Trapman, J,.(1998) Frequent Inactivation of PTEN in Prostate Cancer Cell Lines and Xenografts. *Cancer Research.* **58**. 2720-2723.

Wagenlehner, F, M,. Elkahwaji, J, E,. Algaba, F,. Bjerklund-Johansen, T,. Naber, K, G,. Hartung, R,. and Weidner, W,. (2007) The role of inflammation and infection in the pathogenesis of prostate carcinoma*. BJU international*. **100,** 733-737

Wajant, H,. Pfizenmaier, K,. and Scheurich, P,. (2003) Tumor necrosis factor signalling. *Cell Death & Differentiation*. **10**, 45–65

Wang, Y,. Branicky, R,. Noë, A,. and Hekimi, S,. (2018) Superoxide dismutases: Dual roles in controlling ROS damage and regulating ROS signalling. *Journal of cell biology*. **217**, 1915-28

Weinbacha, E, C,. and Elbert, P, S,. (1985) Effects of succinyl acetone on growth and respiration of L1210 leukemia cells. *Cancer letters.* **26,** 253-259

Wenpeng, Y,. and Henneberg, M,. (2018) Prostate Cancer Incidence is Correlated to Total Meat Intake– a Cross-National Ecologic Analysis of 172 Countries. *Asian Pacific journal of cancer prevention.* **19,** 2229-2239

Whitaker-Menezes, D,. Martinez-Outschoorn, U, E,. Flomenberg, N,. Birbe, R, C,. and Witkiewicz, A, K,. (2011) Hyperactivation of oxidative mitochondrial metabolism in epithelial cancer cells in situ: visualizing the therapeutic effects of metformin in tumor tissue. *Cell Cycle*. **10,** 4047–64.

Wyman, J,. (1948) Heme Proteins. *Advances in Protein Chemistry*, **4,** 407-531

Xie, T,. Peng, W,. Liu, Y,. Yan, C,. Maki, J,. Degterev, A,. Yuan, J,. and Shi, Y,. (2013) Structural Basis of RIP1 Inhibition by Necrostatins. *Structure.* **21**, 493-499

Ye, W,. and Zhang, L,. (2004) Heme controls the expression of cell cycle regulators and cell growth in HeLa cells. *Biochemical and biophysical research communications.* **315,** 546-54

Yoon, S,. Kovalenko, A,. Bogdanov, K,. and Wallach, D. (2017) MLKL, the Protein that Mediates Necroptosis, Also Regulates Endosomal Trafficking and Extracellular Vesicle Generation. *Immunity.* **47,** 51-65

Zhang J., and Ferreira G. C. (2002) Transient state kinetic investigation of 5-aminolevulinate synthase reaction mechanism. *Journal of Biological Chemistry.* **277,** 44660-44669

Zilka, O,. Shah, R,. Li, B,. Angeli, J, F,. Griesser, M,. Conrad, M,. and Pratt, D, A,. (2017) On the Mechanism of Cytoprotection by Ferrostatin-1 and Liproxstatin-1 and the Role of Lipid Peroxidation in Ferroptotic Cell Death. *ACS Central Science*. **3**, 232-243

Zorov, D. B., Juhaszova, M., and Sollott, S. J. (2014). Mitochondrial reactive oxygen species (ROS) and ROS-induced ROS release. *Physiological reviews.* **94**, 909–950.